



Salmirinne, Irni Onerva (2022) *Bioinformatic and biochemical characterization of arabidopsis thaliana protein nch1 and links to plant immunity*. MSc(R) thesis.

<http://theses.gla.ac.uk/82852/>

Copyright and moral rights for this work are retained by the author

A copy can be downloaded for personal non-commercial research or study, without prior permission or charge

This work cannot be reproduced or quoted extensively from without first obtaining permission in writing from the author

The content must not be changed in any way or sold commercially in any format or medium without the formal permission of the author

When referring to this work, full bibliographic details including the author, title, awarding institution and date of the thesis must be given

Enlighten: Theses

<https://theses.gla.ac.uk/>
research-enlighten@glasgow.ac.uk

BIOINFORMATIC AND
BIOCHEMICAL
CHARACTERIZATION OF
ARABIDOPSIS THALIANA
PROTEIN NCH1
AND LINKS TO PLANT
IMMUNITY

Irni Onerva Salmirinne, BSc.Hons.

*Thesis submitted in fulfilment of the requirements for
the Degree of Master of Science by Research, MSc.(R)*

*School of Life Sciences,
College of Medical, Veterinary & Life Sciences
University of Glasgow*

May 2022

© Irni Salmirinne, 2021-2022

Abstract

NCH1 (NRL PROTEIN FOR CHLOROPLAST MOVEMENT 1) is a plant protein postulated to play a role in plant immunity, in addition to being a component of the plant blue light signalling pathway directly downstream of the phototropin blue light receptors. Confocal microscopy of mCitrine-tagged NCH1 *Arabidopsis* lines and bifluorescence complementation (BiFC) experiments in *Nicotiana benthamiana* suggest that in its native state, *Arabidopsis* protein AtNCH1 exists as a dimer, therefore confirming the similar results reported previously in its potato ortholog StNRL1. AtNCH1 was also found to localize at the plasma membrane both in the dark and after blue light treatment both in transgenic *Arabidopsis* hypocotyls and in the transient *Nicotiana benthamiana* expression system. Preliminary confocal microscopy studies on the putative phosphorylation-deficient variant, NCH1^{S602A-S604A}, also exhibited similar localization in the plasma membrane in *N. benthamiana*. As it was hypothesised that NCH1 could play a role in *Arabidopsis* immunity against the hemibiotrophic bacterium *Pseudomonas syringae* pv. *tomato* DC3000 (*Pst* DC3000), flood assay data suggested that double mutant *nch1-1/rpt2-3* plants showed inconclusive differences in impairment in immunity against *Pst* DC3000 in comparison to the wild type Col-0 plants. Further perspectives to the role of NCH1 in plant immunity include the determination of the phosphorylation state, and the roles of potential NCH1 interacting partners, including potential hetero interactions with NRL family proteins, on *Arabidopsis* immunity.

Table of Contents

Abstract	2
Author's Declaration	5
List of Tables and Figures	6
Acknowledgements	8
Abbreviations	9
1. Introduction and Theoretical Background	11
1.1. Plant Immunity	11
1.1.1. Plant Immunity Models.....	11
1.1.2. Extracellular Detection: Plant Basal Defences, MAMPs, and MTI	13
1.1.3. Plant Pattern Recognition: MAMP receptors.....	15
1.1.4. Intracellular Detection: Compatible and Incompatible interactions, ETS and ETI.....	19
1.1.5. Mechanisms of the Plant Immune Responses and Systemic Acquired Resistance	23
1.2. <i>Pseudomonas syringae</i> and <i>Pst</i> DC3000	27
1.2.1. <i>Pseudomonas syringae</i> and <i>Ps</i> pathovars.....	27
1.2.2. <i>Pseudomonas syringae</i> : Genetic Mechanisms of Virulence	28
1.2.3. <i>Pst</i> DC3000 Life Cycle	31
1.3. Plant Photobiology.....	34
1.3.1. Plant Photomorphogenesis	34
1.3.2. Plant Light Receptors and Light Signalling	37
1.3.3. Blue Light Signalling: Phototropins and Phototropin Signalling	40
1.3.4. NRL Proteins	43
1.3.5. NCH1 in Plant Light Signalling.....	46
1.3.6. Convergences of Plant Light Signalling and Immunity: Chloroplasts and NCH1	47
1.4. Experimental Aims and Strategies.....	50
2. Materials and Methods	51
2.1. Bioinformatics	51
2.2. Localization of NCH1 protein in <i>Arabidopsis thaliana</i>	52
2.3. NCH1 Dimerization.....	54
2.4. NCH1 Phosphorylation.....	59
2.5. Flood Assay of <i>Pst</i> DC3000-Infected <i>Arabidopsis thaliana</i> seedlings.....	62
3. Biochemical Characterisation of NCH1	66
3.1. Introduction and Bioinformatic Analysis.....	66
3.2. Subcellular Localization of NCH1 <i>in silico</i> and <i>in vivo</i>	73
3.3. Site-Directed PCR Mutagenesis: Putative Dimerization Mutant <i>nch1</i> ^{D28N-K42Q}	79
3.4. NCH1 protein Homodimerization.....	83
3.5. The Effect of NCH1 Phosphorylation Status on NCH1 Localization.....	87
3.6. Discussion of Findings	92
4. The Effect of NCH1 on Immunity in <i>Arabidopsis</i>	94
4.1. Introduction	94
4.2. <i>Pst</i> DC3000 Time course Experiment: Visual Assessment of the Infection Cycle	97
4.3. <i>Pst</i> DC3000 Time Course Experiment: Bacterial Titre in WT <i>Arabidopsis</i>	100

4.4.	Quantification of Bacterial Titre in NRL Mutant Plants.....	102
4.5.	Flood Assay Method Optimization.....	105
4.6.	Discussion of Findings	109
5.	Conclusion & Discussion.....	111
	REFERENCES.....	113
	APPENDIX 1: PCR Thermocycler programmes	121
	APPENDIX 2: <i>Pst</i> DC3000 Flood Assay Data Statistics (DPI3).....	122

Author's Declaration

I declare that, except where explicit reference is made to the contribution of others, that this thesis is the result of my own work and has not been submitted for any other degree at the University of Glasgow or any other institution.

Signature: _____

Irni Salmirinne

May 2022

List of Tables and Figures

Figure 1.1. Examples of Arabidopsis PRR-proteins, their types, domain composition, and target MAMPs, associated co-receptors and their intracellular downstream signalling components.	15
Figure 1.2 Arabidopsis MTI signalling pathways during flg22 MAMP recognition, and their negative feedback regulation.	18
Figure 1.3 Basic dynamics of plant-pathogen interactions and the relationship between MTI and ETI responses.	19
Figure 1.4 Molecular strategies for plant R-proteins and examples of their function.	21
Figure 1.5 The zig-zag model of plant immunity and plant-pathogen interactions.	22
Figure 1.6 Interconnected mechanisms of plant systemic acquired resistance.	25
Figure 1.7 Pseudomonas syringae and genetic mechanisms for virulence.	29
Figure 1.8 Pseudomonas syringae life cycle and compatible interaction in planta.	33
Figure 1.9 Examples of normal photomorphogenesis in Arabidopsis, photomorphogenic mutants, and their phenotypes.	35
Figure 1.10 Plant light signal transduction pathways.	35
Figure 1.11 Overview of plant photoreceptors, their approximate absorbed wavelengths, and their bound chromophore cofactors.	37
Figure 1.12 Schematic representation of the domain structure of the three plant BL photoreceptor families.	39
Figure 1.13 Phot-activation is initiated by a light-dependent conformational change in the protein.	41
Figure 1.14 Inactive and active phot1-photoreceptors absorb light in distinct patterns.	42
Figure 1.15 NRL-protein subfamily members exhibit conserved domain structures.	44
Figure 1.16 Light signalling pathways and plant immunity are connected through chloroplasts.	46
Figure 1.17 Model for chloroplast stromule function in pro-immunity signalling during ETI.	48
Figure 2.1 Comparison of the old and new flood assay protocols.	63
Figure 3.1 Bioinformatic analysis of the NCH1 gene locus, exon structure and protein crystal structure.	67
Figure 3.2 NCH1 transcript expression patterns in Arabidopsis organs and tissues during development.	68
Figure 3.3 Amino acid residue characteristic analysis of AtNCH1 protein.	70
Figure 3.4 Phylogenetic analysis of NCH1.	72
Figure 3.5 NCH1 is predicted to localize into the plasma membrane and/or cytoplasm, and interacts with at least 3 other proteins.	74
Figure 3.6 Hydropathy plots for the prediction of potential transmembrane domains in three Arabidopsis NRL subfamily member proteins, NCH1, RPT2, and NPH3.	75
Figure 3.7 Probabilities and placements for potential transmembrane domains in three Arabidopsis NRL subfamily proteins NCH1, RPT2, and NPH3, based on protein sequence data.	76
Figure 3.8 NCH1 localization is not influenced by BL.	78
Figure 3.9 The schematic structure of the 35S-SPYNE and 35S-SPYCE BiFC vectors used in this study.	79
Figure 3.10 Cloning strategy for the BiFC vectors used in this study.	80
Figure 3.11 Results of the Gibson assembly reaction can be visualised as an electrophoretic mobility shift in the DNA gel electrophoresis.	81
Figure 3.12 Plasmid maps for 35S-SPYCE nch1 D28N-K42Q and 35S-SPYNE nch1 D28N-K42Q.	82
Figure 3.13 Schematic overview of the BiFC method used in this study.	83
Figure 3.14 WT AtNCH1 forms dimers in planta.	85
Figure 3.15 Mutagenesis of salt bridge residues D28N and K42Q prevents AtNCH1 dimerization in Nicotiana benthamiana.	86
Figure 3.16 NCH1 protein contains multiple putative phosphorylation sites.	89
Figure 3.17 Expression of GFP-containing binary vectors in N. benthamiana.	90
Figure 3.18 Preliminary confocal micrograph data on the subcellular localisation of the AtNCH1 putative phospho-mutant NCH1 ^{S602A-S604A} suggests NCH1 localization is not determined by its phosphorylation status.	91
Figure 4.1 Models of NCH1 function in plant immunity.	96
Figure 4.2 Schematic overview for the time course experiment methodology.	98
Figure 4.3 Visual assessment of Pst DC3000 Infection in WT Arabidopsis.	99
Figure 4.4 Pst DC3000 population growth curve in WT Arabidopsis.	100
Figure 4.5 The effect of NCH1 genotype on Pst DC3000 infectivity in Arabidopsis.	104
Figure 4.6 Visual comparison of the old and the new flood assay methods.	107
Figure 4.7 Comparison of the old flood assay method and the new one developed after optimization.	108

Table 1.1 Examples of plant pathogenesis-related (PR) proteins, induced by the plant systemic acquired resistance.	26
Table 1.2 Overview of <i>Pst</i> DC3000 Effectors.	30
Table 1.3 NRL-subfamily protein requirements and assigned functions in various phototropin-mediated responses in <i>Arabidopsis</i>	43
Table 2.1 Confocal microscope protocol and parameters for time lapse imaging during <i>NCH1</i> localization experiment.	53
Table 2.2 BiFC co-infiltration combinations for studying <i>NCH1</i> protein dimerization in planta.	56
Table 2.3 Confocal microscope settings used for the imaging and Z-stack scans during the BiFC dimerization experiment.	57
Table 2.4 Confocal microscope settings used for the imaging and Z-stack scans during the <i>NCH1</i> phosphorylation experiment.	61

Acknowledgements

I would like to recognize the assistance of the funding bodies and the University of Glasgow MVLS and the James Hutton Institute for the material support of this study, and Dr. Eirini Kaiserli, Prof. John Christie, Dr. Eleanor Gilroy, for Prof. Paul Birch, and Dr. Stuart Sullivan for their contributions to this work.

Special thanks for Dr. Noriyuki Suetsugu, Mr. Franco Vegliani, Dr. Lingfeng Xia, and the Karnik Lab for their contributions to the materials and background knowledge concerning this project, and Dr. William Rooney for his invaluable help with the development of the flood assay methods. I would also like to thank my specialist academic mentor Ms. Jenny Charters for her unwavering guidance.

I am particularly grateful for Prof. Gareth Jenkins for his profound support and encouragement that inspired me and helped me throughout the writing process of this thesis, but most importantly made me believe in my abilities.

Lastly, I would like to extend my gratitude to Mr. Juuso Kallinkoski and Capt. Johannes Kallinkoski and their families for supporting me through the hard times and helping me have faith in the future. I am deeply indebted to my partner Mx Isobel Mckenna for her unparalleled emotional support, and for believing in me at times when I struggled to believe in myself. You are my star, and your love moves planets. I love you!

Abbreviations

AA: Amino acid	Ef-Tu: Elongation factor Tu	MeSA: Methyl salicylate
ABA: Abscisic acid	ETI: Effector-triggered immunity	$\frac{1}{2}$ MS: Half-strength Murashige-Skoog medium
bHLH: Basic helix-loop-helix transcription factor	ETS: Effector-triggered susceptibility	MTHF: Methenyl-tetrahydro-folate
BIC1: BLUE-LIGHT INHIBITOR OF CRYPTOCHROMES1	FAD: Flavin adenine dinucleotide	MTI: MAMP-triggered immunity
BiFC: Bimolecular fluorescence complementation	FKF1: FLAVIN BINDING-KELCH-F- BOX 1	NB-LRR/NCR: Nucleotide-binding leucine-rich repeat
BL: Blue light	flg22: Phytoimmunogenic 22-amino acid peptide of bacterial flagellin	NBS: Nucleotide binding site
BP: Base pair	FLS2: FLAGELLIN-SENSING 2	NCH1: NRL PROTEIN FOR CHLOROPLAST MOVEMENT 1, syn. NRL31 , AtSR1IP1: Syn. NCH1
BTB-POZ: Bric a brac tram track broad complex - pox virus zinc finger domain	FMN: Flavin mononucleotide	NELG: Nuclear encoded chloroplast gene
bZip: Basic zipper transcription factor	FT: FLOWERING LOCUS T	NPH3: NONPHOTOTROPIC HYPOCOTYL 3
CCT: CRYPTOCHROME C-TERMINUS	G3P: Glycerol-3-phosphate	NPR 1/3/4: NON-EXPRESSOR OF PATHOGENESIS-RELATED 1/3/4
CDPK: Calcium-dependent protein kinase	GFP: Green fluorescent protein	NPY: NAKED PINS IN YUCCA
CEL: conserved effector locus	HA: Haemagglutinin	NRL: NPH3/RPT2 -LIKE protein
CHUP1: CHLOROPLAST UNUSUAL POSITIONING	HR: Hypersensitive response	OD: Optical density, measured at 600 nm
CIB: CRYPTOCHROME-INTERACTING bHLH	HY5: ELONGATED HYPOCOTYL 5	PAMP: Pathogen-associated molecular pattern, synonymous with PAMP
Col-0: <i>Arabidopsis thaliana</i> Columbia ecotype	HYA: HY5-homolog	Pfr: Phytochrome far-red
COI1: CORONATINE-INSENSITIVE 1	ICD: INF1-triggered cell death	phot: Phototropin photoreceptor holoprotein
COP1: CONSTITUTIVE PHOTOMORPHOGENESIS 1	JA: Jasmonic acid	PHOT: Phototropin photoreceptor apoprotein
COR: CORONATINE	JA-Ile: Jasmonoyl-isoleucin conjugate	PHR: PHOTO LYASE-HOMOLOGY REGION
cp-actin: Chloroplast actin	LB: Luria-Bertani medium	Phy A-E: phytochrome A-E
cry1/2: Cryptochrome 1 / 2	LKP2: LOV-KELCH PROTEIN 2	PIF: PHYTOCHROME-INTERACTING FACTOR
CUL3: Cullin 3	LOV: light-oxygen-voltage-sensing domain	Pr: Phytochrome red
CWDGs: Cell wall-degrading enzymes	LRR: leucine-rich repeat	PRR: Pattern/PAMP-recognition receptor
DAMP: Damage-associated molecular pattern	LYM: Lys-M domain	PSII/I: Chloroplast photosystem II/I
DOT3: DEFECTIVE ORGANIZED TRIBUTARIES3	MAMP: Microbe-associated molecular pattern, synonymous with PAMP	
DPI: Day(s) post-inoculation	MAPK: mitogen-activated protein kinase	
	MCS: Multiple cloning site	
	mCit: mCitrine, a variant of Yellow fluorescent protein	

Pst: *Pseudomonas syringae*
pv. *tomato*

pv: Pathovar

R-gene/protein: Resistance
gene/protein

RLCK: receptor-like
cytoplasmic kinase

RLK: Receptor-like kinase

RLP: Receptor-like protein

ROS: Reactive oxygen
species

RPT2: ROOT
PHOTOTROPISM 2

SA: Salicylic acid

SAR: Systemic acquired
resistance

SCF: Skp1–Cullin–F-box E3
ubiquitin ligase family

SPA1: SUPPRESSOR OF
PHYA1

SPYNE/SPYCE: Split YFP
N-terminal/C-terminal
fragment expression

Syn.: synonymous

TBS: Tris-buffered saline

TBS-T: Tris-buffered saline +
Tween20

T3E: Type 3 Effector

T3SS: Type 3 Secretion
System

UV: ULTRAVIOLET LIGHT

UVR8: UV-RESISTANCE
LOCUS

WT: Wild type

YFP: Yellow fluorescent
protein

ztl: Zeitlupe

1. Introduction and Theoretical Background

This first chapter provides the general introduction and theoretical background to this thesis and the research conducted to the target protein NCH1, covering relevant topics and perspectives from the plant immunity to the microbiology of *Pseudomonas syringae*, and finally, to the plant photobiology. Consequently, this thesis presents the background knowledge in three parts: **1) Plant immunity**, **2) *Pseudomonas syringae* and *Pst* DC3000**, and **3) Plant photobiology**. The links between these three topics and their relevance to the investigation are highlighted and discussed in detail.

1.1. Plant Immunity

1.1.1. Plant Immunity Models

The models to explain plant immunity have changed over time. The earliest modern model that aimed to explain molecular plant interactions was the gene-for-gene hypothesis by Harold Henry Flor, which stated that plant immunity was a result of specific genetic combinations of the host and the pathogen (Flor, 1971): The plant-pathogen interaction was considered either “compatible” if the plant became successfully infected by the microbe virulence factors or elicitors (now called effectors), or “incompatible” if the plant successfully warded off the pathogen. Consequently, for each pathogen-derived avirulence gene, there was postulated to be a host resistance or R-gene to render that gene product dysfunctional, and therefore, unsuccessful in infection (Van Der Biezen and Jones, 1998). In Flor’s own words, “*Each gene in either member of a host-parasite system may be identified only by its counterpart in the other member of the system.*” (Flor, 1971). The model also suggested that the plant defence genes followed Mendelian segregation ratios: the resistance gene was dominant in the plant host, similarly to the dominant avirulence gene in the pathogen (Flor, 1971). While the model was purely based on genetic analysis and failed to give molecular or biochemical explanations for the disease phenotypes resulting from the compatible or incompatible interactions, or alternatively, address instances where a single pathogen elicitor would be universally detected among a range of plant species and families non-specifically (Cook et al., 2015), it formed the basic conceptual framework that was later updated with newer molecular models based on molecular pattern recognition and coevolution in a community ecology context. Importantly, the model gave rise to terms like “avirulence” and “compatibility” that evolved and changed over time from their original meaning of specific genetic combinations based on the Mendelian genetic analysis into modern molecular concepts. Therefore, these concepts are still used outside their original definition as a part of the modern molecular models to describe the nature or quality of the plant-pathogen interactions, and in the relevant plant and pathogen gene nomenclature. For instance, many pathogen effector genes are often named with a prefix “*Avr*” standing for “avirulence”, and similarly, the plant resistance genes encoding for the receptors for these effectors are still termed “R-genes”. Furthermore, the quality of the visible infection phenotypes in plant hosts can still be described as “compatible” or “incompatible” in modern contexts outside the original Mendelian genetic definition.

The advent of the pattern recognition model by Charles Janeway Jr. provided the biochemical framework for the earlier gene-for-gene hypothesis, as it described the existence of pathogen-associated molecular patterns (PAMPs) and pattern recognition receptors (PRRs) (Janeway, 1989). This model was therefore crucial in

explaining the compatible and incompatible interactions through protein-protein recognition events, especially the host ligand-binding receptors recognizing pathogen-derived ligands (Janeway, 1989). While the plant immune system is fundamentally different from the animal adaptive immunity in the way that it lacks antibody-mediated adaptive immunity and mobile immune cells (Han, 2019; Spoel and Dong, 2012), it is based on the same premises of pattern recognition as the animal immune system with toll-like receptors and interleukin receptors, where host receptors bind exogenous ligands in order to facilitate an immune response (Couto and Zipfel, 2016; Medzhitov, 2013; Van Der Biezen and Jones, 1998). Therefore, the model made significant advances in understanding the phytopathology behind the observed compatible and incompatible plant-pathogen interactions and provided molecular explanations based on protein biology for the principles of the earlier gene-for-gene hypothesis, in addition to also addressing the gene-for gene model's weaknesses.

The most widely used modern model in describing plant-pathogen interactions and pathogenesis is the zigzag model by Jones and Dangl (2006). The model develops the ideas of the gene-for-gene hypothesis and microbial ligand models further into concepts like PAMP-triggered immunity (PTI, now also known as MAMP-triggered immunity, MTI) and effector-triggered immunity (ETI), while relating the molecular model to the coevolution of both the pathogen and the plant host in an evolutionary molecular arms race for dominance. The concept of a virulence factor from the gene-for-gene hypothesis was also modernised into the concept of microbial effectors. This model also includes postulated mechanisms for the functions of R-proteins in plant defence: the guard hypothesis suggests that plant R-proteins "guard" key host proteins against effector modification and trigger the plant immune response if their guardee become modified. Therefore, avirulent plant pathogens fail to breach the plant immune system by targeting sub-cellular plant proteins guarded by R-proteins, where the modification or removal of the guardee indicates the presence of a pathogen, consequently activating the plant defence response and resulting in a host immune reaction (Jones and Dangl, 2006).

Some of the limitations of the zigzag model include its rigid division into different plant immunity and susceptibility phases and their respective defence-related molecules, while in reality, these would be taking place simultaneously in different parts of the plant, be mediated by overlapping pathways, and change depending on the pathogen (Boller and Felix, 2009; Cook et al., 2015). Another criticism relates to its qualitative approach in describing plant immunity, while in reality there would be less separation between the alternating mechanisms of plant immunity, and the relative susceptibility/immunity would vary depending on the pathogen in question (Cook et al., 2015; Corwin and Kliebenstein, 2017). This also relates to the more realistic assumption that overall plant immunity would follow a continuous distribution, as immunity would be quantitative and polygenic in nature, instead of following simple Mendelian inheritance and the disease status of a plant being a black-and-white division into total plant resistance and total plant susceptibility (Cook et al., 2015; Corwin and Kliebenstein, 2017). Other limitations include reduced accuracy in describing pathogen strategies other than bacterial biotrophy, and its limitations describing mutualist symbiont relationships, non-bacterial pathogens, and defence responses against herbivore insects (Cook et al., 2015).

Indeed, relationships between plants and microbes can take various forms, ranging from positive host effect of mutualistic symbioses where the host and microbe gain advantages from the association, to neutral, and negative antagonistic associations, where the microbe is pathogenic and aims to benefit itself at the expense of the plant host (Ben Khaled et al., 2015; Han, 2019). Therefore, the idea of plant immunity is arguably a more complex issue than just defence against aggressive infections of negative impact to the host. The current plant

immunity model has therefore been further updated from the zigzag model since its introduction in 2006 to include immune elicitors of both host and non-host origin, which has led to concepts like microbe-associated molecular patterns (MAMPs) and damage-associated molecular patterns (DAMPs) (Boller and Felix, 2009). These terms are now used alongside or are preferred to the original concept of PAMPs, as they broaden the scope of host molecular recognition beyond simple pathogen-derived molecules, which is important for portraying the self/non-self/modified self-pattern recognition event correctly. These also provide a broader platform for describing ecological relationships other than microbial antagonism and providing a framework through which mutualistic associations and microbe tolerance by the plant host could be explained (Cook et al., 2015).

Alternative models have also been proposed, including models such as the spatial immunity model (Burgh and Joosten, 2019) and the invasion model (Cook et al., 2015). The spatial immunity model by Burgh and Joosten (2019) divides the plant immune systems into intracellular and extracellular layers, depending on the site of pathogen detection. The invasion model by Cook et al. (2015) aims to address many flaws of the zigzag model, including mutualist associations, and to clarify the perspectives and terminology regarding the plant immune system. In the invasion model, the division into MTI and ETI has been replaced with a collective term “invasion pattern-triggered response” (IPTR), therefore also including ligands other than MAMPs and effectors of microbial origin, such as host-derived DAMPs, as potential immune elicitors (Cook et al., 2015), which is also in line with the MAMP-model described by Boller and Felix (2009).

This thesis describes and utilises the most widely accepted plant immunity models to date, which is the updated zigzag model, with chapter division according to the location of the recognition event. It also utilises canonical and standardised terminology from other models if applicable, such as concepts of compatibility, avirulence and R-genes. In accordance with this, it also prefers the use of the concepts of MAMPs and DAMPs to the more simplistic idea of PAMPs, and therefore replaces the older-styled terms like PTI with MTI, as done before e.g. by Boller and Felix (2009), and Cook et al. (2015). While some plant viral proteins and viral disease markers are recognised by the means of ETI (Couto and Zipfel, 2016), these are beyond the scope of this thesis and therefore omitted.

1.1.2. Extracellular Detection: Plant Basal Defences, MAMPs, and MTI

Plant tissues and the phyllosphere make convenient habitats for many microbes, as they provide a constant supply of nutrients and water to facilitate pathogen multiplication, while also providing favourable growth conditions and shelter from harsh environmental conditions such as drought or UV radiation. Therefore, plants are constantly under microbial attack from different pathogens, ranging from bacteria, oomycetes, and fungi to viruses, nematodes, and herbivorous insects (Lu and Yao, 2018; Panchal et al., 2016). To combat these threats, plants have evolved layers of physical and molecular mechanisms to protect them from microbial attempts to make use of these vast resources. The first line of host defence against plant pathogens are the physical barriers of waxy leaf cuticle and cutin, and plant primary and secondary cell walls composed of tough fibrous cellulose and lignin, which all physically resist pathogen entry to the plant tissues. Plants also have a base level of non-specific antimicrobials, phytoanticipins, present in their tissues (Sels et al., 2008). Collectively, these non-specific means halt microbial attempts in entering the plant surfaces directly, as

pathogens face hostile forces outside plant tissues such as solar UV radiation and dehydration, and may perish even in a matter of hours or days on the epiphytic surfaces if not able to make their way to the safety of plant tissues (Xin and He, 2013). Therefore, many plant pathogens enter the plant through wounds or anatomical openings such as leaf stomata or water pores in order to reach the deeper plant tissues and multiply there (Jones and Dangl, 2006). Some microbes, such as fungi and oomycete pathogens like *Phytophthora infestans*, can even attempt to directly penetrate the plant primary and secondary cell walls by utilising plant cell wall-degrading enzymes such as cellulases, hemicellulases, xylanases, and pectinases (Kubicek et al., 2014) or push directly through the plant epidermis using specialised pressure-generating structures, appressoria (Judelson and Blanco, 2005).

The invading pathogen will cause direct plant tissue damage and/or expose its own surface molecules and epitopes to the plant from the moment it comes into contact with the plant tissues. Therefore, the plant basal immunity against microbial pathogens is based on extracellular host receptor molecules detecting both microbial signature proteins and host-derived damage-associated molecules expected from pathogen invasion (Couto and Zipfel, 2016). Plant basal defence responses are primarily mediated by PRRs, which survey the plant apoplast for fragments of conserved pathogenic molecules, such as bacterial flagellin, peptidoglycan, and elongation factor Tu (EF-TU), fungal chitin, and oomycete INF1-elicitor proteins that act as danger signals (Birch et al., 2009; Boller and Felix, 2009; Chaparro-Garcia et al., 2015; Couto and Zipfel, 2016). These types of microbial signatures collectively comprise the MAMPs, formerly known as PAMPs, therefore indicate the presence of invading organisms in the plant tissues (Boller and Felix, 2009; Jones and Dangl, 2006). Consequently, basal plant immunity is regarded to be associated with the innate detection of conserved, slowly evolving pathogen epitopes, that are integral and structural to the pathogen and cannot, therefore, be discarded or extensively modified easily (Jones and Dangl, 2006).

While pathogens have their own molecular MAMP-signatures that plant PRRs can sense, there are also separate PRR-receptors that monitor the apoplast for the plant's own damage signature, immunogenic endogenous positive feedback molecules, or any other traces of physical tissue damage, that would result from pathogen attempts to penetrate the cell walls (Boller and Felix, 2009; Kimura et al., 2017; Yamaguchi et al., 2010). These kinds of self-derived signals constitute the DAMPs. While many of these receptors are unknown, known examples include PEPR1/2 (receptors for wounding-associated peptide Pep1) and WAK1 (cell wall fragment and oligogalacturonide receptor), among others (Boller and Felix, 2009; Brutus et al., 2010; Kimura et al., 2017). DAMPs detected by these receptors would result from cell walls being penetrated either chemically, by the means of cell wall-degrading enzymes (CWDGs) (Kubicek et al., 2014), or physically, such as by herbivore insect feeding (Erb et al., 2012). Therefore, the binding of the DAMP-ligands to their corresponding receptors notify the plant immune system of the abnormal presence of modified self-derived material, such as loose cellulose or glycans and cell wall fragments, cutin monomers, oligogalacturonides, and plant wound associated signalling molecules, such as phytochemicals (Boller and Felix, 2009; Burgh and Joosten, 2019; Han, 2019). This ensures, that the plant immune system can be induced by both pathogen- and host-derived material, and will result in the initiation of an immune reaction (Han, 2019). Importantly, there is also evidence for host processes that specifically modify MAMPs and DAMPs into short peptides that will be recognised by plant receptors (Wang et al., 2020).

The detection of MAMPs and DAMPs in the extracellular spaces by plant cell PRRs triggers a receptor kinase activation event and a consequent downstream signalling cascade from the plasma membrane to the nucleus, where transcription factors will initiate the transcription of plant defence genes. This type of plant immunity response is termed the microbe-triggered immunity, MTI (also known as PAMP-triggered immunity, PTI), which will eradicate the microbe before it gets a foothold. MTI is a non-specific and generic immune response, that can be elicited by different classes of pathogens from bacteria to fungi and oomycetes (Boller and Felix, 2009). Therefore, it is the first layer of inducible plant immune responses, as the plant has to regulate its energy and resource use and re-route these limited resources to its immunity only when necessary (Couto and Zipfel, 2016). A classic example of the function of PRRs and MAMP triggered immunity is the detection of bacterial flagellin, for example arising from *Pseudomonas syringae* infection, by the plant receptor FLS2, which is reviewed in detail in the next chapter. Other notable MAMP plant PRR pairs include fungal chitin and receptor CERK1, and bacterial EF-Tu peptide efr-18, and plant receptor EFR (Chaparro-Garcia et al., 2015; Wang et al., 2020).

1.1.3. Plant Pattern Recognition: MAMP receptors

The plant extracellular pattern recognition receptor (PRR) proteins fall into two major classes: **a)** receptor-like kinases, and **b)** receptor-like proteins (Wang et al., 2020), which are both introduced in **Figure 1.1**.

The first class, receptor-like kinases (RLKs), are single-pass transmembrane proteins that function in plant growth and development in addition to their role in immunity (Tang et al., 2017). As seen in **Figure 1.1** (white rectangular labels), they have a three-domain protein structure: **1)** N-terminal extracellular-sensing domain that constitutes of conserved motifs for MAMP detection, **2)** a central transmembrane domain, and **3)** a C-terminal cytoplasmic kinase that plays a role in attracting and activating the protein-interacting partners that will convert

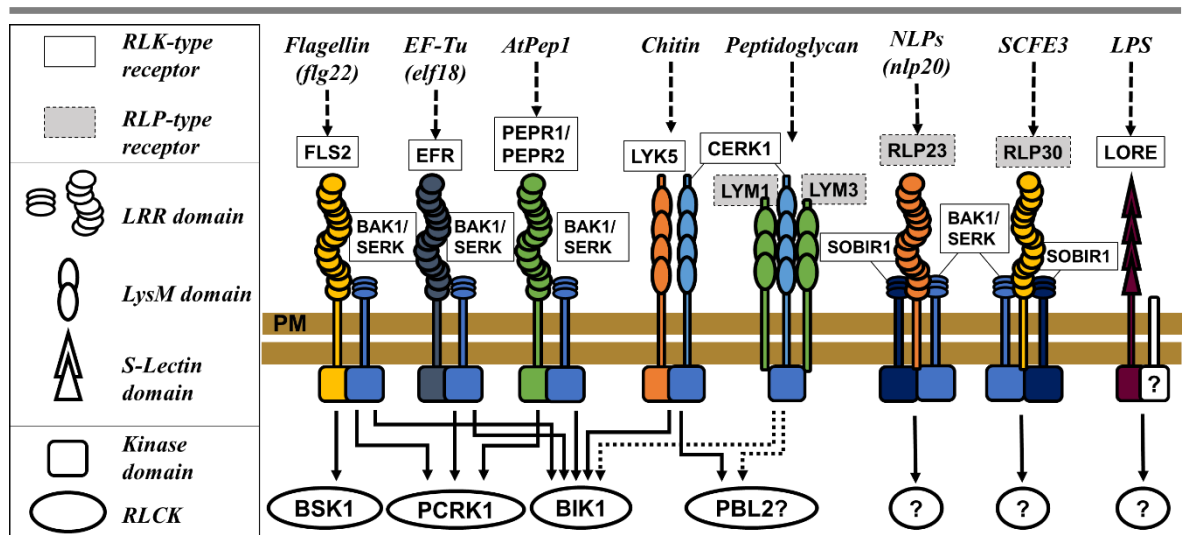


Figure 1.1. Examples of *Arabidopsis* PRR-proteins, their types, domain composition, and target MAMPs, associated co-receptors and their intracellular downstream signalling components.

The pathogen MAMPs are recognized by plant PRRs facing into the extracellular space (top), while their or their signalling partners' kinase/signalling domains are directed into the cytoplasm (bottom). Note the lack of intracellular kinase domain in RLP-type receptors (grey rectangular labels), such as RLP21/30 and LYM1/3, and the influence of interacting partners and the extracellular domains on the downstream signalling component/ RLCK (white oval labels) association for the fine-tuning of the immune response. **PM:** Plasma membrane. Figure modified after Couto and Zipfel (2016).

the extracellular signal into an intracellular signalling cascades (Ben Khaled et al., 2015). Furthermore, RLK-receptors are further divided into subfamilies according to their N-terminal domain motifs, such as leucine-rich repeat (LRR) domains for protein-based ligand detection, LysM domains (LYM) for carbohydrate-based epitopes like fungal chitin, lectin-type PRRs for bacterial structural components like the lipopolysaccharide (LPS) layer, and EGF-like PRRs for detecting plant DAMPs, of which the LRR proteins are the best understood (Couto and Zipfel, 2016).

The second class of plant receptors is the receptor-like proteins (RLPs), which have an N-terminal extracellular receptor domain, and a single-pass transmembrane domain (see grey rectangular labels in **Figure 1.1**). However, unlike RLKs, RLPs distinctively lack a cytoplasmic C-terminal kinase domain or other intracellular signalling motifs (Couto and Zipfel, 2016), and therefore, must associate with RLKs or other kinases, such as SOBIR, during activation by ligand-binding to mediate their defence signalling functions (Couto and Zipfel, 2016; Tang et al., 2017). Consequently, their signalling function is dependent on protein-protein interactions with other proteins that possess functional cytoplasmic signalling domains.

To relay the message of extracellular ligand-binding all the way to the nucleus, receptor-like cytoplasmic kinases RLCKs form the next step in the intracellular signalling cascade (see white oval labels in **Figure 1.1**). RLCKs function in the downstream signalling below the RLKs and RLPs to connect them with the cytoplasmic signalling cascades, and consequently, integrate different ligand-binding signals to fine-tune the MTI-response, as they interact with different receptors with differential affinities (Couto and Zipfel, 2016; Wang et al., 2020). A well-studied example of RLCKs is BIK1 (also seen in **Figure 1.1**) involved in flagellin-flg22 sensing. It is activated by phosphorylation during ligand-binding, and becomes released into the cytoplasm to activate downstream cascades as a functional kinase (Tang et al., 2017).

A classic example of a PRR-protein signalling event is the recognition of the 22-amino acid fragment fls22 epitope by the plant RLK-PRR FLAGELLIN SENSITIVE-2 (FLS2), which also demonstrates all these layers of interconnected signalling networks (Boller and Felix, 2009; Jones and Dangl, 2006; Wang et al., 2020). Bacterial motility organ protein flagellin is such an essential integral and structural pathogen signature, that its recognition is widely conserved among plants (Ben Khaled et al., 2015). **Figure 1.2** presents the hierarchy of the cellular events during MAMP-PRR binding, such as FLS2 ligand-binding, and the negative regulatory loops involved in the attenuation of the defence signalling for homeostasis. The binding of the bacterial flagellin MAMP flg22 to the receptor FLS2 (presented on the blue background in **Figure 1.2**) initiates an activating conformational change in the receptor, which triggers the heterodimeric FLS2-BAK1 (BAK1, aka. SERK3) complex formation at the plasma membrane. After this, the cytoplasmic RCLK BIK1 joins the complex and becomes phosphorylated by the bound BAK1 (grey background in **Figure 1.2**). In turn, BIK1 phosphorylates both FLS2 and BAK1, and as a RCLK, BIK1 is released into the cytoplasm to phosphorylate or otherwise promote the activation of further downstream signalling targets, such as calcium-dependent protein kinases (CDPKs) and the mitogen-activated protein kinase (MAPK) cascade (green background in **Figure 1.2**). In addition to flg22 signalling, BIK1 RCLK is shared by a couple of different plant MAMP and DAMP PRRs and therefore is an early MTI signal integrator (Couto and Zipfel, 2016). The activated FLS2 and BAK1 receptors are internalised and recycled through vesicle trafficking and the late endocytic pathway, which suggests a potential feedback mechanism to control the duration of the receptor activation (Bozkurt et al., 2015; Couto and Zipfel, 2016). MTI by fls22 signalling is also characterised by the initial signature ROS

burst, which has both direct antimicrobial effects and signalling functions: This is initiated by activated BIK1 phosphorylating a membrane-bound NADPH oxidase RBOHD, therefore activating it, and changing the redox state of the cytoplasm in the course of the ROS burst (Couto and Zipfel, 2016). BIK1 also stimulates calcium channel activation, and Ca^{2+} ions flow into the cell, triggering the activation of CDPKs, which further initiates a calcium-dependent activation of the cytoplasmic signalling components (Wang et al., 2020). As free cytoplasmic BIK1 is an active kinase, cytoplasmic signalling cascades are mediated by two parallel mitogen-activated protein kinase (MAPK) cascades, which will eventually activate WRKY transcription factors in the nucleus (red background in **Figure 1.2**) in order to stimulate the transcription of plant defence genes and the consequent production of antimicrobial agents, plant hormones and other signalling molecules (yellow background in **Figure 1.2**) (Couto and Zipfel, 2016).

The resulting MTI response aims to halt the microbial invasion before it gets a foothold of the plant, but with enough sensitivity and scalability in order to avoid excess, uncontrollable immune reactions and autoimmunity (Couto and Zipfel, 2016). Therefore, MTI is considered to be the milder version of the plant immune reaction, and does not involve cell death nor hypersensitive response, while still resulting in increased plant immunity and systemic immunity signalling (Jones and Dangl, 2006). The ROS burst triggers signalling for the closing of stomata, which will form an anatomical barrier for pathogen entry (Couto and Zipfel, 2016). In order to provide further mechanical barriers, the plant reinforces its cell walls directly at the location of the initial infection to hinder pathogen entry to the cells (Xin and He, 2013). Cell wall reinforcement is achieved through increased cell wall synthesis, component crosslinking and callose deposition (Sels et al., 2008; Wang et al., 2020). Antimicrobial defence genes stimulated by the signalling cascades promote the biosynthesis of phytoalexins, such as camalexin (Corwin and Kliebenstein, 2017). Furthermore, systemic changes are achieved through plant hormone signalling (see yellow background in **Figure 1.2**), especially salicylic acid (SA), and involve the inhibition of plant growth hormones such as auxin and brassinosteroids, which are antagonistic with systemic SA signalling (Couto and Zipfel, 2016). Plant hormone signalling by SA is further detailed in section 1.1.5.

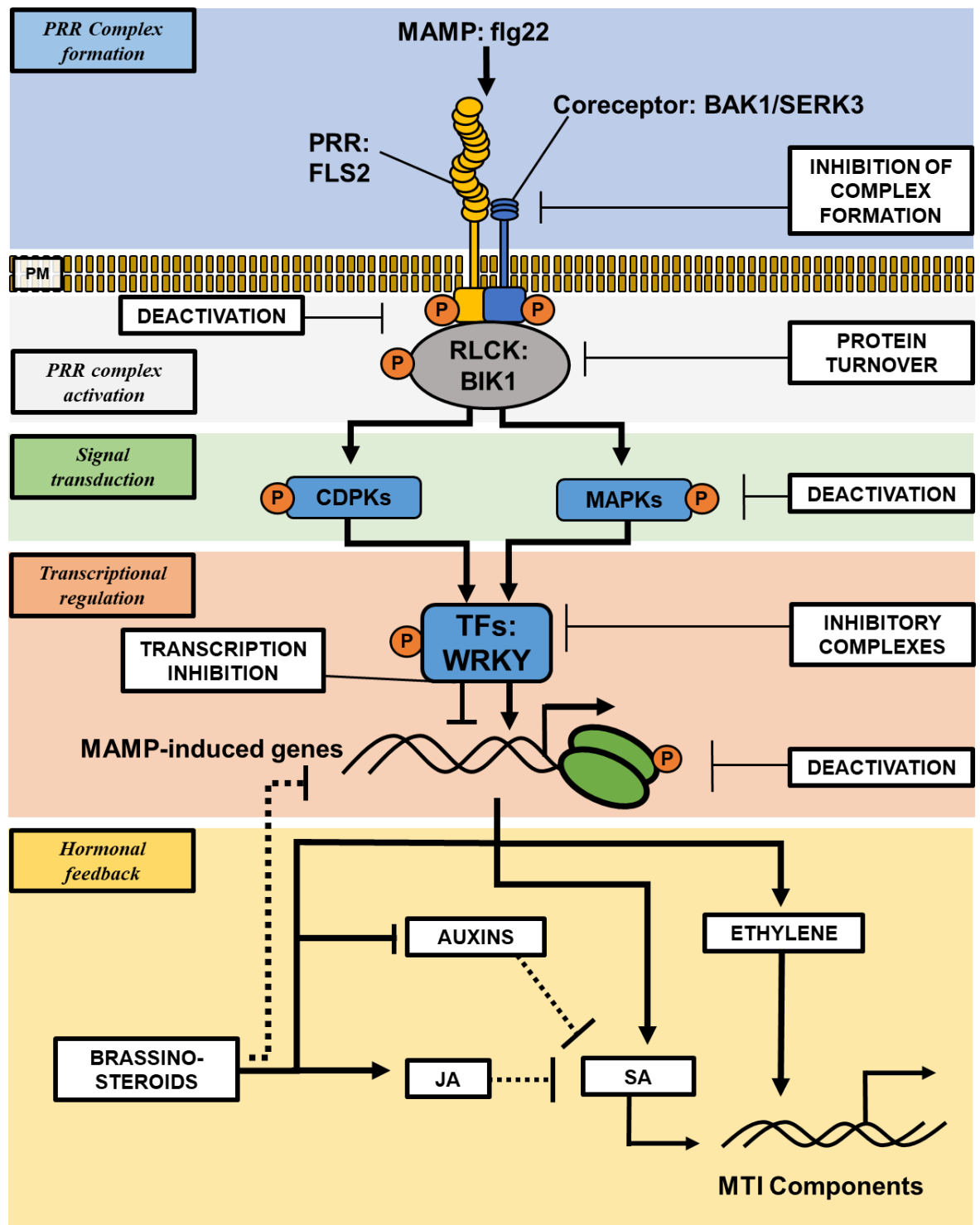


Figure 1.2 *Arabidopsis* MTI signalling pathways during flg22 MAMP recognition, and their negative feedback regulation.

Overview of the plant MTI inducing signalling pathways during bacterial flagellin MAMP flg22 detection, and the related negative feedback loops to tightly control the duration and scale of the immune response. This includes the initial MAMP binding by the PRR FLS2 at the plasma membrane (**blue background**), and the consequent heterotrimeric PRR signalling complex (FLS2-BAK1-BIK1) formation and activation through phosphorylation (**grey background**), the activation of cytoplasmic signalling transduction cascades (**green background**) by BIK1-dependent phosphorylation and/or activation of calcium-dependent protein kinases (CDPKs) and the MAPK-cascade, transcriptional regulation (**red background**) in the nucleus by the modification of transcription factors (e.g WRKYs), and the systemic plant-wide hormonal signals (**yellow background**). **PRR**: Pattern recognition receptor; **MAMP**: Microbe-associated molecular pattern; **RLCK**: Receptor-like cytoplasmic kinase, **TF**: Transcription factor, **P**: Phosphate; **JA**: Jasmonic acid, **SA**: Salicylic acid. Figure modified after Couto and Zipfel (2016).

1.1.4. Intracellular Detection: Compatible and Incompatible interactions, ETS and ETI

As MTI is detrimental for pathogen survival and viability within the plant tissues, pathogens participate in biochemical warfare to attenuate and reverse the plant immunity signalling cascades before they result in a full-blown plant immune response (Jones and Dangl, 2006), as shown in **Figure 1.3**. Effectors are defined as microbe-derived molecules that aim to influence the plant immune system, either for mutualistic symbiotic or antagonistic association (Cook et al., 2015), and they are characteristically highly polymorphic between different pathogens and their pathovars (Barrett and Heil, 2012). Therefore, they are a specialised functional adaptation that facilitates the pathogen entry and spread into the surrounding tissues and population growth within the plant phyllosphere (Cook et al., 2015; Upson et al., 2018). There are two potential outcomes that can result from the pathogen utilising effectors: **a**) the pathogen may either succeed in its attack against the plant, resulting in a compatible interaction and effector-triggered susceptibility (ETS), or **b**) it may be detected interfering with the plant immunity, resulting in avirulence and incompatibility by plant effector-triggered immunity (ETI). When a pathogen manages to overcome plant immunity through the use of intracellular effectors, the interaction between the pathogen and the host has is referred to as a compatible interaction, and the pathogen will be successful in infecting the plant, consequently resulting in ETS (Flor, 1971; Jones and Dangl, 2006).

Plant proteins crucial for the MAMP-triggered immunity or other parts of the plant immune response and immune-related signalling are prime targets for pathogen influence in order to facilitate pathogen presence and multiplication while undetected by the plant immune system, and therefore, the same protein targets are shared by multiple pathogens and their effectors (Win et al., 2012). Consequently, pathogen effectors aim to modify, inhibit the activity or synthesis of, target these components for degradation, or otherwise render them dysfunctional (Boller and Felix, 2009; Kamoun, 2006). Indeed, many pathogen effectors are protein-modifying

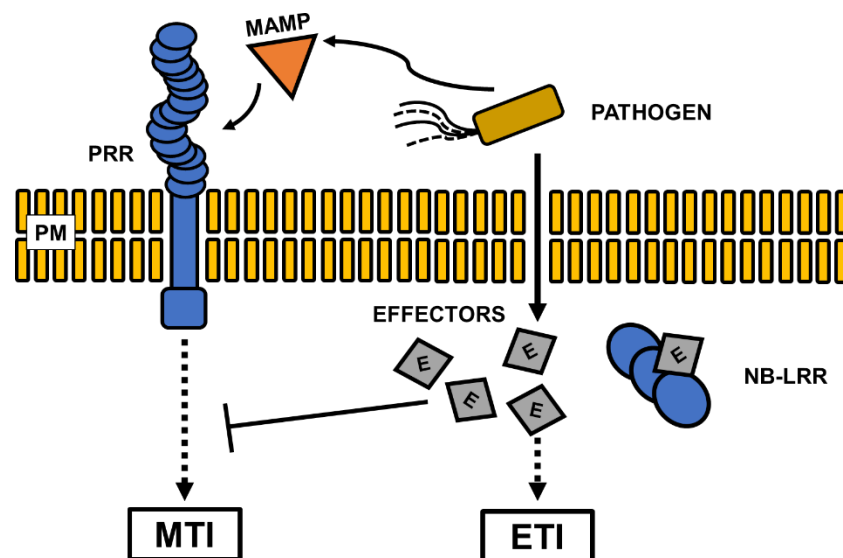


Figure 1.3 Basic dynamics of plant-pathogen interactions and the relationship between MTI and ETI responses.

While plants detect pathogen presence from the free extracellular pathogen signature MAMPs with their PRR-receptors, pathogens may interfere with this recognition process by utilising intracellular effectors that will target the plant MTI-pathway. However, the plant may detect the presence of microbial effectors or the chemical modifications made by these effectors with their intracellular R-proteins, such as NB-LRR receptors, triggering ETI and a stronger immune response than the more generic MTI response. Figure modified after Li and Zhang (2016)

enzymes such as kinases, dephosphorylases, and ubiquitinases. Other types of effectors include toxins, and plant growth regulators, plant hormones, or phytohormone mimics. For example, the bacterium *Pseudomonas syringae* utilises all these means as its invasion strategy and pathogenesis (Xin and He, 2013).

Pathogen effectors are administered into the plant tissues by a variety of methods. Gram-negative bacteria, such as the hemibiotrophic *Pseudomonas* species, utilise a specialised anatomical apparatus called the Type 3 secretion system (T3SS) (Lindeberg, 2012), which typically secretes up to 30-40 different effectors at the time. While this is quite a meagre number in comparison to fungi and oomycetes, which, can produce even 300-400 different effector proteins at a given instance and utilise specialised anatomical structures called haustoria that form close intracellular associations with their target cells, even the lower number of bacterial effectors is enough to manipulate host immunity. Consequently, almost any stage of the MAMP-signalling cascade can be interfered with by *Pseudomonas syringae* pv. *tomato* DC3000 effectors -- either by extracellular or intracellular means (Xin and He, 2013). For *Pseudomonas syringae* pv. *tomato* DC3000, these will be detailed in section 1.2.2. The number and type of effectors a pathogen has also depends on the ecological niche of the pathogen. Some plant pathogens are ecological generalists that can infect various plants and plant families as their life strategy, consequently relying on high effector numbers or structurally more adaptable general effectors of which targets are shared by many plant families with moderate similarity. For example, the oomycete *Phytophthora cinnamoni*'s host range covers over 1000 plants from numerous unrelated taxa (Barrett and Heil, 2012). These general effectors, therefore, should interact with their targets in a less specific manner than specialist pathogen effectors (Barrett and Heil, 2012). Interestingly, a human and animal pathogen secretome study by Blanco et al. (2018) indeed found generalist bacteria to utilise secreted proteins with flexible protein conformations and prevalent intrinsically disorganized regions, therefore able to accommodate a larger number of targets, providing a molecular explanation to the greater adaptability of generalist pathogens' secreted proteins to various hosts. In contrast to ecological generalists, specialist pathogens with their diversified strains and pathovars have evolved into occupying specialist niches, infecting very limited host ranges such as plants of a particular species or family. This is exemplified by the numerous *Pseudomonas syringae* pathovars that differ from each other only in their host preferences (Xin et al., 2018). While the compatibility and non-compatibility of the interactions are more black-and-white than generalists', they can readily infect their host plants with their vast but specific effectors (Corwin and Kliebenstein, 2017). Therefore, plant pathogens -- whether a generalist or a specialist -- with a compatible set of effectors to their hosts' intracellular immune receptors (gene-for-gene recognition) will stumble in their attempts and become detected by plant defences, resulting in avirulence and a successful plant immune reaction by ETI (Corwin and Kliebenstein, 2017; Jones and Dangl, 2006).

To sense the presence of pathogenic effectors in the intracellular landscapes and to trigger the ETI, plants have evolved intricate intracellular receptor systems called resistance (R) proteins that can sense the presence of pathogen effectors either directly or indirectly by monitoring key plant immunity components for modifications. The cytoplasmic R-proteins often belong to the group of intracellular nucleotide-binding site (NBS) proteins, that have characteristic leucine-rich repeat (LRR) domains for ligand-binding similarly to extracellular PRRs. These form the group of NB-LRR (also known as NLR) receptors and are currently the most widely understood class of NBS proteins (Wang et al., 2020). These plant R-proteins may employ various molecular strategies for detecting pathogen effectors, which are detailed in **Figure 1.4**. These fall broadly into categories of **1**) direct recognition of the effector, **2**) through guard proteins (guard hypothesis, (Jones and

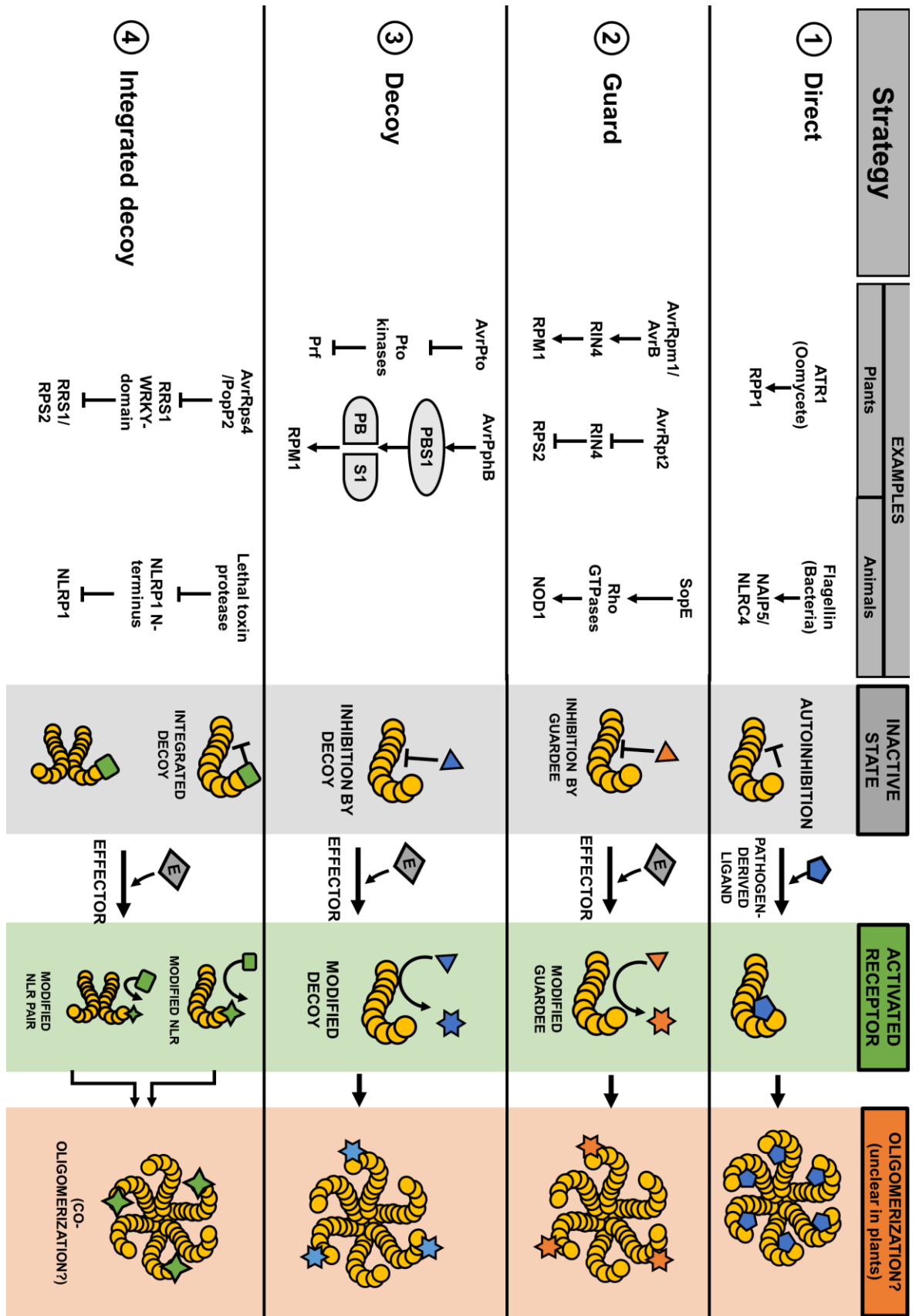


Figure 1.4 Molecular strategies for plant R-proteins and examples of their function.

Plant R-protein strategies in the recognition of intracellular pathogen effectors, example plant R-proteins and their target effectors, and possible examples of corresponding animal immune proteins with similar functions. **1) Direct recognition:** the cytoplasmic NB-LRR binds the pathogen effector ligand directly. **2) Guard:** the NB-LRR guards a molecular target and triggers a defence response if the target is modified by the pathogen effector(s). **3) Decoy:** NB-LRR guards a molecular facsimile of an effector target and triggers an immune response if the decoy becomes modified by pathogen effector action. **4) Integrated decoy:** similar in function to nr. 3, but the decoy is an integral part of the R-protein. Figure after Jones et al. (2016).

Dangl, 2006)), or 3-4) through molecular decoys (decoy hypothesis, van der Hoorn and Kamoun (2008)). According to the guard hypothesis, R-proteins guard the target protein for post-translational modifications (Jones and Dangl, 2006). A classic example of this is *Arabidopsis* protein RIN4 guarded by the R-protein RPM1: RIN4 is targeted by *Pseudomonas syringae* effectors AvrRp1 and AvrB for ribosylation and phosphorylation, but RPM1 will detect these modifications, therefore triggering ETI (Redditt et al., 2019). R-proteins may also take the shape of intracellular decoy proteins that are structurally reminiscent of the signalling cascade components, which consequently intercept generalist avirulent effectors and trigger the immune response, leading to the ETI and hypersensitive response (van der Hoorn and Kamoun, 2008). These decoy proteins are thought to arise from genetic duplication events, consequent functional redundancy between the proteins and the coevolution between plant ETI and ETS: As plant immune proteins are overcome by more sophisticated pathogen effectors, new ones evolve and the old ones may undergo a separate evolutionary path into decoys (van der Hoorn and Kamoun, 2008). Therefore, there may be R-proteins monitoring for modifications in the decoy bait, or the decoys becoming integrated into parts of the R-protein structure itself (Jones et al., 2016).

As millennia have passed, the co-evolution of the plant immune system and the pathogen has given plants the intracellular means to monitor against the pathogen's attempts to interfere with the MTI, which puts an evolutionary selection pressure on the pathogen to develop novel effectors to remain undetected by the plant immunity. This is often referred to as the red queen hypothesis: Organisms need to constantly evolve in order to maintain the status quo. This is exemplified by the zigzag model of plant-pathogen interactions (Jones and Dangl, 2006), illustrated in **Figure 1.5**. After the pathogens evolve new effectors that result in plant susceptibility by ETS, the plant needs to evolve new R-genes or other resistance molecules to keep up the immunity and initiate successful ETI before succumbing to infection and perishing on a population scale (Jones and Dangl, 2006). The evolutionary zigzag between the host immunity and susceptibility or periods of plant

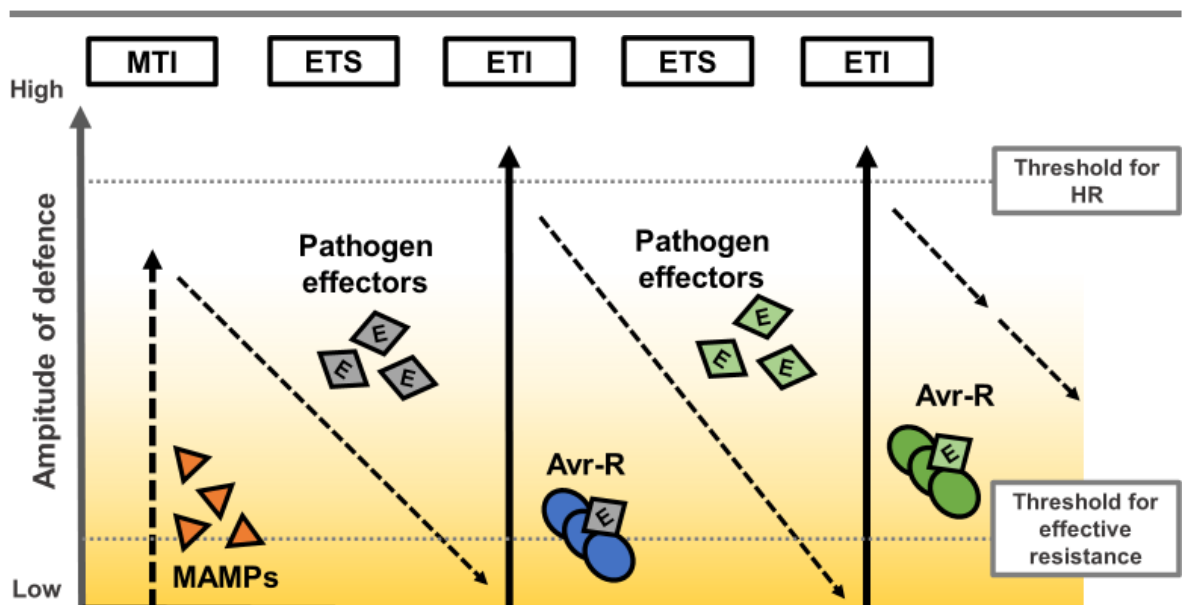


Figure 1.5 The zig-zag model of plant immunity and plant-pathogen interactions.

The model shows the relative strength of the plant immune response (Y-axis) depending on the type and location of MAMP-perception (X-axis): early extracellular detection of the pathogen will give rise to a milder MTI-response, whereas intracellular effectors elicit a strong and specific ETI-response, involving the hypersensitive response and consequent controlled cell death. Over time, red queen dynamics develop, and the plants and pathogens will undergo co-evolution, resulting in alternating periods of host susceptibility by ETS and immunity by ETI. Figure after Jones and Dangl (2006)

ETI and ETS, is the basis of the red queen dynamics between the plant and the pathogen, resulting in a constant molecular arms race between the pathogen the plant host (Han, 2019; Jones and Dangl, 2006). However, it is important to note that the red queen dynamics are more pronounced with specialist pathogens with tight coevolutionary relationships with their host plants and the contrary may be true in the case of generalist pathogens: instead of tightly coupled coevolution with a single host species and/or plant family, the evolutionary associations would appear more like a network, involving various host species in various extents and at different times (Barrett and Heil, 2012).

As a result of the red queen dynamics, different facets of plant immunity face differential selection pressures by the pathogen effector evolution (Jones and Dangl, 2006). While structural pathogen MAMP molecules such as flagellin and chitin cannot be easily or quickly replaced by the pathogen to make them unrecognisable by the plant PRRs, the evolution of individual effectors is more rapid, as these will be employed to hide the traces of structural molecules that cannot be replaced. These effectors therefore function to interfere with the plant immune system directly, or target pathogen MAMPs themselves for modification in order to avoid detection by the plant extracellular receptors (Cook et al., 2015). Avirulent effectors that the plant hosts recognise more widely will be evolutionarily disfavoured at the expense of pathogen molecules that still facilitate ETS. Therefore, especially in the case of specialist pathogens infecting only a narrow host range, effector evolution may be rapid (Cook et al., 2015; Upson et al., 2018) and give rise to vastly functionally redundant effectors (Xin and He, 2013).

1.1.5. Mechanisms of the Plant Immune Responses and Systemic Acquired Resistance

The original zigzag model (seen in **Figure 1.5**) hypothesised the plant immune reactions, MTI and ETI, to give rise to differential levels of immunity (Jones and Dangl, 2006). However, many processes and molecules perform parallel or overlapping functions during the immune reaction, and therefore, may cross the boundaries of strict MTI-ETI dichotomy (Cook et al., 2015). Therefore, it is important to note, that different plant defence processes are often shared as a part of the same phenomenon and are not necessarily mutually exclusive.

In contrast to the generic early intervention response of the MTI, ETI will culminate in strong specialised defence responses both locally and in distal sites of the plant. The local defence response in the infected tissue involves the programmed cell death of the affected cell(s), known as the hypersensitive response (HR). This pathogen-triggered controlled apoptosis effectively functions to contain and limit the spread of the infection to the surrounding tissues by barricading the pathogen to the affected area and starving the pathogen of nutrients and water, while simultaneously activating other pathogenesis-related (PR) genes, the production of phytoalexins and plant cell wall components (Xin and He, 2013). MTI and ETI also give rise to systemic immunity within plants. Systemic acquired resistance (SAR) primes the distal sites for the secondary pathogen infection, providing the plants with a systemic resistance that can last up to months and also provide transgenerational resistance against pathogens (Kachroo and Robin, 2013; Liu et al., 2011). This mechanism of systemic pathogen resistance and tissue priming is dependent on SA, which is synthesised by isochorismate synthase in the chloroplasts and/or phenylamine ammonia-lyase pathway in the cytosol (Lu and Yao, 2018; Wildermuth et al., 2001). Importantly, systemic resistance can also be induced artificially in a laboratory setting

with chemicals and molecules structurally reminiscent of plant systemic resistance molecules, such as SA (Sels et al., 2008).

The pathways of SAR initiation and mobile immune signal mobilisation are presented in **Figure 1.6**. The initial SAR signal originates from the local tissues facing the pathogen and starts with the production of SAR inducer compounds, that include **a**) azelaic acid and with its derivative glycerol-3-phosphate (G3P), **b**) dihydroabietinal amine (DA), and **c**) SA and its volatile derivative methyl salicylate (MeSA), which also functions as a mobile signal and moves with the phloem sap (Kachroo and Robin, 2013; Lu and Yao, 2018). Most azelaic acid acts locally, and is converted into G3P, which in turn is modified into a currently unknown mobile signalling component that moves in the plant tissues associated with DIR1 protein (Kachroo and Kachroo, 2020). This is a rapid reaction, which starts within 4-6 hours of initial pathogen contact (Kachroo and Robin, 2013). In addition to this, key defence genes that encode for components of various defence-related and/or antimicrobial functions, such as PR genes, are upregulated during the systemic response. The currently known plant PR-proteins have structurally and functionally diverse products, ranging from direct antimicrobials, such as antifungals, chitinases, glucanases, to pathogen membrane-permeabilizing agents and components that regulate ROS, and further to proteins that aid with the plant cell wall rigidification process and physical defences (Joshi et al., 2021; van Loon et al., 2006; Sels et al., 2008). The known plant PR proteins and their functions are summarised in **Table 1.1**. PR gene expression is dependent on the SAR signalling, as in mutant *Arabidopsis* plants lacking the SA receptor genes *NPR1* (*NONEXPRESSOR OF PATHOGENESIS-RELATED GENES 1*), *NPR3* and *NPR4*, these genes are not up-regulated (Backer et al., 2019).

Jasmonic acid (JA) is another key plant defence hormone, which is important for defence responses against herbivorous insects (together with abscisic acid, ABA) and necrotrophic bacteria (together with ethylene), and has an antagonistic effect on the plant SA pathways (Couto and Zipfel, 2016; Lu and Yao, 2018): JA and SA controlled pathways are therefore mutually exclusive and will affect one another negatively. Intriguingly, biotrophic and hemibiotrophic pathogens use this feature to their advantage and alter the plant systemic signalling with their own secreted plant hormone mimics in order to manipulate the course of the immune reaction, and to shift the equilibrium of the immune response away from SA-mediated SAR to a less harmful JA response for the bacterium (Xin and He, 2013): *Pst* DC3000 for example, is known to use a phytotoxin functionally similar to the functional plant hormone/ amino acid conjugate jasmonic acid- isoleucine (JA-Ile) called coronatine to achieve this, also triggering other aberrant or mistimed plant responses favourable for the pathogen invasion, such as stomatal opening (Geng et al., 2012; Lu and Yao, 2018). Therefore, plant defence networks, their control hubs and overall dynamics provide an important target for pathogen influence, as will be discussed more in detail in the next chapter.

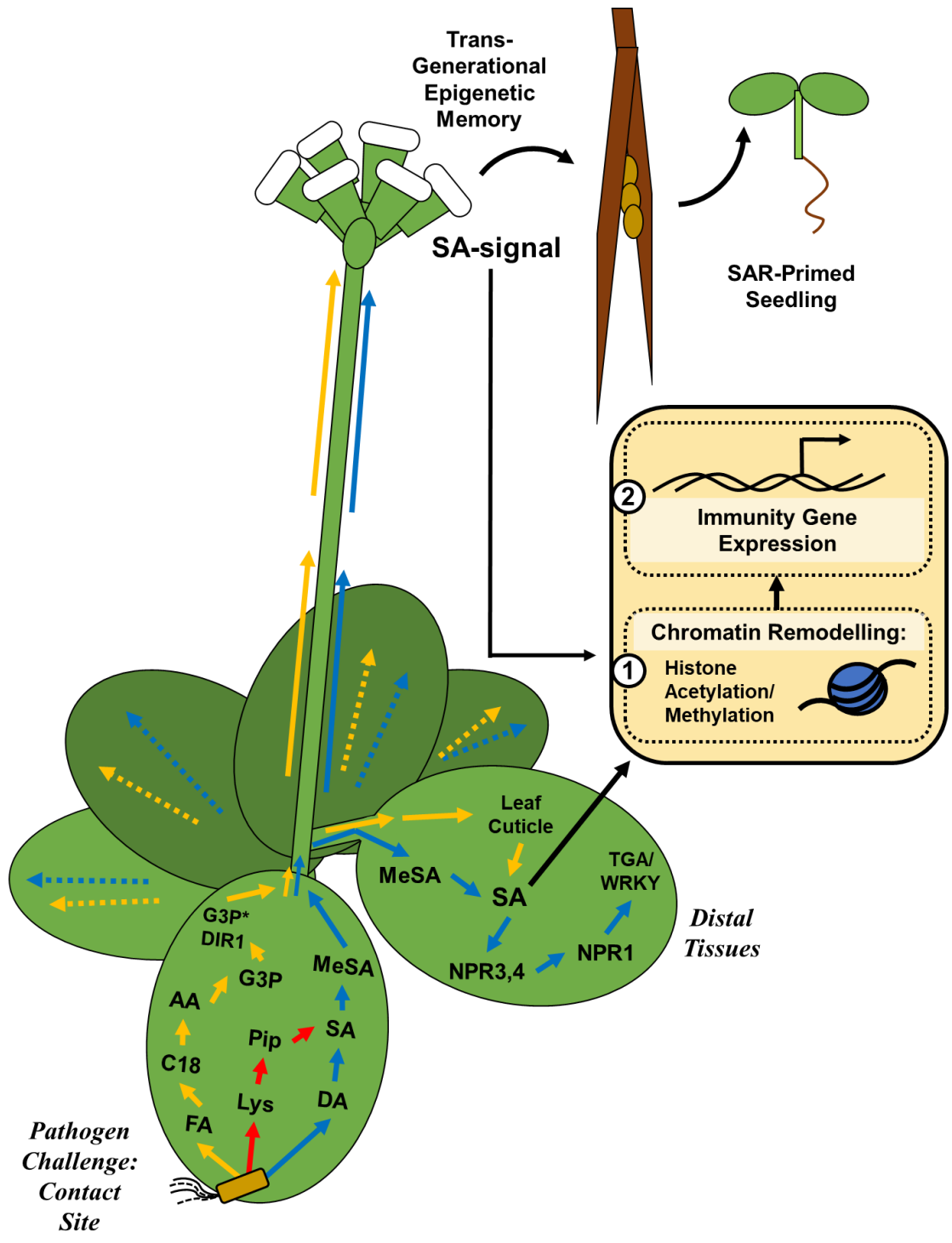


Figure 1.6 Interconnected mechanisms of plant systemic acquired resistance.

Orange: Pathogen contact initiates the intracellular release of 18-carbon fatty acids (C18 FA) from the plasma membrane, which stimulates azelaic acid (AA, abbreviation in this figure only) production, and its further processing into G3P. G3P is further processed into a signalling molecule (currently unknown, termed G3P* in the figure) that will move systemically together with the protein DIR1. In the distal tissues, successful SAR requires an intact leaf cuticle.

Red: Pathogen contact stimulates lysine conversion into pipercolic acid (Pip), priming the tissues for SA accumulation.

Blue: Simultaneously to lysine conversion, dihydroabietal amine (DA) accumulates. While DA and AA may move to some extent from the local tissues, DA and PIP initiate the local synthesis and accumulation of SA, whose volatile derivative, methyl-salicylate (MeSA) is thought to be the mobile systemic signal. MeSA may be converted back into SA in distal sites, which is sensed by SA-receptors NPR3 and NPR4, which prime the distal sites against infection by stimulating TGA and WRKY-transcription factors.

The systemic SA-signal is thought to remodel the chromatin, which can also bring about transgenerational epigenetic memory of the infection for the progeny.

Figure after Kachroo and Robin (2013).

Table 1.1 Examples of plant pathogenesis-related (PR) proteins, induced by the plant systemic acquired resistance.

Table compiled from Sels et al. (2008) (a), van Loon et al. (2006) (b), and Joshi et al. (2021) (c). Items on grey background are putative PR-proteins.

Family	Type member ^{a,c}	Gene symbols ^b	Typical size (kDa)	Properties ^{a,b,c}	Proposed target(s)
PR-1	<i>Nicotiana tabacum</i> PR-1a	<i>ypr1</i>	15	Antifungal ^{a,c}	Unknown ^a
PR-2	<i>Nicotiana tabacum</i> PR-2	<i>ypr2</i> , [<i>gns2</i> (<i>'glb'</i>)]	30	β -1,3-Glucanase ^{a,c}	Fungal β -1,3-Glucan ^{a,c}
PR-3	<i>Nicotiana tabacum</i> P, Q	<i>ypr3</i> , <i>chia</i>	25–30	Chitinase (class I,II,IV,V,VI,VI) ^{a,c}	Microbial chitin ^a
PR-4	<i>Nicotiana tabacum</i> R	<i>ypr4</i> , <i>chid</i>	15–20	Chitinase (class I,II) ^{a,c}	Microbial chitin ^a
PR-5	<i>Nicotiana tabacum</i> S	<i>ypr5</i>	25	Thaumatococin-like ^{a,c}	Microbial membrane ^a
PR-6	<i>Solanum lycopersicum</i> Inhibitor I	<i>ypr6</i> , <i>pis</i> (<i>'pin'</i>)	8	Proteinase-inhibitor ^{a,c}	Unknown* ^a
PR-7	<i>Solanum lycopersicum</i> P ₆₉	<i>ypr7</i>	75	Endoprotease ^{a,c}	Unknown* ^a Microbial cell walls? ^b
PR-8	<i>Cucumis sativus</i> chitinase	<i>ypr8</i> , <i>chib</i>	28	Chitinase (class III) ^{a,c} Lysozyme ^b	Chitin ^a
PR-9	<i>Nicotiana tabacum</i> lignin-forming peroxidase	<i>ypr9</i> , <i>prx</i>	35	Peroxidase ^{a,c}	Unknown* ^a Plant cell wall lignification catalysis? ^b
PR-10	<i>Petroselinum crispum</i> PR1	<i>ypr10</i>	17	Ribonuclease-like ^{a,c}	Unknown* ^a
PR-11	<i>Nicotiana tabacum</i> class V chitinase	<i>ypr11</i> , <i>chic</i>	40	Chitinase (class I) ^{a,c}	Microbial chitin ^a
PR-12	<i>Raphanus raphanistrum</i> Rs-AFP3	<i>ypr12</i>	5	Defensin ^{a,c}	Microbial membrane ^a
PR-13	<i>Arabidopsis thaliana</i> THI2.1	<i>ypr13</i> , <i>thi</i>	5	Thionin ^{a,c} Membrane permeabilization ^c	Microbial membrane ^a
PR-14	<i>Hordeum vulgare</i> LTP4	<i>ypr14</i> , <i>ltp</i>	9	Lipid-transfer protein ^{a,c} Membrane permeabilization, lipid catabolism ^c	Microbial membrane ^a
PR-15	<i>Hordeum vulgare</i> OxOa (germin)	<i>ypr15</i>	20	Oxalate oxidase ^{a,c} Superoxide dismutase activity ^b	Unknown* ^a
PR-16	<i>Hordeum vulgare</i> OxOLP	<i>ypr16</i>	20	Oxalate oxidase-like ^{a,c} Superoxide dismutase activity ^b	Unknown* ^a
PR-17	<i>Nicotiana tabacum</i> PRp27	<i>ypr17</i>	27	Antiviral, antifungal ^c Proteinase-like activity ^c	Unknown* ^a Pathogen cell walls? ^c Plant signalling? ^c
PR-18	<i>Helianthus annuus</i> HaCHOX <i>Lactuca sativa</i> LsCHOX	-	60 ^c	Carbohydrate oxidase ^{b,c}	Fungal β -1,3-Glucan ^c
PR-19	<i>Pinus sylvestris</i> SpAMP <i>Macadamia integrifolia</i> MiAMP1	-	8 ^c	Antifungal, Glucan-binding ^c	Fungal β -1,3-Glucan ^c

*: No *in vitro* antimicrobial activity reported ^a

1.2. *Pseudomonas syringae* and *Pst* DC3000

1.2.1. *Pseudomonas syringae* and *Ps* pathovars

Pseudomonas syringae (*Ps*) is a rod-shaped gram-negative bacterium and one of the most common crop plant pathogens globally (Lu and Yao, 2018; Xin et al., 2018). Its numerous different pathovars cause bacterial speck disease in almost all economically significant crop plants, infecting notable fruit crops and fresh produce like tomatoes and peppers from the family *Solanaceae*, and exotic fruits like mangoes and kiwifruits among others – of which kiwifruits have been affected by a significant bacterial bleeding canker outbreak in New Zealand, Asia, Chile and southern Europe since 2008 (McCann et al., 2017; Rooney et al., 2020; Xin and He, 2013; Xin et al., 2018). The bacterium is motile with its polar flagella which facilitate swimming and swarming (Xin and He, 2013). In the affected plants and tissues, classic *Ps* symptoms include chlorosis and localized necrotic wounding with distinctive water-soaked lesions as the pathogen secretes effector proteins into the host and induces the accumulation of fluid into the apoplast (Elizabeth and Bender, 2007; Xin et al., 2018). As it has the ability to infect the whole phyllosphere including fruits, leaves and stems, the bacterial speck disease results in the overall reduced fitness of the mother plant and consequent economic losses: a *Ps* infection in the fruits is a significant reason for crop rejection due to bacterial spoilage and reduced quality of the fresh produce (Gutiérrez-Barranquero et al., 2019; Ríó-Álvarez et al., 2014; Rooney et al., 2020).

Different plant pathogen strains, such as in the case of *Ps* species, tend to exhibit a large variety in the plants they infect, and strains that seem otherwise the same appear to differ only in their host preferences: These classes of pathogen strains that exhibit differences smaller than subspecies level are termed “pathovars”, abbreviated “pv.” (Bradbury, 1983). There are over 60 *Ps* pathovars with only slight differences in their host plant preferences, making *Ps* with all its pathovars collectively a number 1 on the top-10 list of bacterial pathogens (Gutiérrez-Barranquero et al., 2019; Mansfield et al., 2012). A laboratory-made tomato pathovar with rifampicin antibiotic resistance, *Pseudomonas syringae* pv. *tomato* DC3000 (*Pst* DC3000), has become a popular and successful model system for bacterial pathogens, as it can infect the model plant *Arabidopsis thaliana* (Cuppels, 1986; Whalen et al., 1991). This *Arabidopsis*-*Pseudomonas* pathosystem has since provided great insights into plant-pathogen interactions and bacterial effector functions, facilitated by the vast amount of research performed on the *Arabidopsis* model plant (Xin and He, 2013). Therefore, the *Arabidopsis*-*Pseudomonas* pathosystem is ideal for the studies on the links of plant immunity with other plant functions and well-studied signalling pathways, such as light signalling.

1.2.2. *Pseudomonas syringae*: Genetic Mechanisms of Virulence

As can be deduced from its ecological niche as a specialist plant pathogen, the *Pst* DC3000 genome encodes various mechanisms to interfere with the plant immune system, including highly specialised effectors and phytotoxins. With a complete genome sequence since 2003 (Buell et al., 2003), the *Pst* DC3000 genome has been thoroughly analysed for the presence of effector genes and other virulence mechanisms, which have given great insight into the molecular strategies of bacterial virulence. To successfully infect plants and avoid being detected by the different layers and mechanisms of plant immunity, *Pst* DC3000 utilises 34 effectors, whereas other *Ps* pathovars, such as *P. syringae* pv. *japonica*, may use as little as only 9 effectors (Lindeberg, 2012). These bacterial effectors are collectively called Type-3 effectors (T3E), as they are administered by the bacterial type-3 secretion system (T3SS), characteristic for Gram-negative bacteria (Lindeberg, 2012; Lu and Yao, 2018). T3SS injection pilus acts as a syringe, that injects the secreted effectors directly into the plant cell cytoplasm, and its components are encoded in the *Pst* genome in the conserved effector locus (CEL) (Geng et al., 2012). The importance of T3Es is that collectively, all the different effectors can practically jam any stage of the MAMP triggered immunity, as seen in **Figure 1.7** and **Table 1.2**: they can, for example, inhibit PRR complex formation and MAMP recognition, interfere with the cytoplasmic defence signalling and MAPK cascade, tamper with mRNA processing, modify R-proteins, re-route vesicle traffic, interfere with mitochondrial function, and target chloroplasts for inhibition of ROS production and SA biosynthesis (Xin et al., 2018). In an organismal scale, these changes can translate into abnormal plant hormone production and signalling patterns, and abnormal timings of normal plant responses -- all necessary for the pathogen life strategy and viability (Panchal et al., 2016; Xin et al., 2018).

Coronatine (Cor) is one of the most important *Pst* phytotoxins and is largely accountable for the plant symptoms during the disease cycle, including chlorosis that results from chlorophyll degradation, and abnormal plant responses, such as stomatal opening and down-regulation of SA signalling. It is a polyketide compound and a functional mimic of the bioactive plant defence hormone-amino acid conjugate JA-Ile, which in plants confers resistance against necrotrophic pathogens and insects, but is also antagonistic to the SA signalling normally activated by hemibiotrophs like *Pst* (Katsir et al., 2008; Toum et al., 2016). Cor phytotoxin yields many favourable outcomes for the pathogen, such as the opening or re-opening of stomata (as ROS and MTI typically cause rapid stomatal closure as a mechanism of physical barrier defence) which facilitates further pathogen entry from the leaf surfaces (Toum et al., 2016). In addition to this, it can lead to the prevention of MTI and consequent SAR, which together increase *Pst* virulence and fecundity, and result in increased disease symptoms in the plant (Geng et al., 2012).

In normal healthy plant cells, JA-Ile hormone conjugate performs the switch of resource allocation between defence and growth, as JA is a negative regulator of vegetative growth and a positive indicator of tissue damage, in addition to its role in biotic stress signalling (Katsir et al., 2008). In order to facilitate pathogen invasion and to be able to multiply in the apoplast without being targeted by the plant immune system, Cor functions to re-route signalling towards a less harmful direction for the pathogen: as SAR would be detrimental to *Pst*, a mistimed JA-mediated immunity compromises MTI and plant defences appropriate for hemibiotrophic bacterial pathogens like *Pst* (Geng et al., 2012). While Cor has multiple targets within plant cells, it functions mainly through the suppression of SA by mimicking JA-Ile and agonistically activating the cellular F-box

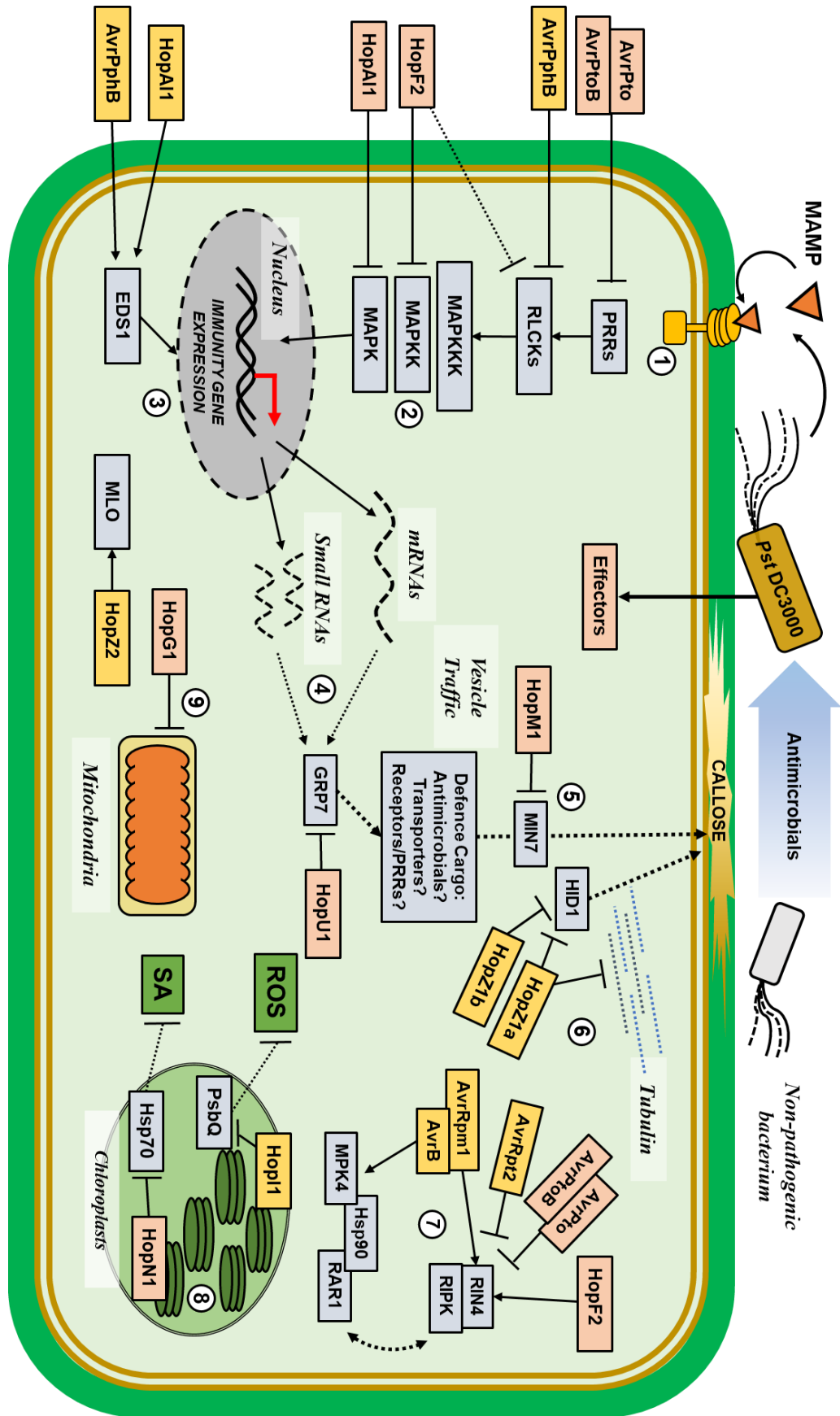


Figure 1.7 *Pseudomonas syringae* and genetic mechanisms for virulence.

Red background denotes known *Pst* DC3000 effectors, and yellow background denotes known effectors from other *Ps* pathovars, blue rectangular items are host target proteins. Note how *Pst* effectors can interfere redundantly with practically all steps and components of the plant immune system: **1)** MAMP-recognition and RLCKs, **2)** the MAPK-cascade, **3)** ETI and SA-mediated immunity protein EDS1, **4)** Gene transcripts, **5)** Vesicle trafficking and vesicle cargo, **6)** the cytoskeleton, **7)** R-protein RIN4 and **8)** chloroplast processes, and **9)** mitochondrial processes. Figure after Xin and He (2013).

Table 1.2 Overview of *Pst* DC3000 Effectors.

Left Known *Pst* DC3000 Type-3 Effectors, their plant targets and target processes, and if available, other information on the particular effector featured in this thesis. **Right** *Pst* DC3000 effectors with unknown plant host targets. Tables modified and compiled from Xin et al. (2018), and Xin and He (2013).

<i>Pst</i> DC3000 Type-3 Effectors	Host target	Host process	Other	<i>Pst</i> DC3000 Effectors With Unknown Plant Targets	
	–	JA			
AvrB	RIN4, MPK4, HSP90, RAR1	RIN4 complex	See Fig. 1.4. and Fig. 1.7, ⑦	AvrE	
AvrE	PP2A	–		HopI1	
AvrPphB	BIK1, PBS1, PBLs	MTI	See Fig. 1.4. and Fig. 1.7, ①	HopAA1-1	
AvrPto	RIN4	RIN4 complex	See 1.7, ⑦	HopAA1-2	
	FLS2, EFR, BAK1	MTI	See Fig. 1.4. and Fig. 1.7, ①	HopR1	
AvrPtoB	RIN4	RIN4 complex	See 1.7, ⑦	HopQ1	
	FLS2, CERK1, BTI9, BAK1	MTI	See 1.7, ①	HopY1	
	FEN, R _{HopAD1}	ETI		HopO1	
	–	ABA		HopV1	
AvrRpm1	RIN4	RIN4 complex	See Fig. 1.4. and Fig. 1.7, ⑦	HopAO1	
AvrRps4	EDS1	EDS1	See Fig. 1.7, ③	HopA1	
	WRKY TFs	MTI	See Fig. 1.4.	HopH1	
AvrRpt2	MPK4,MPK11	MTI		HopC1	
	AUX/IAA	Auxin		HopE1	
	RIN4	RIN4 complex	See Fig. 1.4. and Fig. 1.7, ⑦	HopY1	
HopA1	EDS1	EDS1	See 1.7, ③	HopS1	
	–	Proteasome		HopAM1	
HopAF1	MTN1,MTN2	Ethylene		HopK1	
HopAI1	MPK3, MPK6, MPK4	MTI	See Fig. 1.7, ②		
HopAM1	–	ABA			
HopAO1	–	Proteasome			
HopB1	BAK1	MTI			
HopBB1	JAZ	JA			
HopD1	NTL9	ETI			
HopE1	MAP65	Microtubule			
HopF2	BAK1, MKK5	MTI	See Fig. 1.7, ①, ②		
	RIN4	RIN4 complex	See Fig. 1.7, ⑦		
HopG1	–	Proteasome			
	Kinesin	Actin			
HopI1	–	SA			
	HSP70	Chloroplast	See Fig. 1.7, ⑧		
HopK1	–	Chloroplast			
HopM1	–	Proteasome			
	MIN7	Water balance	See Fig. 1.7, ⑤		
HopN1	PsbQ	Chloroplast	See Fig. 1.7, ⑧		
HopQ1	–	Cytokinin			
HopU1	GRP7 and GRP8	Gene transcripts	See Fig. 1.7, ④		
HopW1	Actin	Actin			
HopX1	JAZ	JA			
	JAZ	JA			
HopZ1a	GmHID1	Phytoalexin	See Fig. 1.7, ③		
	Tubulin	Microtubule	See Fig. 1.7, ③		
HopZ1b	GmHID1	Phytoalexin	See Fig. 1.7, ③		
HopZ4	RPT6	Proteasome			

protein and JA-Ile receptor COI1 that functions as the substrate adapter of the E3 ubiquitin ligase SCF^{COI1}. This ubiquitin ligase plays a role in the targeted degradation of proteins with Jasmonate Zim (JAZ) domains, which are the repressors of the SA pathway through MYC2 (Geng et al., 2012; Katsir et al., 2008). However, Cor has also been found to have 1000-fold higher bioactivity than normal JA-Ile in tomato plants, causing further magnification of the SA signalling perturbation, and a significant shift in the plant systemic defence hormone equilibrium (Katsir et al., 2008).

As C3 and C4 plants close their stomata for the night when plant defences are naturally downregulated, stomatal closure also acts as a barrier for pathogen penetration. To prolong the time window of the temporally coordinated invasion, *Pst* can utilise its effectors and phytotoxins to hijack the host immune system and to force the plant to perform abnormal responses favourable for the pathogen, both when outside and inside the plant tissues. As night is ideal for *Pst* motility and cooler ambient temperature encourages water condensation and mist on plant surfaces, Cor can be used by *Pst* in the epiphytic phase to force the stomata open against the normal diurnal stomatal cycle and block the MTI induced closure signal (Panchal et al., 2016). Some of these plant pathways targeted by *Pst* Cor phytotoxin intriguingly involve the plant circadian clock pathways ultimately governed by plant photoreceptors. For instance, Cor has been found to negatively regulate the *Arabidopsis* circadian clock genes by reducing the amplitude and extending the period of clock components in a JA receptor-dependent manner, therefore reprogramming the plant circadian clock for increased pathogenesis: *Pst* strains lacking Cor biosynthesis gene were also found less virulent in plants grown on a diurnal cycle, and the disease phenotype appears to be at least partially light-dependent (Gao et al., 2020; Panchal et al., 2016).

1.2.3. *Pst* DC3000 Life Cycle

Once a plant pathogen is inside the plant tissues, the course of the infection will depend on the life strategy and nutritional requirements of the pathogen. Biotrophic pathogens, which evolutionarily originate from plant mutualists evolving pathogenic traits, complete their life cycles solely in live plants, whereas necrotrophic bacteria, which in contrast evolutionarily originate from saprotrophs gaining the ability to infect live plants, kill the host plant to multiply in the dead plant tissues (Jones and Dangl, 2006). However, *Pst* DC3000 is an example of a hemibiotrophic pathogen: hemibiotrophs exhibit both biotrophic and necrotrophic phases firstly starting by infecting live plants and multiplying in live plant tissues, but then switching strategies over the course of the infection and eventually killing the plant (Xin and He, 2013).

Following its hemibiotrophic life cycle (**Figure 1.8**), the *Pst* colonisation of a plant can be divided into epiphytic and endophytic phases (Río-Álvarez et al., 2014). *Pst* DC3000 starts its infection epiphytically on the surfaces of healthy plants (**Figure 1.8 A**). Bacteria are transmitted to the healthy leaf surfaces from infected plants by rain and liquid droplets, and high environmental humidity promotes infection. Once on the leaf surface (**Figure 1.8 B**), the bacteria are motile and utilise quorum sensing and photo- and chemotactic cues to swarm inside the plant tissues through natural openings such as open stomata or wound sites by utilising their flagellae for swimming (**Figure 1.8 C**). Alternatively, *Pst* can also employ special ice nucleation proteins as a virulence strategy in order to directly inflict wounds on the host plants and to make entrances for swift

colonisation (Xin et al., 2018). Unlike many other *Ps* strains and pathovars in the wild, the laboratory strain *Pst* DC3000 is a weak epiphyte and most vulnerable when in touch with the abiotic environment (Feil et al., 2005). Therefore, the phyllosphere and the apoplast are the ideal environments for *Pst* DC3000, and the endophytic phase inside the plant tissues is characterised by aggressive bacterial multiplication (Río-Álvarez et al., 2014) (**Figure 1.8 D**). Through the extensive use of its effectors to attenuate plant defences, the *Pst* population will enter its exponential growth phase until it reaches its peak, and plateaus. As plant nutrients and other resources become locally depleted with the increasing bacterial population and activity (incl. secreted phytotoxins and effectors), the infection will shift to the necrotrophic phase and plant tissues will become visibly chlorotic and necrotic (Xin and He, 2013) (**Figure 1.8 E**).

In addition to the mechanisms of infection, also the timing of the bacterial invasion is important to ensure the maximal viability and virulence for the *Pst*. As many plant processes, including the immune reaction, are regulated by light, and the plant immune reactions involve molecular components such as ROS and SA made in the chloroplasts in the daylight (Kangasjärvi et al., 2012; Kimura et al., 2017; Wildermuth et al., 2001), pathogens can gain an advantage by infecting the host plants at times they are naturally the most vulnerable and unable to achieve peak immunity (Río-Álvarez et al., 2014). Therefore, *Pst* DC3000 has its own set of photoreceptors that monitor for different light conditions and times of the day: these include the blue light receptors, such as LOV domain receptors, BLUF, PYP and cryptochromes, two bacteriophytochromes for red light detection, and a light-activated proton pump proteorhodopsin (Río-Álvarez et al., 2014). Studies by Río-Álvarez et al. (2014) and Santamaría-Hernando et al. (2018) found that white and blue light wavelengths, in addition to high irradiation, discouraged *Pst* motility, induced the bacterial T3SS genes and promoted tethering to the plant surfaces, together with bacterial biofilm formation. In contrast, lower light intensities, darkness, and monochromatic red light promoted bacterial mobility, swarming behaviour, and more severe disease phenotype, and triggered a reduction in the coronatine phytotoxin production. Therefore, the pathogens need to divide the phases of invasion into the motile phase outside the plant and static phases inside the plant tissues, as the timing of the infection is important, and correctly timed flagellar motility will determine the outcome of the infection. Most bacterial movement must occur outside the peak daylight hours for the pathogens to make it to the safety of the phyllosphere before the plant regains its full immune power in the daylight, and the attachment and quorum sensing in full daylight conditions also primes the pathogen for T3SS effector injection in order to suppress the peak immunity when optimal light conditions are present for the plant. It is also notable, that root-infecting *Pseudomonas* species, namely *P. putida* and *P. fluorescens*, have been found to lack the LOV domain blue photoreceptors, providing further evidence for the importance of the environmental light cues in the virulence of the phyllospheric pathogens such as *Pst* DC3000 (Río-Álvarez et al., 2014).

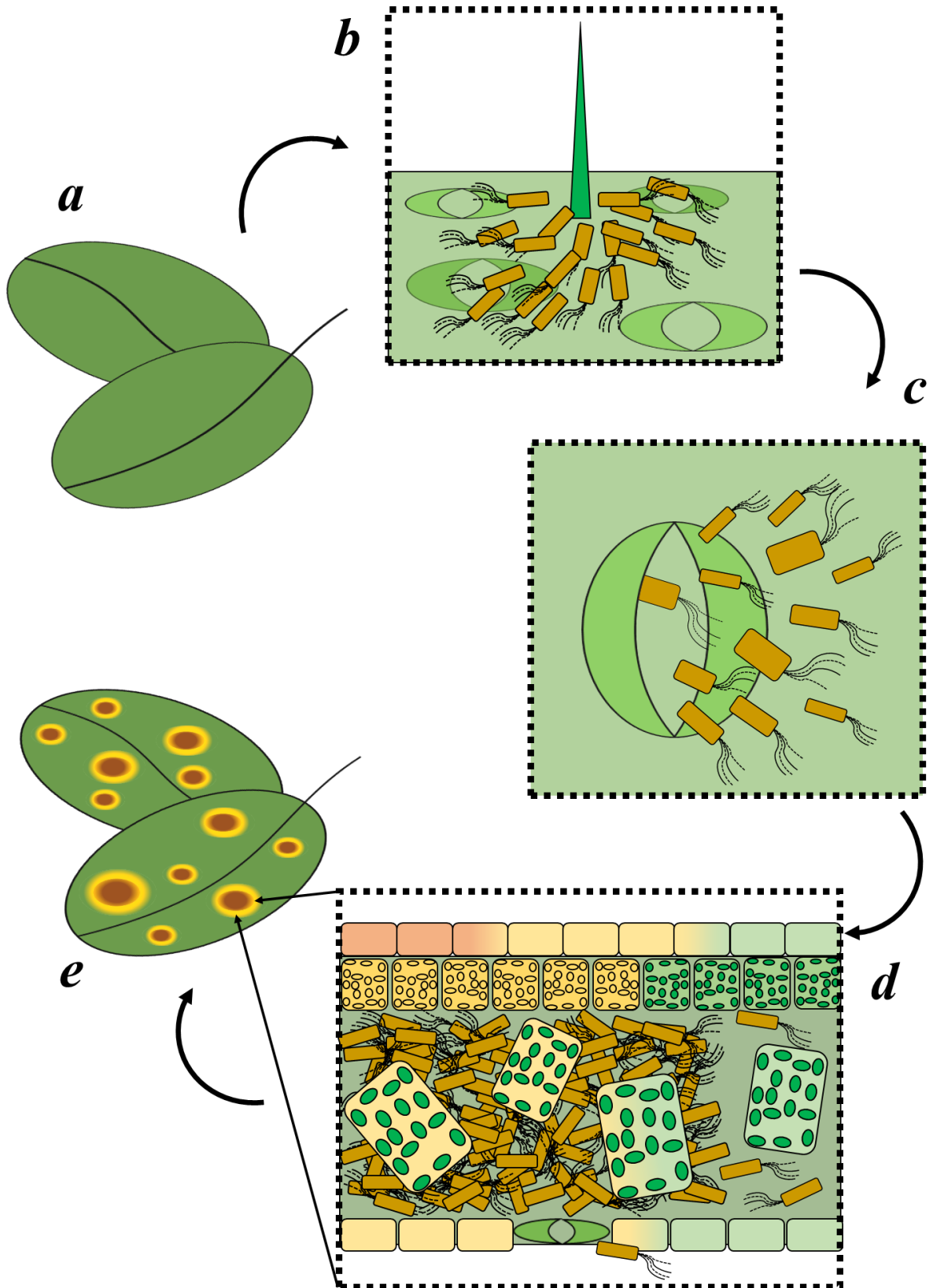


Figure 1.8 *Pseudomonas syringae* life cycle and compatible interaction *in planta*.

A simplified schematic diagram detailing a compatible interaction between *Ps* and a host plant, and the course of the infection (not to scale). **a**) Infection will start on the leaf surface of a healthy plant; **b**) bacteria are transmitted to the top of the leaf, and initiate the motile phase and swarming behaviour; **c**) the pathogens invade the plant through wound sites or open stomata, or alternatively, utilise their effectors to initiate stomatal opening; **d**) *Ps* multiplies in the apoplast, which is its favoured habitat, while simultaneously suppressing both inter- and intracellular plant signalling through effectors and phytotoxins; **e**) Plants develop the characteristic disease phenotype, including necrotic lesions and chlorosis. Figure after Xin and He (2013).

1.3. Plant Photobiology

1.3.1. Plant Photomorphogenesis

Photomorphogenesis refers to plant growth and development in response to the visible light portion of the electromagnetic spectrum. It involves plant photoreceptors specific to particular wavelengths of visible light, which allow the gathering of environmental information in order to trigger downstream signalling cascades for the optimal regulation of the plant genomic plasticity (Folta and Carvalho, 2015). Therefore, the higher plant life cycle involves several light-dependent phase changes (Kim et al., 2017). The first light-dependent process for the plant is the red light-dependent seed germination, where a brief environmental red light signal functions as the trigger for germination in many species (Bae and Choi, 2008). The germination conditions determine the first photomorphogenic life strategy decision (see left yellow frame, “WT”, in **Figure 1.9**): in the darkness, the nascent wild type seedling will go through skotomorphogenesis and grow a tall hypocotyl in the search of light, with its apical hook turned inwards to protect the folded cotyledons during growth through the soil layers (Perrella et al., 2020). At this stage, the seedling is etiolated and coloured white or pale yellow. De-etiolation and phase change from the seedling stage to the juvenile vegetative state occurs when the seedling senses light for the first time. This triggers the massive light-dependent transcriptome remodelling and chromatin reorganization and changes the plant from dark-grown etiolated phenotype to photosynthesising light-grown de-etiolated phenotype (Paik and Huq, 2019). During de-etiolation, the hypocotyl extension stops, the apical hook uncurls and the cotyledons expand and flatten, and the plant colour turns green with the conversion of chloroplast precursor etioplasts into functional chloroplasts (Kim et al., 2017; Wu, 2014), as seen in **Figure 1.9** (right yellow frame, “WT”).

The stark differences between the etiolated and de-etiolated phenotypes have allowed the thorough research of the photomorphogenic regulatory genes, and their consequent determination as positive or negative factors of photomorphogenesis, as shown in **Figure 1.9**. Mutants in positive regulators of photomorphogenesis, such as phytochrome or cryptochrome photoreceptors, signalling nodes, and positive transcription factors, appear to be undergoing skotomorphogenesis even if grown in light (Kim et al., 2017; Wu, 2014). The opposite is true for the negative regulators of photomorphogenesis, which are, for example, key E3 ubiquitin ligase components that degrade the light signalling proteins in the dark. These mutants have a distinctive phenotype seen in darkness: the seedlings are coloured pale or white as they are etiolated but appear morphologically de-etiolated as if they had sensed light (Wu, 2014). Therefore, photomorphogenic mutations affect different steps in the plant signal transduction pathway, from the light receptor proteins to the downstream signalling components, signalling nodes and signal integrators, and their negative regulatory loops to photomorphogenesis-promoting transcription factors, as shown in **Figure 1.10**.

As light is among the most important environmental factors for the plant (Kim et al., 2017), roughly 1/3 of the *Arabidopsis* genome is controlled in a light-dependent fashion (Ma et al., 2001). Photoreceptors gather environmental information that will direct the organism-wide decision making and commitment from one life phase to another: the transitions have to be made swiftly and they are irreversible, and therefore, the cost of a badly timed life phase commitment is reduced viability and reduced number of seeds at best, and death at worst. Photoreceptor input and other environmental information can be pooled and assessed in signalling nodes and signal integrator points. One major signalling node for plant photoreception is the ELONGATED HYPOCOTYL 5 (HY5) bZip transcription factor, which is the main photomorphogenic switch controlling

	Dark-grown	Light-grown	
	WT	Negative regulator mutant	WT
Photoreceptors		---	<i>PhyA, PhyB, Cry1, Cry2</i>
Chromatin remodeling enzymes		<i>hd1/hda19 epp1/pkl</i>	<i>(taf1), gcn5, hda15</i>
Transcription factors		<i>pifq, bbx24, bbx25, gbf1, bzip16, zbh1</i>	<i>hy5, hyh, hfr1, laf1, pat1, fhy3, far1, bbx4, bbx20, bbx21, bbx22, gata2</i>
Splicing factors		<i>skip</i>	<i>rrc1</i>
miRNA processing		<i>ago1 (?)</i>	---
Translation factors		<i>eif3h</i>	---
Protein degradation factors		<i>cop/det/fusca, spa, pks1, eid1</i>	<i>afr, max2/ore9</i>

Figure 1.9 Examples of normal photomorphogenesis in *Arabidopsis*, photomorphogenic mutants, and their phenotypes.

Wild type example seedling phenotypes in dark (black background) and light (yellow background) are shown inside yellow frames. Negative photomorphogenesis regulator-mutants (green background) exhibit de-etiolated phenotype in the dark, whereas positive regulator mutants (red background) exhibit etiolated phenotype in the light. Figure after Wu (2014).

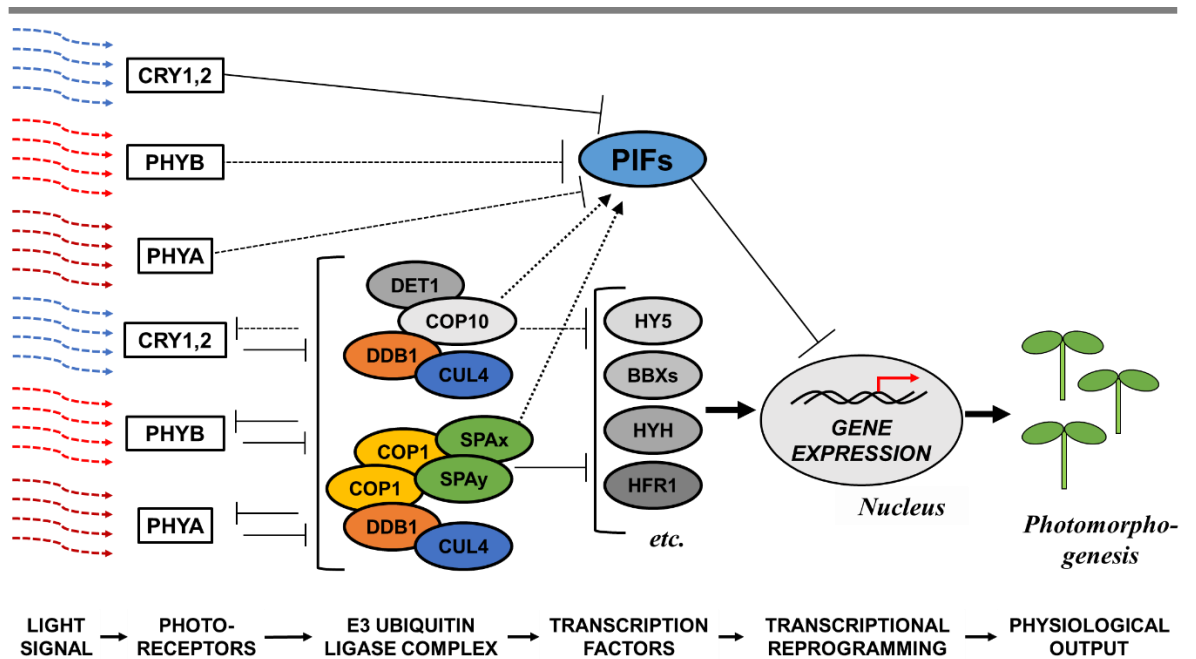


Figure 1.10 Plant light signal transduction pathways.

Signal transduction from the initial light signal (left) and its detection by photoreceptors to the removal of negative regulators (E3 ubiquitin ligase complexes) and stimulation of positive transcription factors and signal integrators. All these factors will alter the gene expression and result in transcriptional reprogramming, which underpins photomorphogenic development and de-etiolation. Compare with Figure 1.9 above. Figure after Xu (2020).

hypocotyl extension and interacts with 3000 gene loci (Lee et al., 2007): the default in the dark is the negative regulation and destabilisation of HY5 transcription factor through targeted degradation, and only sufficient sum of the environmental factors can promote hypocotyl growth by removing the negative regulation and stabilising HY5. *hy5* mutants have long hypocotyls regardless of light conditions, but *hy5* also exhibits functional redundancy e.g. with transcription factor HYH (Xu, 2020). The key regulator behind the targeted HY5 degradation and suppression of photomorphogenesis in the dark is the COP1-SPA E3 ubiquitin ligase, which is a negative regulator of photomorphogenesis (see **Figure 1.9** and **Figure 1.10**). Light-dependent photoreceptor signalling cascades, therefore, function to inhibit COP1-SPA repressor function to allow the expression of photomorphogenic genes (Kim et al., 2017).

Once the plant has sensed light and gone through de-etiolation, the plant will simultaneously start the entrainment of its circadian clock using its cryptochrome and Zeitlupe family photoreceptors (Paik and Huq, 2019; Wu, 2014). The seedling will also begin to optimise its growth for the establishment of the seedling and correct its growth habit to maximise photosynthesis: this directional growth and solar tracking, and shade avoidance are mediated by phototropins and phytochromes, respectively (Bae and Choi, 2008; Kutschera and Briggs, 2016). In too high light conditions, photoreceptors coordinate photoprotection. Plant flavonoid biosynthesis is UV-B light stimulated and plays a role in plant photoprotection and colouring (Jenkins, 2014), while the chloroplasts undergo phot2-mediated photorelocation and avoidance movement (Suetsugu and Wada, 2007). Photoreceptors will also play a role in the correct timing of phase changes of the plant, which is especially important for annuals. Vegetative growth is therefore constantly optimised to maximise photosynthesis and to gather resources and energy for future spread by sexual or asexual reproduction. In addition to this, phytochromes, cryptochromes, and Zeitlupe family photoreceptors time the reproduction by adjusting flowering time to correctly time the pollination, coordinate the time of seed setting, and in perennials, aid with cold acclimation (Paik and Huq, 2019; Perrella et al., 2020).

1.3.2. Plant Light Receptors and Light Signalling

As plants are sessile organisms and must rely on the plasticity of their genome for their survival, light provides a vital environmental cue for plant growth and development. Therefore, to gather important information regarding their surroundings and to regulate this genomic plasticity to make the most out of their fixed habitat, higher plants have evolved five classes of specialised photoreceptors to assess the wavelength, duration and direction of light (Christie et al., 2015; Jenkins, 2014): Red and far-red light receptors phytochromes A-E (phy A-E), blue light (BL) and UV-A receptors phototropins 1 and 2 (phot1 and phot2), cryptochromes 1 and 2 (cry1 and cry2) and zeitelupe family photoreceptors ztl, fkl1 and lkp2, and finally, the UV-B receptor UVR8 (Christie et al., 2015; Jenkins, 2014; Paik and Huq, 2019), as seen in **Figure 1.11**. According to Paik and Huq (2019), all 5 classes of photoreceptors share three key similarities despite their molecular differences and different modes of action: **1)** the ability to convert photon energy input into photoreceptor activation through a conformational change in the protein; **2)** the ability to relay the activation information forward in the signalling chain through protein post-translational modifications, and **3)** the ability to self-regulate through receptor de-sensitisation and negative feedback loops (Paik and Huq, 2019).

A typical photoreceptor structure consists of an apoprotein frame without the pigment, and the chromophore, which is a small organic cofactor pigment molecule that absorbs light. Together they comprise the photoreceptor holoprotein, where the small light-dependent chemical reactions within the chromophore are transformed into large structural and functional changes in the protein structure. Photoreceptors and their cofactors are presented in **Figure 1.11**. Phytochromes bind phytochromobilin as its cofactor, and BL receptors phototropins, Zeitlupes, and cryptochromes bind flavin-based cofactors as their main chromophore, such as flavin mononucleotide (FMN, in Zeitlupes) or flavin adenine dinucleotide (FAD, in phototropins and cryptochromes) (Bae and Choi, 2008; Christie et al., 2015). In contrast to all the other plant photoreceptors, the UV-B photoreceptor UVR8 does not have an inorganic chromophore, as its photoreceptive function is mediated by a triad of aromatic amino acid tryptophan residues (Christie et al., 2012; Jenkins, 2014).

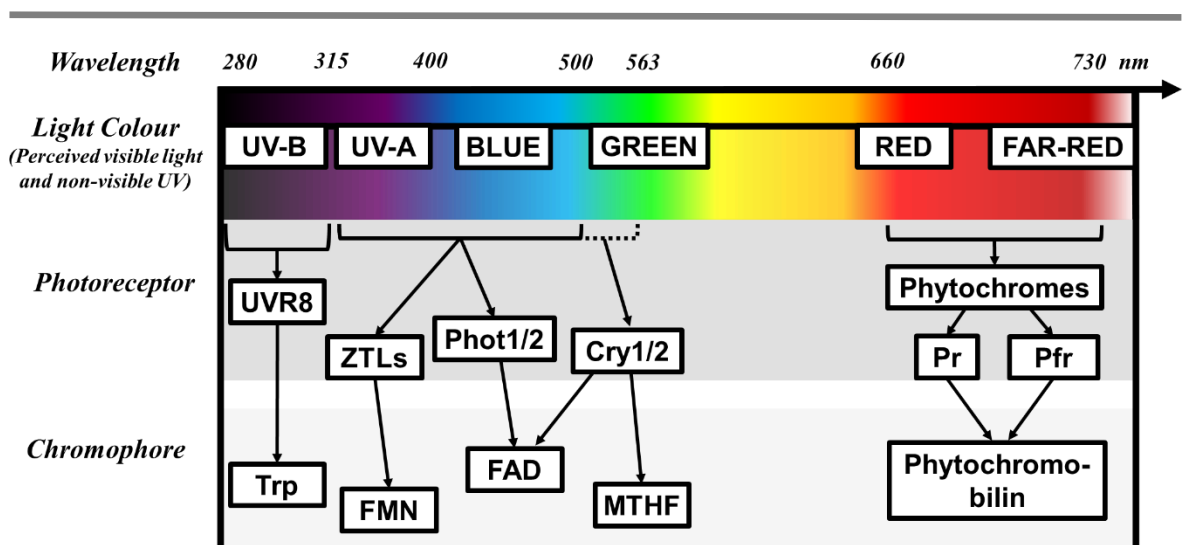


Figure 1.11 Overview of plant photoreceptors, their approximate absorbed wavelengths, and their bound chromophore cofactors.

Figure compiled after Heijde and Ulm (2012) and Folta and Carvalho (2015) .

Plant photoreceptors have specialised to perceive different wavelengths of visible and UV light, originating from the sun as white light. Therefore, light wavelength and intensity determine the exact cellular pathway and responses activated in the plant cell.

Phytochromes

Phytochromes are the main red light sensors in plants, which detect red and far-red light at 600-750 nm with their covalently attached linear tetrapyrrole phytochromobilin chromophore (Mroginski et al., 2011; Paik and Huq, 2019). There are five distinct types consisting of phytochromes A-E, of which PhyA plays a distinct role from the rest during de-etiolation: photolabile PhyA is rapidly degraded in light, whereas PhyB-E are all stable (Bae and Choi, 2008). The photoreceptor is synthesised in the cytosol in the inactive Pr form and is a dimer in all conditions: activation by red light and the consequent photoisomerisation of the chromophore induces the photoconversion of the full photoreceptor into the active Pfr form with exposed interaction surfaces and localization signals (Bae and Choi, 2008). Furthermore, activation also triggers the protein relocalization from the cytoplasm to the nucleus. In the nucleus, Phys initiate the degradation of basic helix-loop-helix (bHLH)-transcription factors, phytochrome interacting factors (PIFs), and inactivate the repressor and light signal integrator COP-SPA (as seen previously in **Figure 1.10**), therefore removing negative regulation and promoting and stabilising positive photomorphogenic regulators, such as LAF, HY5 and HYH, and HFR, resulting in light-dependent gene transcription (Paik and Huq, 2019; Perrella et al., 2020).

The active Pfr absorbs different wavelengths of light to the Pr form and will be consequently photoconverted back into inactive Pr in far-red light or darkness rapidly, resulting in constantly changing pools of active and inactive Phys in various ratios termed photoequilibria. The cellular Pfr-Pr photoequilibrium is crucial in assessing the exact light environment experienced by the cells for key plant life strategy decisions, including de-etiolation mediated by PhyA, among others (Rivadossi et al., 2008; Sakuraba et al., 2014). Phytochromes are also vital for the plant shade avoidance reaction, as natural conditions such as canopy shade filter red wavelengths out from sunlight, enriching the remaining light passing through the leaves in far-red wavelengths. Excess far-red light gives the plant information about being shaded, and therefore encourages hypocotyl or stem growth to gain access to sunlight and greater photosynthetic efficiency (Paik and Huq, 2019). Other major functions involve the sequential senescence of older shaded leaves (Sakuraba et al., 2014; Ueda et al., 2020), and the control of flowering time where the high Pfr to Pr ratio promotes flowering in long-day plants while inhibiting it in short-day plants (Perrella et al., 2020). There is also evidence for Phys as environmental multi-sensors, integrating information not only from the light conditions alone but also from temperature, functioning as a thermosensor for controlled cold acclimation response (Paik and Huq, 2019; Perrella et al., 2020).

Blue Light Signalling: Zeitlupe family

The Zeitlupe family consists of three members that exhibit partial functional redundancy: zeitlupe (*ztl*), lov-kelch protein (*lkp2*) and flavin binding kelch repeat f-box1 (*fkf1*), all of which contain a photosensory LOV domain with an FMN cofactor similarly to phototropins, an F-box E3 ubiquitin ligase domain, and a kelch repeat domain for protein-protein interactions, as seen in **Figure 1.12** (Christie et al., 2015). They function mainly in the plant circadian clock, circadian entrainment and flowering time: for example, *ztl* regulates key components of the circadian clock, such as cyclin DOF factors, and *fkf1* binds a flowering time regulator GIGANTEA and signalling component to ultimately induce FT-dependent flowering (Christie et al., 2015).

Blue light Signalling: Cryptochromes

Cryptochromes *cry1* and *cry2* are flavoproteins, which bind FAD as the primary chromophore, and a methenyl tetra hydro folate (MTHF) as an antenna chromophore inside the photolyase homology region (PHR) domain. Signalling functions are performed by the cryptochrome C-terminal (CCT) domain in response to light activation, as seen in **Figure 1.12** (Christie et al., 2015). *cry1* has key functions in de-etiolation and hypocotyl growth suppression, whereas *cry2* controls photoperiodicity and flowering time (Christie et al., 2015). Phylogenetically, they originate from photolyases, which mediate light-dependent DNA repair in cells: therefore, *Arabidopsis* CRY3 is a DNA repair protein and not a functional photoreceptor (Fantini and Facella, 2020).

BL activation leads to receptor phosphorylation and consequent dimerization and nuclear body formation, all inside the nucleus (Christie et al., 2015). The *cry2* receptor also exhibits rapid desensitisation by targeted degradation, while both photoreceptors trigger negative feedback by activating inhibitors Blue light inhibitor of cryptochromes1 (BIC1) (Christie et al., 2015; Paik and Huq, 2019). Downstream signalling is mediated by activation of positive regulators, such as cryptochrome interacting bHLH (CIB) transcription factors inside the

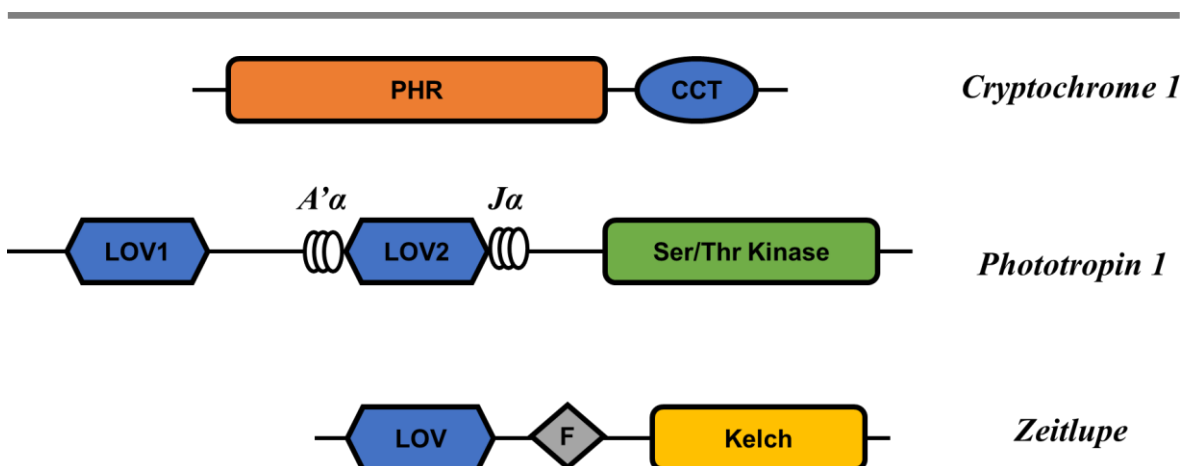


Figure 1.12 Schematic representation of the domain structure of the three plant BL photoreceptor families.

Cryptochromes: Photolyase homology region (PHR), cryptochrome C-terminus (CCT).

Phototropins: Light-oxygen-voltage-sensing 1 & 2 (LOV1&2), with regulatory A'α and Jα-helices, and a C-terminal Ser/Thr kinase domain.

Zeitlupe: LOV-domain, F-box (F), Kelch-repeat.

Figure after Christie et al. (2015).

nuclear bodies, the PIF transcription factors shared with Phys, interaction with the negative regulator COP-SPA, plant hormone auxin, and the forementioned feedback proteins BICs (Fantini and Facella, 2020; Paik and Huq, 2019).

UV-B and UVR8

UVB resistance locus 8 (UVR8) functions mainly in photoprotection against UV-B, inducing flavonoid sunscreen synthesis, upregulated DNA repair and photomorphogenesis (Jenkins, 2014). UVR8 monomer is a 7-bladed beta-propeller protein, and in the inactive homodimer, the monomers are superimposed and held together by salt bridges, electrostatic interactions and hydrogen bonds (Christie et al., 2012). UVR8 does not possess a separate chromophore, but the UV-B light reception is mediated by a triad of conserved tryptophan residues in the dimer interface protonates the salt bridges holding the dimer together, releasing the active monomers into the cytosol from the inactive dimer (Christie et al., 2012). Monomers accumulate in the nucleus, where they bring about the changes in gene expression by interacting with COP1 and stabilising HY5, further initiating significant gene expression changes and chromatin remodelling (Jenkins, 2014).

1.3.3. Blue Light Signalling: Phototropins and Phototropin Signalling

The phototropin family has two members in *Arabidopsis*, phot1 and phot2 (Haga et al., 2015), which absorb blue and UV-A light at wavelengths at 320-500 nm. They are hydrophilic membrane-associated proteins that localize to the plasma membrane in fluorescent tagging experiments and undergo rapid activation and consequent autophosphorylation when illuminated with BL (Christie et al., 2015, 2018). Phot photoreceptors also exhibit dynamic relocalization patterns in response to light. Phot1 relocates into the cytoplasm and into cytosolic strands, whereas phot2 mostly maintains its position at the plasma membrane while a small subpopulation of the phot2 receptors undergoes trafficking into the Golgi apparatus (Christie et al., 2015; Kong et al., 2006).

Functionally, phototropins allow the determination of light direction and the modulation of plant growth response by transforming the light-induced receptor activation patterns into plant hormone gradients. This is the result of the phot-dependent direction of plant hormone auxin fluxes within the plant tissue, resulting in photomorphogenic growth responses and ultimately, the optimisation and maximisation of photosynthesis. (Christie et al., 2015; Haga et al., 2015; Pedmale and Liscum, 2007). Both phot BL receptors exhibit redundant functions in plant photomorphogenesis, such as phototropism, stomatal opening, chloroplast accumulation, and leaf flattening. However, while phot1 functions in low to moderate light, phot2 is more specialised to detect high light intensities to initiate photoprotective responses, such as chloroplast avoidance reaction (Łabuz et al., 2012; Suetsugu and Wada, 2017). Consequently, the photoreceptor expression patterns are also light-responsive. While phot1 photoreceptor expression is downregulated in response to BL, phot2 expression is light-induced consistent with its role in photoprotective signalling (Łabuz et al., 2012).

The phot structure (see **Figure 1.12**) involves **a**) two LOV (light-oxygen-voltage) domains LOV1 and LOV2 that contain the non-covalently attached oxidised FMN chromophore and therefore directly sense BL, and a regulatory linker between these two domains that function in protein-protein interactions, such as with 14-3-3 proteins; **b**) a LOV2 linker region that plays a role in regulatory modifications through its conserved $J\alpha$ helix; **c**) a C-terminal AGCVIII-type serine/threonine kinase, which is activated through the phosphorylation reactions within the activation loop (Christie et al., 2015, 2018). In the dark, the photoreceptor is folded in a way that the kinase's active site is obstructed and therefore inactive (**Figure 1.13 A**). Activation by BL functions as the start of the phot photocycle, triggering a covalent, dark reversible cysteinyl adduct formation between the FMN chromophore and a cysteine residue (Cys-966) within a conserved 3_{10} helix of the LOV2 domain apoprotein, as shown in **Figure 1.14 A**. The 3_{10} -helix is a type of protein secondary structure, where the arrangement of the amino acids in the helical conformation is more tightly wound, with 3 residues per turn in contrast to 3.6 residues per turn in α -helices. In addition to this, the helix comes with almost 0.5\AA taller helical rise and at least 0.4\AA higher helical pitch per turn than α -helices, therefore making it also longer and thinner in comparison to α -helices (Vieira-Pires and Morais-Cabral, 2010) and promoting the region's flexibility. The conformational changes in the LOV2 domain therefore further translate into the unfolding and displacement of the C-terminal $J\alpha$ helix and the A' α helix between LOV1 and LOV2 domains, exposing the functional kinase domain, as shown in **Figure 1.13 B** (Christie et al., 2015; Konold et al., 2016). This then leads to the receptor autophosphorylation event, an activated signalling state, and the dissociation of the photoreceptor from the plasma membrane and its interacting partners, such as NPH3 (Christie et al., 2015; Haga et al., 2015). The activation also changes the light absorption pattern of the photoreceptor: a dark-state phototropin absorbs both BL and UV-A light at a peak of 450 nm (LOV₄₅₀ state), whereas a photobleached receptor absorbs light only at UV-A region with a peak at 390 nm (LOV₃₉₀ state), as shown in **Figure 1.14 B**.

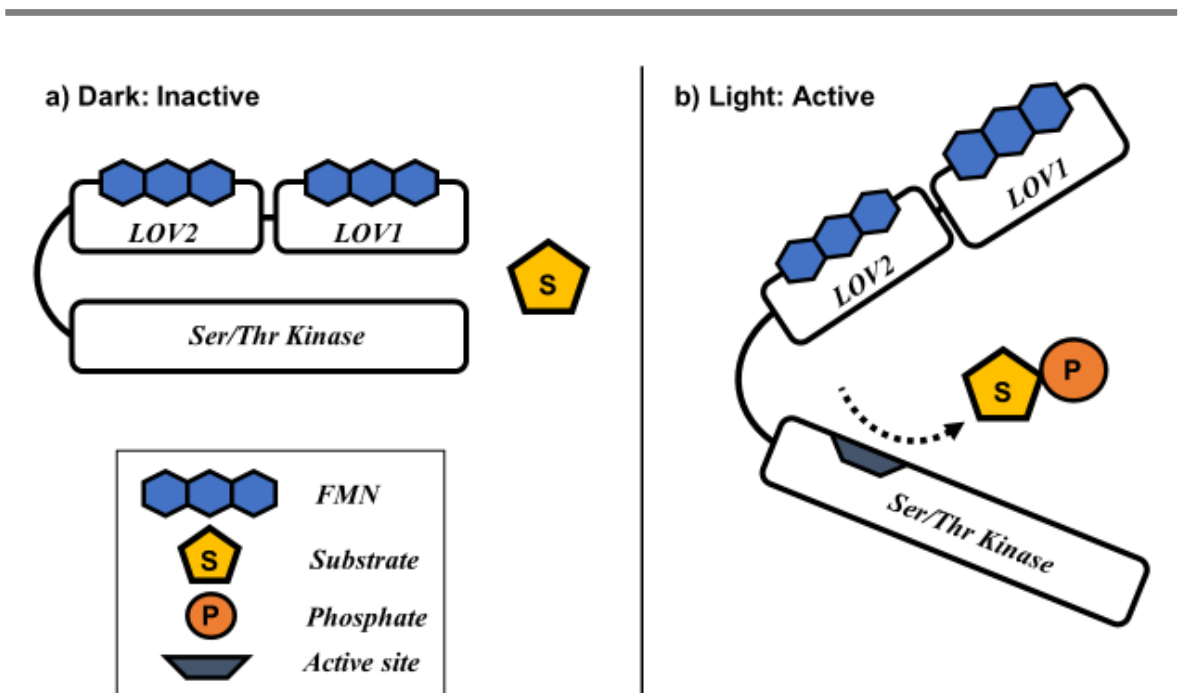


Figure 1.13 Phot-activation is initiated by a light-dependent conformational change in the protein.

A schematic graphic portraying the conformational changes during phot-activation, from **A**) inactive conformation in dark, to **B**) active conformation that underpins phot ser/thr-kinase function. Figure after Kimura and Kagawa (2006).

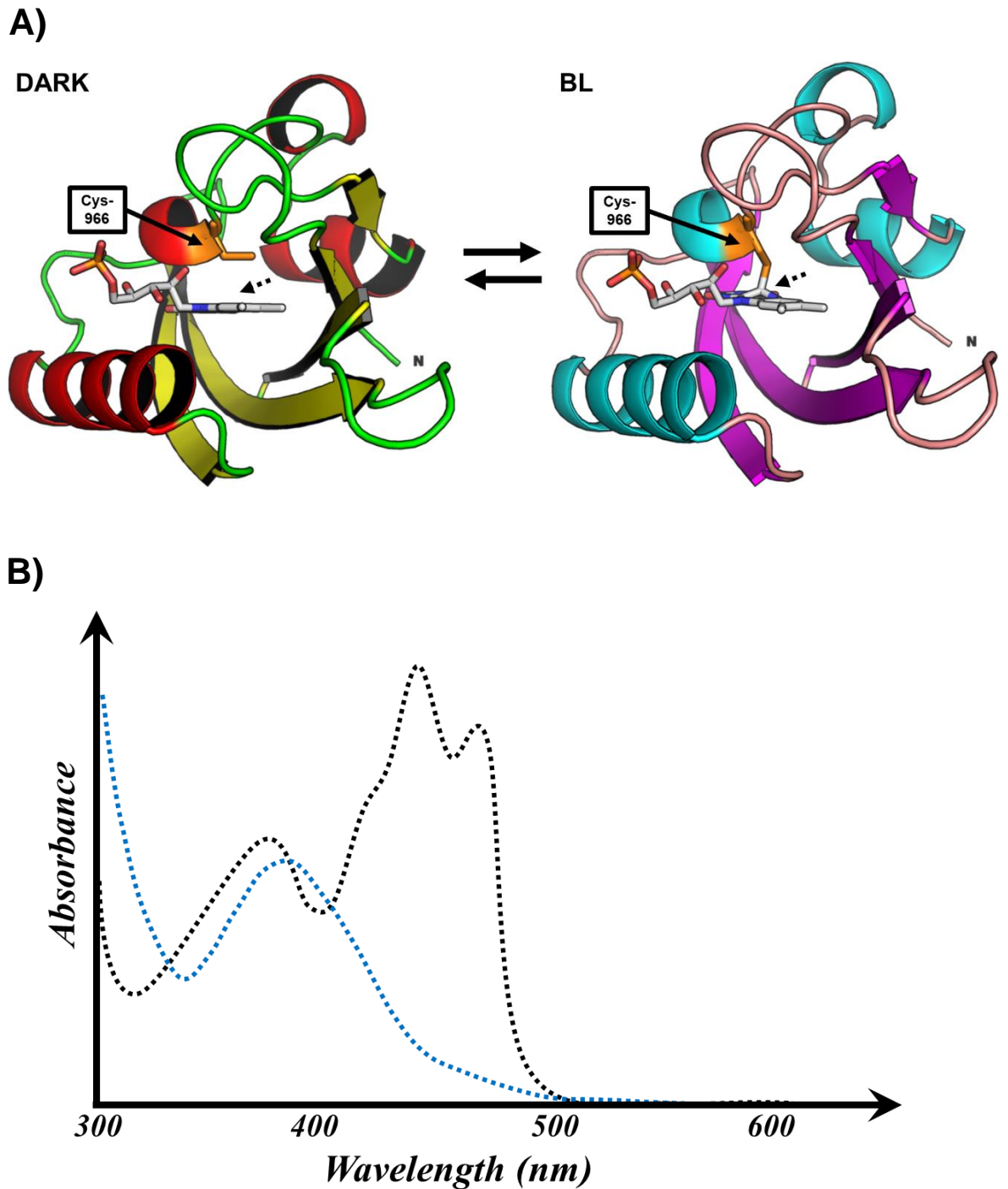


Figure 1.14 Inactive and active phot1-photoreceptors absorb light in distinct patterns.

A) The light-dependent cysteinyl adduct formation between the FMN chromophore and the Cys-966 residue (orange) within the conserved 3_{10} helix of the *Arabidopsis* phototropin LOV2-domain (pictured) underpins the change in its activity in response to BL. Note the deformation of the chromophore structure (dashed arrow) from linear conformation to a convex shape during the formation of the covalent thiol bond between the chromophore and the apoprotein.

3D figures constructed using the PyMOL Molecular Graphics System, Version 1.6, Schrödinger, LLC, according to the Protein Data Bank Phototropin1G28.pdb and Phototropin 1JNU.pdb files (2013).

B) Relative absorbance during phototropin LOV domain photocycle, with dark-state molecule LOV₄₅₀ (black) absorbing light both at UV-A and BL ranges with a peak absorption at 450 nm, and the BL-activated LOV₃₉₀ molecule exhibiting absorption only at the UV-A range with a peak absorption at 390 nm. Figure after Christie et al. (2015).

1.3.4. NRL Proteins

NPH3/RPT2 -LIKE (NRL) family of proteins consists of proteins with the eponymous NPH3 domain, which is postulated to play a role in protein-protein interactions (Christie et al., 2018; Zhang et al., 2014). There are 33 NRL family proteins in angiosperms such as *Arabidopsis*, some of which have photosignalling and/or organogenesis related functions based on the modulation of auxin fluxes and their direction (Celaya and Liscum, 2005; Christie et al., 2018). A subfamily of three proteins out of 10 *Arabidopsis* NRLs with assigned functions have been discovered to interact directly with phot1, mediating plant blue light response signalling events downstream of phot1 and the resulting plant responses, detailed in **Table 1.3: NON-PHOTOTROPIC HYPOCOTYL3 (NPH3, syn. RPT3), ROOT PHOTOMORPHISM 2 (RPT2), and NRL PROTEIN FOR CHLOROPLAST MOVEMENT 1 (NCH1, syn. NRL31, AtSR1IP1)** (Christie et al., 2018; Suetsugu et al., 2016a). These NRL proteins modulate both auxin-dependent and -independent branches of the phot signalling (Suetsugu et al., 2016a).

NPH3, which is the best characterised NRL protein of the family, functions to regulate phot1 activation and phototropism, while RPT2 functions independently of auxin gradients through the regulation of NPH3 (Christie et al., 2018; Suetsugu et al., 2016a). Their mutants show defects in the shoot or root phototropism, or leaf positioning and expansion, as the proteins function in directing auxin hormone fluxes in response to light (Christie et al., 2018; Suetsugu et al., 2016a). NPH3 has **a**) an N-terminal coiled-coil domain, **b**) an NPH3 domain and **c**) a C-terminal BTB-POZ (bric-a-brac tram track broad – pox virus zinc finger) domain, (see **Figure 1.15**) thought to play a role as a substrate adapter for a cullin type E3 ligase, CRL3^{NPH3} that appears to target phot1 in BL. Phot1 function can be directed by ubiquitination modifications, as polyubiquitination results in the degradation of the phot1, while in contrast, monoubiquitination initiates the photoreceptor sub-cellular trafficking process (Choi et al., 2014; Christie et al., 2018; Suetsugu et al., 2016a). The C-terminal end is required for phot photoreceptor interaction and plasma membrane association (Christie et al., 2018).

Table 1.3 NRL-subfamily protein requirements and assigned functions in various phototropin-mediated responses in *Arabidopsis*.

+ : The process is dependent on the protein in question ; - : The process is independent of the protein.

Table modified after Christie et al. (2018).

Phot Response	NRL Proteins Required		
	NPH3	RPT2	NCH1
Phototropism	+	+	
Petiole positioning	+	+	
Leaf expansion	+	+	
Chloroplast accumulation		+	+
Chloroplast avoidance	-	-	-
Nuclear avoidance	-	-	-
Stomatal opening	-	-	-
Destabilization of chloroplast <i>Lhcb</i> mRNA	+		
Inhibition of hypocotyl elongation	-		
Circadian control of PS II photosynthetic efficiency	-		

Many NRL family proteins appear to be modified in a post-translational fashion. For example, NPH3 has a well-established activity pattern characterised by phosphorylation in the dark or by receptor desensitization in continuous light stimulus, and light-dependent dephosphorylation in BL (Christie et al., 2018). This modification is reversible and depends on the ambient light conditions. In etiolated seedlings, phosphorylated NPH3 functions by directly associating with phot1 from its C-terminus at the plasma membrane (Pedmale and Liscum, 2007). During the first positive phototropism, when the hypocotyl senses light with its phot1 photoreceptor, phot1 undergoes light-dependent autophosphorylation and controls the phosphatase performing the dephosphorylation of the interacting regulator NPH3. Dephosphorylation of NPH3 in response to BL activates it, leading to the dissociation of NPH3 and phot1 from each other, and the consequent relocalization of these proteins (Christie et al., 2018; Haga et al., 2015; Pedmale and Liscum, 2007). phot1 relocalizes into the cytosol and cytoplasmic strands (Wan et al., 2008), while NPH3 exhibits a rapid relocalization response into cytoplasmic microdomains which disappear both during continuous irradiation and in the dark (Haga et al., 2015). However, to fine-tune the plant responses in continuous irradiation, both NPH3 and RPT2 constitute a protein complex together with the activated phot1 photoreceptor during the second positive phototropism that occurs in continuous light (Christie et al., 2018; Haga et al., 2015). Therefore, RPT2 functions to modulate phot1 and NPH3 activity in constant light for receptor desensitization (Haga et al., 2015).

While most NRL proteins outside of the phot-dependent subfamily of NPH3, RPT2 and NCH1 have unknown functions, some of them have been found to regulate auxin-dependent plant development and organogenesis, and exhibiting partial functional redundancy with each other: NPH3 with RPT2, and RPT2 in turn with NCH1 (Christie et al., 2018; Reuter et al., 2021). Outside this subfamily, related NRL proteins called NAKED PINS

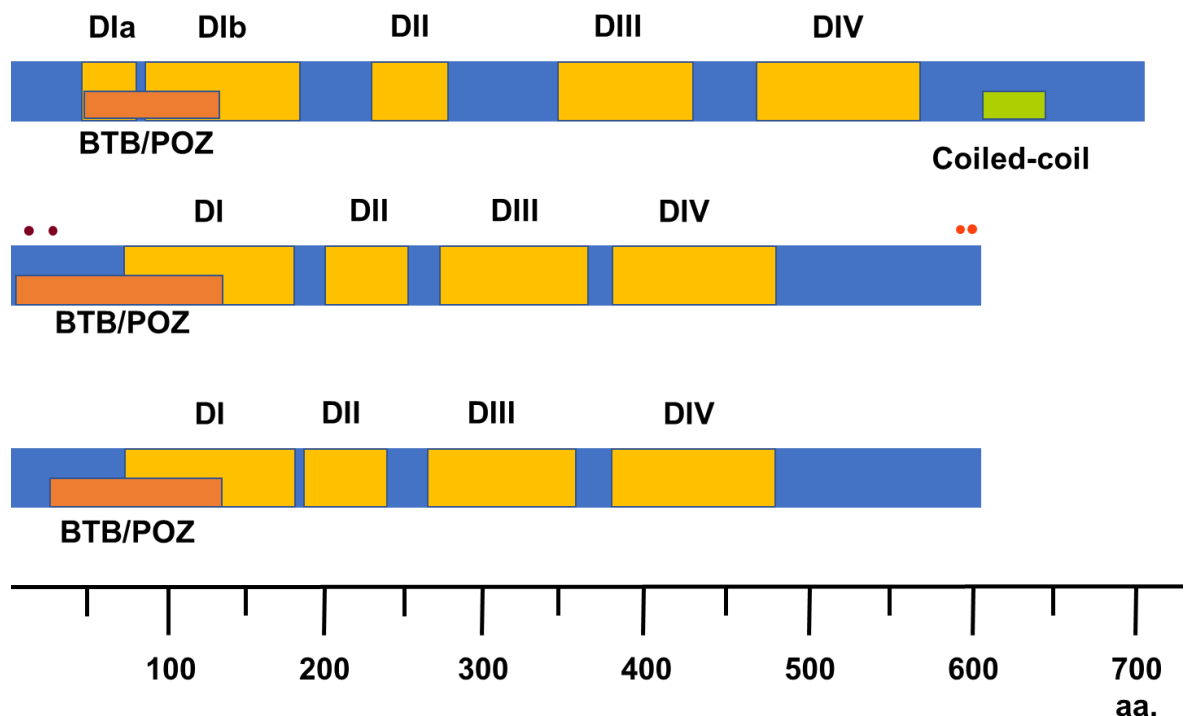


Figure 1.15 NRL-protein subfamily members exhibit conserved domain structures.

Schematic representation of three key NRL protein family members' protein domain structures, showing the BTB/POZ-domain, conserved NPH3 domain regions (DI-DIV), coiled-coil domains, and the relative protein sizes in number of amino acid (aa) residues. Purple and red dots represent the approximate locations of the putative dimerization and phosphorylation sites on the NCH1 protein, respectively. Note the similarity between NCH1 and RPT2 proteins, and the lack of the C-terminal coiled coil domain. **phot1**: Phototropin 1, **NCH1**: NRL PROTEIN FOR CHLOROPLAST MOVEMENT 1. Figures after Celaya and Liscum (2005), Suetsugu et al. (2016), and Suetsugu and Wada (2017).

IN YUCCA (NPY, aka. NRL6-7 and NRL20-21) are auxin efflux transporters that control auxin movement during plant development and gravitropism, and DEFECTIVE ORGANIZED TRIBUTARIES3 (DOT3, syn. NRL23) affects leaf shape and vein patterns by directing auxin fluxes during leaf morphogenesis and leaf vein formation (Christie et al., 2018; Suetsugu et al., 2016a). Indeed, DOT3 and another NRL protein, MACCHI BOU4 (MAB4, syn. NPY1) have been suggested to exhibit at least partial redundancy with NPH3 (Reuter et al., 2021), yet is not part of the core NRL subfamily consisting of NPH3, RPT2 and NCH1. One NRL protein with a known function, SETH6, is an essential protein for pollen germination and pollen tube formation during flower pollination and fertilization (Christie et al., 2018; Huang et al., 2013).

1.3.5. NCH1 in Plant Light Signalling

NCH1 and the functionally redundant RPT2 exhibit partially overlapping roles in the auxin-independent branch of phot downstream responses, especially in regulating the chloroplast accumulation (Suetsugu et al., 2016a). The structure of NCH1, with orthologs *StNRL1* in potato *Solanum tuberosum* (He et al., 2018; Yang et al., 2016) and *MpNCH1* in *Marcantia polymorpha* liverwort, is typical to the NRL proteins and very similar to that of RPT2, as seen in **Figure 1.15**. The protein structure includes **a**) a BTB-POZ domain, and **b**) an NPH3 domain (conserved regions I-IV) (Suetsugu and Wada, 2017). NCH1 is also known to exhibit E3 ubiquitin ligase substrate adapter activity (He et al., 2018; Zhang et al., 2014).

As blue light signalling through phot1 provides a key cue for plants and, therefore, controlling a range of physiological responses, NCH1 functions as a signalling node combining the phot photoreceptor signalling input about the environmental BL conditions with the auxin-independent chloroplast accumulation movement, see **Figure 1.16 A** (Christie et al., 2018; Suetsugu et al., 2016a). Consequently, NCH1 couples these light signals into physical movement provided by the intracellular cytoskeleton, made of a specialised type of actin, chloroplast (cp) actin (Suetsugu and Wada, 2016; Suetsugu et al., 2012). NCH1 therefore functions to optimise the chloroplast accumulation (see **Figure 1.16 B**) to promote light harvesting in favourable light conditions and to help the chloroplasts to navigate to the top of the mesophyll cells to maximise their light capture (Kong and Wada, 2014). However, NCH1 is not involved in the photoprotective phot2-mediated branch including the chloroplast avoidance reaction nor stomatal opening (Suetsugu et al., 2016a). In the intracellular environment, NCH1 localizes in the cytoplasmic side of the plant plasma membrane similarly to phot1 and NPH3 (Christie

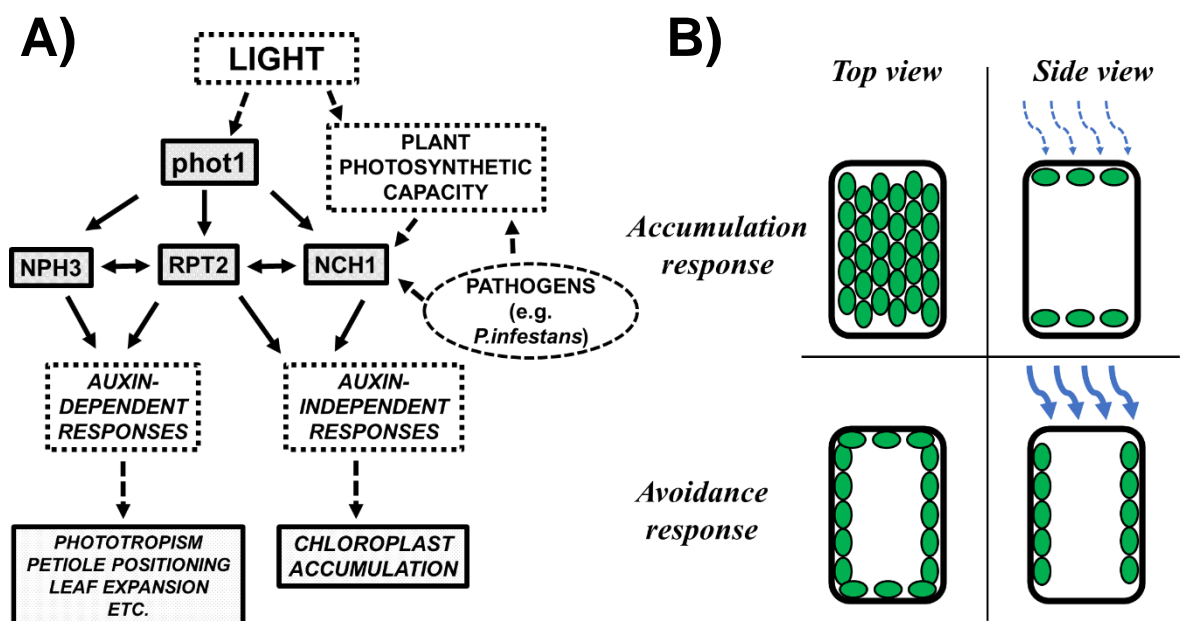


Figure 1.16 Light signalling pathways and plant immunity are connected through chloroplasts.

A) Flow chart of light reception pathways from the initial light signal (top) to photoreception by phot1 and subsequent downstream signalling by NRL proteins. Photosynthetic machinery and photoreception are hypothesised to converge at NCH1, which determines chloroplast accumulation movement, as chloroplasts also mediate defensive functions against pathogens.

B) Chloroplast movement types, including the photosynthesis-maximising accumulation and photoprotective avoidance responses. Chloroplast accumulation response governed by both NCH1 and the functionally redundant RPT2 occurs in low BL conditions. In contrast to this, chloroplast avoidance reaction involving phot2 signalling independent of NRL proteins occurs in damagingly high light intensities, causing the chloroplasts to escape to the peripheries of the cells, with the topmost chloroplasts sacrificing themselves to shade both other chloroplasts and the nucleus to protect them from photodamage. Figure B after Suetsugu and Wada (2007)

et al., 2018), but unlike in the case of phot1 and NPH3, the preliminary results suggest NCH1 does not exhibit dynamic light induced localization patterns. In addition, the potato ortholog *StNRL1* has been reported to function as a homodimer (He et al., 2018). Bioinformatics analysis has also revealed, that NCH1 has putative phosphorylation sites and dimerization sites, marked in red in **Figure 1.15**.

1.3.6. Convergences of Plant Light Signalling and Immunity: Chloroplasts and NCH1

Chloroplasts play a multifaceted role in plant defence responses. Chloroplast photosystems PSII and PSI are central to the generation and management of ROS, which is an essential intracellular immunity signal during the plant MTI and ETI responses (Lu and Yao, 2018). ROS is generated as a dangerous side product by the photosynthetic light capture and electron transport processes in the presence of excess photons, but in small quantities, ROS is also required for several immunity-related functions: **1)** it is used in signalling for defence gene activation; **2)** utilized directly as an antimicrobial; **3)** it triggers cell wall rigidification; **4)** it is required for antimicrobial, e.g. phytoalexin production; **5)** For the HR and **6)** the cellular lipid peroxidation leading to the HR; **7)** for vesicle trafficking processes; and **8)** for the internalisation and trafficking of PRRs after MTI receptor activation (Lu and Yao, 2018). As plants attempt to minimise ROS generation in normal circumstances, immunity signalling must shift this balance from tight control over ROS production at the chloroplast photosystems towards higher tolerance and generation of more cellular ROS available for immune response (Sowden et al., 2018). Therefore, because ROS is an important signalling factor for immunity, *Pst* effectors have consequently been found to downregulate photosynthesis and CO₂ assimilation very early on during the infection: their effectors were found to target nuclear-encoded chloroplast-targeted genes (NECGs) to reduce photosynthesis-related gene expression and to diminish the MTI signature ROS burst (de Torres Zabala et al., 2015). Similarly, metabolic modelling found plant photosynthesis to be down-regulated by the oomycete pathogen *Phytophthora infestans* effectors during infection (Botero et al., 2018).

Chloroplasts are very dynamic organelles and also exhibit movement patterns and morphology changes outside the binary accumulation/avoidance movement patterns. During pathogen challenge, chloroplasts have been reported to generate stroma-filled projections called stromules, which can link the chloroplasts with different intracellular organelles including the nucleus (Caplan et al., 2015). Stromules are often seen in response to stress, including the external application of plant signalling molecules such as ROS, H₂O₂, and SA, and have therefore been proposed to provide connections for signalling and transport functions (Caplan et al., 2015; Kumar et al., 2018; Savage et al., 2021): indeed, Caplan et al. (2015) found stromules to be a positive HR signal during ETI, but not during a lower intensity MTI. Chloroplasts also exhibit distinct movement and morphology change patterns during the plant ETI response: The first step is the upregulation of chloroplast stromules, the second is the initiation of stromule-to-nucleus connections, third is the physical chloroplast movement and perinuclear clustering, and the last one the accumulation of defence-related proteins and ROS into the nucleus before commencing the cellular HR (Caplan et al., 2015). Therefore, chloroplasts and stromules are thought to be a potential positive feedback mechanism to trigger the HR, while also containing and lining the affected cell's area. This is possibly for cell-to-cell communication with the surrounding cells after HR (Caplan et al., 2015).

An example on the proposed mechanism and function of the stromules during ETI-type immunity (Caplan et al., 2015) is presented in **Figure 1.17**. Tobacco mosaic virus effector p50 is bound by chloroplast protein N-receptor interacting protein 1 (NRIP1), which moves out from the chloroplast into the cytoplasm to associate with the p50 effector. The p50-NRIP1 complex is recognized by the guard NB-LRR R-protein N as a type of indirect recognition, as the guardee NRIP1 bridges the connection between the R-protein and the p50 effector, and the p50 effector can only be sensed if NRIP1 is present. Relocalization of NRIP1 into the cytoplasm and the N receptor activation initiate the pro-immunity signalling and the chloroplast stromule formation. Stromules bridge the spatial difference between the signal-producing chloroplast and the signal receiving nucleus, and therefore cytoskeletal framework of actin and myosin XI and other cytoskeleton-interacting proteins (e.g. actin-anchoring protein WIT) ensure physical proximity between the chloroplast and the nucleus. As chloroplasts are the source of pro-defence signalling molecules such as SA and ROS during ETI, the physical proximity between the stromule/chloroplast and the nucleus increases the local concentration of chloroplast-produced pro-immunity signalling components (ROS, SA, NRIP1) in the areas immediately surrounding the nucleus. Furthermore, cytosolic ROS and SA-signals promote further stromule formation from the chloroplasts as a positive feedback mechanism. Therefore, the high pro-defence molecule concentration in the perinuclear area is important to initiate a further positive feedback loop between the chloroplast and the nucleus, eventually culminating in a successful ETI defence signalling and response including the HR. (Caplan et al., 2008, 2015).

BL signalling and chloroplast movement machinery are well connected in land plants, with phot1-dependent processes coordinating and polymerising short filament cp-actin and phot2-dependent avoidance processes depolymerising cp-actin for avoidance movement (Kong et al., 2020). On the chloroplast outer envelope, CHUP1 protein provides nucleation and connection points for the actin filaments, linking the plasma membrane and chloroplasts together, while BL regulates CHUP1 distribution in a phot-dependent manner (Kong et al., 2020; Suetsugu et al., 2016b). Stromule movement is also mediated by the actin cytoskeleton, and

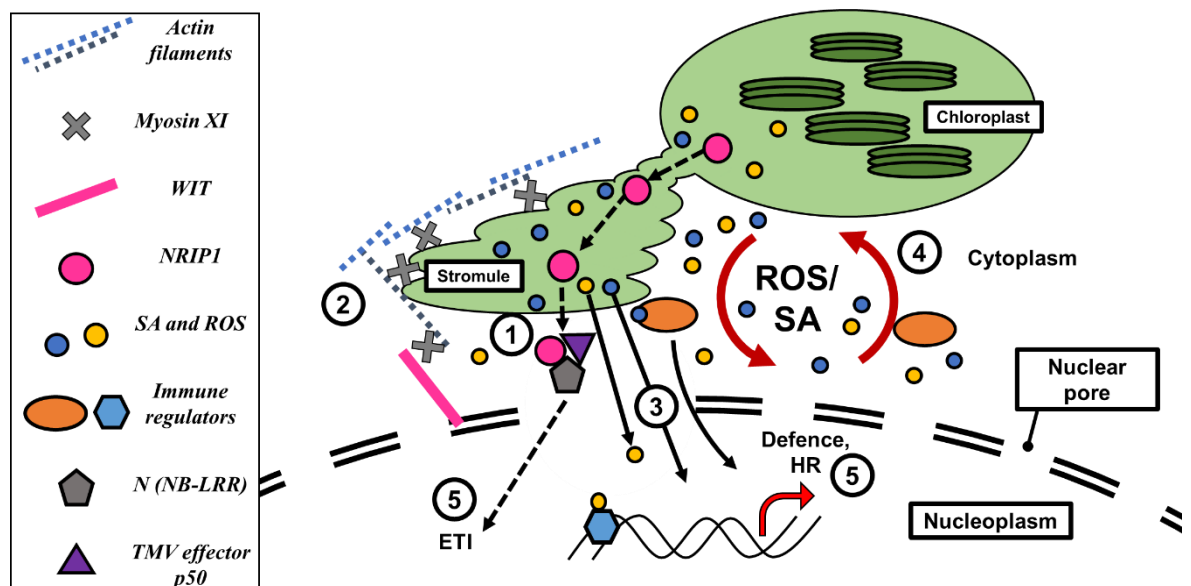


Figure 1.17 Model for chloroplast stromule function in pro-immunity signalling during ETI.

1) Chloroplast protein NRIP1 relocates in the cytoplasm and forms a complex with TMV effector p50 (black dashed arrows), and this complex is recognized by NRIP1's guard protein NB-LRR called N. **2)** Stromule formation commences, with the actin cytoskeleton and their interacting proteins (e.g. WIT) anchoring the stromule into the nuclear envelope. **3)** The transport of pro-defence molecules, e.g. SA and ROS (black arrows), from the chloroplast to the cytoplasm, increasing local concentration of pro-immune and pro-HR signals in the areas immediately surrounding the nucleus, initiating **4)** a positive feedback loop (red arrows) and **5)** the ETI pro-defence signalling together with HR and systemic signalling into the surrounding tissues. Figure after Gu and Dong (2015) and Caplan et al. (2015).

interestingly, the chloroplast movement-associated protein *CHUPI* has also been found to be an important factor for chloroplast morphology and stromule regulation during pathogen challenge. *chup1* knockout plants have been reported to exhibit a constitutive stromule phenotype with higher rates of HR in comparison to wild type cells (Caplan et al., 2015).

As chloroplasts are believed to evolutionarily originate from the endocytosis event of a photosynthetic prokaryote (Zimorski et al., 2014) there is intriguing new evidence of chloroplasts having retained some ability of their single-celled prokaryote progenitors to contribute to immunity against other incoming microbial threats. Savage et al. (2021) found chloroplasts to mobilise, accumulate and associate with the oomycete haustorial membrane during *P. infestans* infection in 40% of the examined *P. infestans* haustoria. This active movement response was light-independent but actin-dependent, and the chloroplasts returned to the haustoria after attempts to pull them away from it using optical tweezers. They also exhibited an increased number of stromules in comparison to the mock-treated cells that were also directed towards the host-pathogen interface. However, the expression of a pathogenic effector that down-regulates MTI in *Nicotiana benthamiana* was found to result in a reduced number of stromules, providing further evidence on their defence-related function (Savage et al., 2021). While the genetic mechanisms of these chloroplast movement patterns are unknown and the possibility of pathogen effector interference cannot be excluded (Savage et al., 2021), cellular components regulating chloroplast movement could be potential targets for pathogen effectors during ETS.

In addition to its function in phot signalling, there is some evidence for the direct role of NCH1 in immune functions in plants, intriguingly independent of the role of NCH1 in BL signalling and chloroplast function. Investigations by Zhang et al., (2014) and He et al. (2018) reported NCH1 to function as a ubiquitin E3 ligase substrate adapter, performing the targeted ubiquitination of plant immune targets. However, while He et al. (2018) hypothesised the potato ortholog of NCH1, *StNRL1*, to be a negative regulator of pro-immune response components, therefore preventing autoimmunity and a type of HR, INF1-triggered cell death (ICD), in the absence of pathogen challenge, Zhang et al., (2014) found *AtNCH1* to be a positive regulator of plant defence response, removing the repression of SAR inducing genes such as *EDS1* in response to pathogen-induced Ca^{2+} flux. Furthermore, the potato ortholog *StNRL1* was also found to be a susceptibility or S-factor, meaning a plant protein targeted by the pathogen – in this case the oomycete *P. infestans* – effectors (He et al., 2018; Yang et al., 2016), suggesting NCH1 having an immunity-related function evolutionarily important enough for the pathogen to evolve a specialised effector protein for rendering NCH1 dysfunctional. The experimental evidence for the role of NCH1 in plant immunity will be reviewed more closely in section 4.1.

1.4. Experimental Aims and Strategies

This report describes the theoretical background of the plant immune and photoreceptor biology, and strategies and approaches taken to characterise the links between plant blue light and immunity signalling. The main aim of this project is to gain a better understanding of the links between plant BL and immunity signalling by studying the potential significance of *AtNCH1* protein in *Arabidopsis thaliana* immunity. This work entails the biochemical characterisation of the NCH1 protein and investigation of its involvement in these pathways. Therefore, the experimental foci of the project can therefore be divided into two main branches: **1)** the biochemical properties and protein biology of the target protein *AtNCH1*, and **2)** the role of *AtNCH1* in plant immunity against *Pseudomonas syringae* pv. *tomato* DC3000.

The main experimental strategies in the structure-function studies of the NCH1 protein are as follows: **a)** studies on the sub-cellular localization of *AtNCH1* in response to light, by utilising fluorescent protein mCit-tagging and time lapse confocal microscopy in stable transgenic *Arabidopsis* hypocotyls, and following the localization of the fluorescence-tagged mCit-NCH1 protein from dark-grown etiolated seedlings to sustained 10 minute BL irradiation; **b)** analysis of the literature concerning dimerization of the potato ortholog *StNRL1*, and the introduction of synonymous mutations to the *AtNCH1* protein by mutagenesis PCR to create functional NCH1^{D28N-K42Q} BiFC vectors; **c)** use of the both constructed BiFC vectors in the dimerization studies of NCH1, and to study the effects of dimerization mutations D28N and K42Q on the sub-cellular localization of the NCH1 protein, **d)** investigation of the NCH1 phosphorylation status by the introduction of putative phosphorylation site mutations NCH1^{S602A-S604A} to produce an initial binary vector construct for the future study of the roles of C-terminal phospho-mutations on the NCH1 phosphorylation status, intracellular localization and dimerization status; **e)** investigation of the effects of *nch1* BL signalling mutations on plant bacterial disease resistance using *Arabidopsis-Pst* DC3000 pathosystem.

Plant pathology and infection studies were conducted on the *Arabidopsis* model system by developing modified flood assay methods based on those originally devised by Ishiga et al. (2011, 2017). The methods were used with the model plant pathogen *Pseudomonas syringae* pv. *tomato* DC3000 to monitor the susceptibility of wild type (WT) Columbia (Col-0) ecotype *Arabidopsis* and various *nch1* and NRL mutant *Arabidopsis* plants to infection. These assays were conducted on plants with the *rpt2* mutant background to prevent potential functional redundancy between NCH1 and RPT2 proteins.

2. Materials and Methods

2.1. Bioinformatics

Sequence information on the selected *Arabidopsis* genes was gathered from *The Arabidopsis Information Resource* (TAIR; www.Arabidopsis.org) and *Genbank*, with the *NCH1* gene locus number AT5G67385, and splice variant AT5G67385.1 used to produce the protein sequence. For *RPT2*, the gene locus number AT2G30520 was used, and for *NPH3*, locus number AT5G64330. All nucleotide-to-amino acid translations were done from coding sequence information using Benchling. For *35S-SPYNE/SPYCE* BiFC vectors, sequence information was gathered from *Genbank* sequence database with ID EU796372.1. Plasmid maps were constructed using Benchling.

For the *NCH1* protein expression profiles in *Arabidopsis* tissues and organs, BAR eFP ePlant browser (Sullivan et al., 2019; Waese-Perlman et al., 2021; Winter et al., 2007) was used. The computational prediction of the *NCH1* subcellular localization was done using BAR eFP ePlant/eCell browser with data from the SUBcellular location database for *Arabidopsis* proteins, SUBA4 (Hooper et al., 2017). Similarly for the *NCH1* protein-protein interactions chart, the BAR *Arabidopsis* Interactions viewer database was used, originally introduced by Geisler-Lee et al. (2007) and last updated in November 2018, also incorporating data from Biomolecular Interaction Network Database, BIND (Popescu et al., 2007, 2009), and localization data from SUBA4 (Hooper et al., 2017). The computational *NCH1* crystal structure was predicted using the machine learning/AI protein structure prediction tool AlphaFold (Senior et al., 2020).

EMBOSS Pepinfo was used to generate amino acid characteristic overview plot for the *AtNCH1* protein. Hydropathy plots were made using EMBOSS Pepwindow and Kyte and Doolittle methodology, with an amino acid window of 19 aa to predict potential transmembrane domains and helices from the translated sequences detailed above. Separate probability plots were generated for transmembrane regions using TMHMM 2.0 (Krogh et al., 2001). A phylogenetic tree for *NCH1* and related NRL proteins was made using PANTHER 16.0 (Mi et al., 2021).

The putative phosphorylation sites in the *AtNCH1* protein were screened *in silico* using PhosPhAt 4.0 database (Heazlewood et al., 2008), using protein prediction search with the *AtNCH1* TAIR accession number AT5G67385.1.

Multiple sequence alignment between *AtNCH1*, *AtRPT2* and *AtNPH3* was done using Clustal Omega (Sievers et al., 2011), with protein sequence data from UniProt database.

2.2. Localization of NCH1 protein in *Arabidopsis thaliana*

Sterile Plant Tissue Cultures: ½MS (Murashige-Skoog) Medium

Sterile half-strength Murashige-Skoog (½ MS) plant tissue culture medium (1 L, pH 5.6) was made by dissolving 0.222% (w/v) of MS basal salts (Sigma Aldrich, Missouri, US) and 0.5% (w/v) sucrose in double-distilled H₂O while stirring. The pH of the solution was adjusted to 5.6 using 2 mM MES and 0.5 mM Tris, and finally, 1% (w/v) of plant tissue culture-compatible agar (Sigma Aldrich, Missouri, US) was added. The final volume was adjusted to 1 L using double-distilled H₂O, and the resulting solution was bottled in 500mL quantities in 1L volume bottles. The bottles were autoclaved for sterilization using the standard 121°C for 30 min cycle, after which the media was poured on 12cm x 12cm square Petri dishes (Greiner AG, Kremsmünster, Austria) in sterile lateral flow hood conditions, and stored in 4°C fridge conditions until use.

***Arabidopsis thaliana* Seed Sterilisation and Sterile Tissue Cultures**

Transgenic homozygous *Arabidopsis* seeds of genotypes *NCH1::mCit-NCH1* (pDEST, hygromycin resistant), courtesy of Dr. Noriyuki Suetsugu (University of Tokyo), and *NPH3::GFP-NPH3*, courtesy of Dr. Stuart Sullivan (University of Glasgow), were sterilised using methodology by Ishiga et al. (2017). The sterilised seeds contained in microfuge tubes were cold stratified in dark +4°C conditions for 3 days. After this, they were plated on 12cm x 12cm square Petri dishes (Greiner AG, Kremsmünster, Austria) with ½ MS medium (see above), in a density of 16 seedlings per plate. The sealed plates were kept in the laboratory ambient light conditions for 1 h to initiate germination, after which they were wrapped in aluminium foil and grown in the dark for 3 days at room temperature.

Confocal Microscopy and Time Lapse Imaging

For confocal microscopy, the dark-grown etiolated hypocotyls were mounted on microscope slides under a red safelight. *NPH3::GFP-NPH3* plants (courtesy of Dr. Stuart Sullivan, University of Glasgow) were used as a positive control. The samples were scanned, imaged and BL treated using a Leica S8 confocal microscope, and pictures recorded as Z-stacks. The experiment was repeated three times for both *NCH1::mCit-NCH1* and *NPH3::GFP-NPH3* genotypes.

For all irradiation and scanning, the confocal laser power was set to 5%. For confocal microscopy, settings of 500-530 nm were used for the collection of green fluorescent protein (GFP) and mCitrin (mCit) protein fluorescence. Chloroplast autofluorescence cancelling was set to 660-800 nm. It is important to pay attention to the excitation spectra of the fluorescent proteins used (GFP and mCit) and the action spectrum of photos, as the same BL treatment is enough to provide BL treatment for both photos to activate the BL signalling pathway and GFP in the case of the control protein NPH3, but not for mCit, with which separate BL and fluorophore excitation wavelengths are required during imaging, at 488 nm and 514 nm respectively.

For studies on the dynamic NCH1 protein localization in *Arabidopsis* hypocotyls, the confocal microscope laser scanning was used as a source of BL irradiation. In this method (described in **Table 2.1**), the first step was the imaging step, with the confocal microscope set to scan the sample a 15-layer Z-stack with the wavelength appropriate for the chromophore (488 nm for GFP or 514 nm for mCitrin). After this, the second step was the BL treatment, where the sample was irradiated with a confocal microscope blue 488 nm laser for 5 minutes. In the third step, the microscope was set to scan the same cells again as a 15-layer Z-stack, after which the fourth step was a second BL treatment, and the last one a Z-stack imaging step. Therefore, over the course of the protocol, the imaging would be repeated 3 times, resulting in 3 images, and a 5-minute BL treatment would be done twice. The confocal settings were maintained constant for all the samples to ensure even blue light treatment. The final adjustment of images, including the separation into 3 channels, and image brightness and contrast adjustment, was performed using FIJI software (Schindelin et al., 2012) using the same settings to all images in the experiment.

Table 2.1 Confocal microscope protocol and parameters for time lapse imaging during NCH1 localization experiment.

Above: Confocal microscope settings for the imaging steps and Z-stack scans.

Below: Protocol for the sample imaging and BL treatment scans during the dynamic protein localisation experiment.

Format	1024 x 1024 px
Speed	600
Line average	6
Z-stack	15 steps at 1 μ m step, total 14 μ m
Zoom	3x
GFP/YFP smart gain	393,6%

Step	Action	Duration	Wavelength for GFP samples	Wavelength for mCit samples
1	Imaging: Z-stack scan	2 min 20 s	488 nm	514 nm
2	BL treatment	5 min	488 nm	488 nm
3	Imaging: Z-stack scan	2 min 20 s	488 nm	514 nm
4	BL treatment	5 min	488 nm	488 nm
5	Imaging: Z-stack scan	2 min 20 s	488 nm	514 nm

2.3. NCH1 Dimerization

*Site Directed PCR Mutagenesis of Putative Dimerization Mutant *nch1*^{D28N-K42Q}*

The putative dimerization-deficient *nch1* variant *nch1*^{D28N-K42Q} was constructed using PCR site-directed mutagenesis to mutagenize putative salt bridge sites at D28 and K42 as follows (with the mutated nucleotide in bold and underlined):

D28N: F-primer sequence:

5' - TTC TTC TCA AGA AGT ATC TAG **TAA** TGT CAC CGT TCA TGT AGG AG - 3' ;

D28N: R-primer sequence:

5' - CTC CTA CAT GAA CGG TGA CAT TAC TAG ATA CTT CTT GAG AAG AA - 3' .

K42Q: F-primer sequence:

5' - GCT TCG TTT TCA CTG CAC **CAG** TTT CCA CTC ATG TCA A - 3' ;

K42Q: R-primer sequence

5' - TTG ACA TGA GTG GAA ACT GGT GCA GTG AAA ACG AAG C - 3' .

For PCR thermocycler settings, see **APPENDIX 1**. The samples were *DpnI* treated (Promega, Wisconsin, US) after PCR to remove any leftover template and purified using a PCR purification kit QIAquick (Qiagen, Hilden, Germany). The double mutant constructs were amplified using Subcloning Efficiency™ DH5α *Escherichia coli* cells (Thermo Fisher Scientific, Massachusetts, US), purified using a Miniprep kit (Qiagen, Hilden, Germany) and sequenced (Eurofins Genomic Services, Wolverhampton, UK) to confirm the presence of mutations.

PCR methodology was also used to incorporate the desired Gibson assembly compatible overhangs to the *nch1*^{D28N-K42Q} fragment:

35S-SPYNE & 35S-SPYCE Forward primer sequence:

5' - GGCGCGCCACTAGTG GATCC **ATGTCAGCAAAGAAGAAAGATCT** - 3'

35S-SPYNE Reverse primer sequence:

5' - ACTTTTGCTCCAT CCCGGG **AGAGTGTCTCCGATCTTT** - 3'

35S-SPYCE Reverse primer sequence:

5' - CGTATGGGTACAT CCCGGG **AGAAATAGAGTGTCTCCGATCTTT** - 3'

where italicised part is vector-specific, underlined is a reconstituted restriction site (*Bam*HI for forward primer and *Sma*I for reverse primer), and bolded is NCH1 specific sequence. For PCR thermocycler settings, see **APPENDIX 1**.

Gibson Assembly of the NCH1 fragment and BiFC vectors

The PCR-produced *nchI*^{D28N-K42Q} insert already had restriction site compatible overhangs for Gibson assembly. Therefore, both the insert and the BiFC vectors *35S-SPYNE* and *35S-SPYCE* (Walter et al., 2004) were double digested using *Bam*HI and *Sma*I restriction enzymes (both by New England Biolabs, Massachusetts, US) to ensure directional ligation of the *nchI*^{D28N-K42Q} insert and the vector. The insert and vector were combined using Gibson assembly by NEBuilder HiFi Assembly Mix (New England Biolabs, Massachusetts, US) as per manufacturer's instructions, with an insert-to-vector ratio of 3:1 determined using a molar ends calculator to be 75 ng of insert to 100 ng of vector. To monitor for the incorporation of the *nchI*^{D28N-K42Q} insert in the *35S-SPYNE/35S-SPYCE* vector, samples of both the empty vector and the ligation reaction product were visualised on a 0.8% agarose gel with NEB 1 Kb Plus DNA Ladder markers (New England Biolabs, Massachusetts, US).

The same Gibson assembly protocol was used to combine both the target *NCHI* fragments WT *NCHI* and *nchI*^{D28N-K42Q} with the desired *35S-SPYNE* and *35S-SPYCE* vectors. Positive control constructs *35S-SPYNE-NPH3* and *35S-SPYCE-NPH3* were kindly offered by Mr. Franco Vegliani (University of Glasgow). The ready combined BiFC constructs, which are large low copy number plasmids, were amplified using NEB 5 α High Efficiency (New England Biolabs, Massachusetts, US), purified with Miniprep kit (Qiagen, Hilden, Germany) and sequenced (Eurofins Genomic Services, Wolverhampton, UK).

Transient expression system: Agrobacterium Transformation and Infiltration of *N. benthamiana* leaves

Luria-Bertani (LB) broth and agar (pH 7.2), were made from granulated growth media concentrate, "LB-Broth Granulated" and "LB-Agar Granulated" (both Melford Laboratories, Suffolk, UK) respectively, according to the manufacturer's instructions. The solution was bottled in 500 mL quantities in 1L volume bottles and autoclaved for sterilization using the standard 121°C for 30 min cycle.

Electrocompetent GV3101 *Agrobacterium* cells (50 μ l aliquots in microfuge tubes, stored in -80°C) were defrosted on ice, after which 50 μ l of 10% glycerol was added to the cells. Desired plasmids used for the transformation (see **Table 2.2**) were diluted to 100 ng/ μ l concentration. A total of 200 μ l of plasmid was added into the microfuge tube containing the cells, after which the cells were incubated on ice for 30 min. The cells were then transferred into ice-cooled Bio RAD (Hertfordshire, UK) electroporation cuvettes, and electroporated using Bio RAD GenePulser Xcell Microbial system, with the manufacturer's pre-set *Agrobacterium tumefaciens* waveform settings. After electroporation, 900 μ l of ice-cooled LB broth (Melford Laboratories, Suffolk, UK) was added to the cuvette, and the resulting mix was transferred into fresh sterile microfuge tubes. The tubes were then placed in a 28°C shaking incubator for a minimum of 2 hours, and 20 μ l and 200 μ l volumes of these transformed cells were plated on pre-warmed kanamycin-gentamicin (concentration for kanamycin 50 μ g/mL media, gentamicin 25 μ g/mL) double antibiotic LB-agar (Melford Laboratories, Suffolk, UK) Petri dishes (\varnothing 9cm, Sterilin™ Thermo Fisher Scientific, Massachusetts, US). The resulting plates were sealed using Parafilm (Amcor Plc., Zürich, Switzerland) and incubated in a 28°C incubator for 2 days.

The bacterial solution for *N.benthamiana* infiltration was prepared as follows. One colony of the desired transformed *Agrobacterium* was picked from the fresh plates using a sterile plastic loop and diluted into 5mL of LB broth (Melford Laboratories, Suffolk, UK) including gentamicin (25 µg/mL of LB-broth) and the selection antibiotic kanamycin (50 µg/mL LB) and incubated overnight in a 28°C incubator. The suspended cells were centrifuged the next day in a Sorvall Legend centrifuge (Sorvall Thermo Scientific, Massachusetts, US) for 10 mins at 3500 rpm, and resuspended in 10 mM MgCl₂ 10 mM MES (pH 5.6) infiltration buffer. The resulting solution was placed in a 50 mL Falcon tube (Greiner AG, Kremsmünster, Austria) and the bacterial solution was measured using an Eppendorf Biophotometer (Eppendorf, Stevenage, UK) and adjusted for optical density (OD₆₀₀) of 0.4. As BiFC technique requires both the corresponding 35S-SPYNE and 35S-SPYCE vectors to be present and co-infiltrated at the same time into the same leaf tissue, the desired *Agrobacterium* solutions were mixed in 1:1 ratio of 35S-SPYNE and 35S-SPYCE vectors in the following combinations (**Table 2.2**):

Table 2.2 BiFC co-infiltration combinations for studying NCH1 protein dimerization *in planta*.

Table shows the genotypes of the *Agrobacterium* infiltration solutions. The solutions are always co-infiltrated in corresponding 35S-SPYNE + 35S-SPYCE combinations to introduce both N- and C-terminal halves of the YFP-reporter into the plant cells simultaneously.

	SPYNE	SPYCE	Controls
1	35S-SPYNE-NCH1 WT	35S-SPYCE-NCH1 WT	
2	35S-SPYNE-NCH1 ^{D28N-K42Q}	35S-SPYCE-NCH1 ^{D28N-K42Q}	
3	35S-SPYNE-NPH3	35S-SPYCE-NPH3	(Positive control)
4	35S-SPYNE (Empty vector)	35S-SPYCE-NCH1 WT	(Negative control)
5	35S-SPYNE-NCH1 WT	35S-SPYCE (Empty vector)	(Negative control)
6	35S-SPYNE (Empty vector)	35S-SPYCE (Empty vector)	(Negative control)

After mixing the co-infiltration solutions, the bacterial suspension was let sit on the bench for at least an hour. After this, the *N.benthamiana* leaves were infiltrated from the abaxial side with 1 mL disposable Luer syringes, the infiltrated area sketched on the leaf using a permanent marker, and the infiltrated plants moved into SANYO growth chambers (16h day/ 8h night cycle conditions, with the day time temperature set to 26°C and humidity to 60%, and night-time temperature to 18°C and 70%) for 3 days to allow the transient expression of the desired BiFC proteins before harvesting of leaf tissue discs for confocal microscopy and Western blots.

Confocal Slide Preparation and Mounting of Leaf Samples on Microscope Slides

For confocal microscopy, leaf discs (Ø0.8cm) were harvested by punch method. The leaf discs were vacuum treated using a syringe, and with the mounted abaxial side up on the glass microscope slides.

Confocal microscopy

The samples were imaged using a Leica S8 confocal microscope, and the pictures recorded as Z-stacks. The confocal settings (**Table 2.3**) were maintained constant for all the samples. The experiment was repeated 5 times. The final adjustment of images, including the separation into 3 channels, and image brightness and contrast adjustment, was performed using FIJI software (Schindelin et al., 2012) using the same settings to all images in the experiment.

Table 2.3 Confocal microscope settings used for the imaging and Z-stack scans during the BiFC dimerization experiment.

Format	1024 x 1024 px
Speed	600
Line average	6
Laser/ Excitation Wavelength	514 nm, 5%
Collection Wavelengths	500-530 nm
Chloroplast autofluorescence cancelling	660-800 nm
Z-stack	10-15 μ m stack depending on the size of the imaged cell, 1 μ m step size
Zoom	2x
YFP smart gain	393,6%

Western Blots from Infiltrated *N.benthamiana* Leaf Tissue

For Western blots, 3 leaf discs (\varnothing 0.8cm) per infiltrated leaf, corresponding to the leaves imaged in the confocal pictures, were harvested by punch method. The leaf discs, 3 per microfuge tube, were flash-frozen in liquid nitrogen and stored in -80°C freezers.

Protein extraction from the leaf tissue was done by adding 150 μ l of 2x Laemmli sample buffer (125 mM Tris pH 6.8, 4% SDS, 20% glycerol, 10% β -mercaptoethanol, 0.004% bromophenol blue, dH_2O) and grinding the frozen leaf discs in the buffer using a small plastic microfuge tube pestle until homogenous. The samples were boiled using a $+95^{\circ}\text{C}$ heat block for 5 min, after which the samples were spun in a tabletop microcentrifuge at full speed (13 000 rpm) for 5 min. After centrifugation, the supernatant was transferred into fresh microfuge tubes to wait for loading onto gels.

7.5% acrylamide gels were hand-cast using the 0.75 mm glass slide frames and a gel casting kit by Bio RAD. The gels were loaded using 15 μ l of each sample and 5 μ l of Thermo PageRuler Plus Pre-stained 10-250 kDa (Thermo Fisher Scientific) protein ladder, and the SDS-PAGE was run in 1x SDS Running buffer (25 mM Tris, 190 mM glycine, 3.5 mM SDS, dH_2O). The gel was transferred onto a Whatman® Protran® nitrocellulose membrane (Cytiva, Sheffield, UK) using a semi-dry Bio RAD Trans-blot Turbo Transfer system, following manufacturer's instructions and "Low molecular weight" preset programme. The membrane was stained with Ponceau-S / acetic acid solution to examine the protein staining and placed inside a plastic sleeve to visualise

Rubisco large subunit (RbcL) as a loading control. The membrane was blocked for 1h in room temperature on a shaker using a membrane blocking solution made of 8% Marvel skimmed milk powder suspended in 0.1 mM pH 7.4 TBS-T [10% TBS (137 mM NaCl, 27 mM KCl, 100 mM Tris, dH₂O), 0.5% Tween20, dH₂O].

The primary antibody, either anti-HA (monoclonal mouse, 1:10 000 dilution, catalogue # 26183, Invitrogen Thermo-Fisher, Illinois, US) or anti-cMyc (monoclonal rabbit, 1:5000 dilution, catalogue # C3956, Sigma Aldrich, Missouri, US) depending on the target protein tag in question, was added to the 8% blocking solution and incubated overnight in +4°C, after which the membrane was washed twice in TBS-T for 10 minutes. After this, the secondary antibody was added, either anti-mouse 2° (1:10 000 dilution, Promega, Wisconsin, US) for anti-HA, or anti-rabbit 2° (1:10 000 dilution, Promega, Wisconsin, US) for anti-cMyc. The blot was incubated in the secondary antibody solution in room temperature for 1-2h. The final washes were done with TBS-T three times, for 10 minutes each, after which the blot was rinsed with TBS (137 mM NaCl, 27 mM KCl, 100 mM Tris, dH₂O). The development and visualisation of the blot were done with a Fusion chemiluminescence imaging system (Vilber Lourmat, France), using Pierce® ECL Plus (Thermo Scientific, Illinois, US) Western blotting substrate kit according to the manufacturer's instructions.

2.4. NCH1 Phosphorylation

*Site Directed PCR Mutagenesis of Putative Phosphorylation Mutant *nch1*^{S602A-S604A}*

The putative phosphorylation deficient *nch1*^{S602AS604A} insert with restriction site overhangs was constructed using PCR site-directed mutagenesis. A plasmid containing the putative phosphorylation defective *nch1*^{S602AS604A} sequence (courtesy of Dr. Noriyuki Suetsugu, University of Tokyo) was modified to contain *KpnI* and *BamHI* restriction site overhangs. The primer sequences were as follows, with the mutated nucleotides in bold and underlined, and added restriction sites italicised and underlined:

***nch1* insert:**

F-primer sequence

5' - A AAA GGT ACC TTA TGT CAG CAA AGA AGA AAG ATC T - 3' ;

R-primer sequence:

5' - A AAA GGA TCC TCA AGC AAT AGC GTG TCT CCG A - 3' .

For PCR-thermocycler settings, see **APPENDIX 1**.

Ligation of the AtNCH1^{S602AS604A} insert and NPH3::AtNCH1 -GFP vector

The PCR-produced *nch1*^{S602AS604A} insert with the added overhangs, and the *pEZR(K)LC* binary vector (courtesy of Dr. Noriyuki Suetsugu, University of Tokyo), containing the *NPH3::NCH1 -GFP*, were double digested using *KpnI* and *BamHI* restriction enzymes (both by New England Biolabs, Massachusetts, US) to ensure directional ligation of the insert and the vector. The insert and the vector were combined using T4 ligase (New England Biolabs, Massachusetts, US) with an insert-to-vector ratio of 3:1, determined using a molar ends calculator to be 50 ng of insert to 100 ng of vector. The resulting mix was incubated for 1 h at room temperature, after which the resulting mix was used to transform NEB 5α High Efficiency (New England Biolabs, Massachusetts, US) *E. coli* cells for amplification. The plasmid was purified using a Miniprep kit (Qiagen, Hilden, Germany) and sequenced (Eurofins Genomic Services, Wolverhampton, UK), yielding the *NPH3::GFP-nch1*^{S602A-S604A}.

Transient expression system: *Agrobacterium* Transformation and Infiltration of *N.benthamiana* leaves

The method used in this experiment was similar to one detailed before in the “*Transient expression system: Agrobacterium Transformation and Infiltration of N.benthamiana leaves*” section. *NPH3::nch1^{S602A-S604A}-GFP*, *NPH3::AtNCHI WT-GFP* and the positive control *NPH3::AtNPH3-GFP* plasmids were used for the *Agrobacterium* transformation, and the transformed *Agrobacterium* cells were plated on pre-warmed spectinomycin-gentamicin (concentration for spectinomycin 100 µg/mL media, gentamicin 25 µg/mL) double antibiotic LB-agar (Melford Laboratories, Suffolk, UK) Petri dishes (Ø9cm, Sterilin™ Thermo Fisher Scientific, Massachusetts, US). The resulting plates were sealed using Parafilm (Amcor Plc., Zürich, Switzerland) and incubated in a 28°C incubator for 2 days.

NPH3::nch1^{S602A-S604A}-GFP, *NPH3::WT AtNCHI-GFP* and the positive control *NPH3::AtNPH3-GFP* were transiently expressed *in planta* utilising electroporation transformed *Agrobacteria* and *N. benthamiana* model system. 10 mM MgCl₂ 10 mM MES (pH 5.6) infiltration buffer solution was used to suspend the *Agrobacteria* with the desired plasmids directly from the fresh plates containing a bacterial lawn, and the resulting *Agrobacterium* solution was transferred into a 50 mL Falcon tube (Greiner AG, Kremsmünster, Austria). The bacterial solution was measured for optical density using an Eppendorf Biophotometer (Eppendorf, Stevenage, UK). and adjusted for optical density of 0.4 for infiltration. The bacterial suspension was let to sit on the bench for at least an hour. After this, the *N.benthamiana* leaves were infiltrated from the abaxial side with 1 mL disposable Luer syringes, the infiltrated area sketched on the leaf using a permanent marker, and the infiltrated plants were moved into cupboards, where they were kept in constant darkness under a humidifier dome in room temperature for 3 days to allow the transient expression of the desired proteins before harvesting of leaf tissue discs for confocal microscopy and Western blots.

Confocal Slide Preparation and Mounting of Leaf Samples on Microscope Slides

For confocal microscopy, leaf discs (Ø0.8cm) were harvested by punch method. The leaf discs were vacuum treated using a syringe, mounted abaxial side up on the glass microscope slides. All steps from the harvesting of the dark-adapted tissue discs to mounting on microscope slides were done under red safelight for confocal microscopy.

Confocal Microscopy: Localization of the Putative Phosphorylation deficient NCH1 protein in *N.benthamiana* Leaf Tissue

The samples were scanned using a Leica S8 confocal microscope and pictures recorded as single images with following settings (**Table 2.4**):

Table 2.4 Confocal microscope settings used for the imaging and Z-stack scans during the NCH1 phosphorylation experiment.

Format	1024 x 1024 px
Speed	600
Line average	4
Laser/ Excitation Wavelength	488 nm, 5%
Collection Wavelengths	500-530 nm
Chloroplast autofluorescence cancelling	660-800 nm
GFP smart gain	390%

The final adjustment of images, including the separation into 3 channels, and image brightness and contrast adjustment, was performed using FIJI software (Schindelin et al., 2012) using the same settings to all images in the experiment. The experiment was done once and not repeated.

2.5. Flood Assay of *Pst* DC3000-Infected *Arabidopsis thaliana* seedlings

King's B Agar and King's Broth Media for Pst DC3000 Bacterial Cultures

Sterile King's B agar medium (1 L, pH 7.2) was made by mixing 2% (w/v) of peptone (Sigma Aldrich, Missouri, US) in double-distilled H₂O with a magnetic stirrer. 8.61198 mM of K₂HPO₄ (1.5 g/L) and 12.46178 mM MgSO₄ (1.5/L) (both by Sigma Aldrich, Missouri, US) was added, together with 1% (v/v) of glycerol (Thermo Scientific, Massachusetts, US), and mixed until homogeneously suspended. Finally, 1.5% (w/v) of agar was added. The final volume was adjusted to 1 L with double-distilled H₂O, and the resulting solution was bottled in 500 mL quantities in 1L volume bottles. The bottles were autoclaved for sterilization using the standard 121°C for 30 min cycle, after which the media was slightly cooled, and in the case of the new protocol, the desired antibiotic (50 µg rifampicin /mL media) was added. The resulting media was poured on round Petri dishes (Ø9cm, Sterilin™ Thermo Fisher Scientific, Massachusetts, US) in sterile lateral flow hood conditions, and the plates stored in 4°C fridge conditions until use.

Sterile King's broth medium was made for liquid bacterial suspension cultures by mixing 2% (w/v) of peptone (Sigma Aldrich, Missouri, US) in double-distilled H₂O with a stirrer. 8.61198 mM of K₂HPO₄ (1.5 g/L) (Sigma Aldrich, Missouri, US) and 1% (v/v) of glycerol (Thermo Scientific, Massachusetts, US) were added, and all mixed until homogeneously suspended. The final volume was adjusted to 995 mL using double-distilled H₂O, and the resulting solution was bottled. The bottles were autoclaved for sterilization using the standard 121°C for 30 min cycle, after which the solution was cooled and 5mM filter-sterilized MgSO₄ (5 mL of 1M solution) was added post-sterilization to avoid high temperature-induced cloudiness and the effect on the OD₆₀₀ of the broth. For the new protocol, an antibiotic (50 µg rifampicin /mL media) was also added.

Flood assay of Arabidopsis thaliana seedlings: Protocols derived from Ishiga et al. (2011) and Ishiga et al. (2017)

The flood assay method used was optimized over the course of the investigation, and these two protocols (called "old protocol" and "new protocol", respectively) are summarised in **Figure 2.1. A and B**, with key differences highlighted on grey background on the new protocol.

In the original old protocol, *Arabidopsis thaliana* WT Col-0, *nch1-1* and *rpt2-3* single mutant and *nch1-1/rpt2-3* double mutant seeds, courtesy of Dr. Stuart Sullivan, University of Glasgow, were sterilised using methodology by Ishiga et al. (2017). The sterilised seeds, contained in microfuge tubes, were cold-stratified in dark +4°C conditions for 3 days. After this, they were plated on 12cm x 12cm square Petri dishes (Greiner AG, Kremsmünster, Austria) with ½ MS + 0.5% (w/v) sucrose medium (see section 2.2 "Sterile Plant Tissue Cultures: ½MS (Murashige-Skoog) Medium"), in a density of at least 16 seedlings per plate. The plates were sealed from the sides using Micropore tape (3M, Minnesota, US) and placed in controlled environment cabinets on a long day 16h day (light intensity measured at 266 µmol m⁻² s⁻¹) /8 h night cycle in 22°C temperature and grown for 10-14 days.

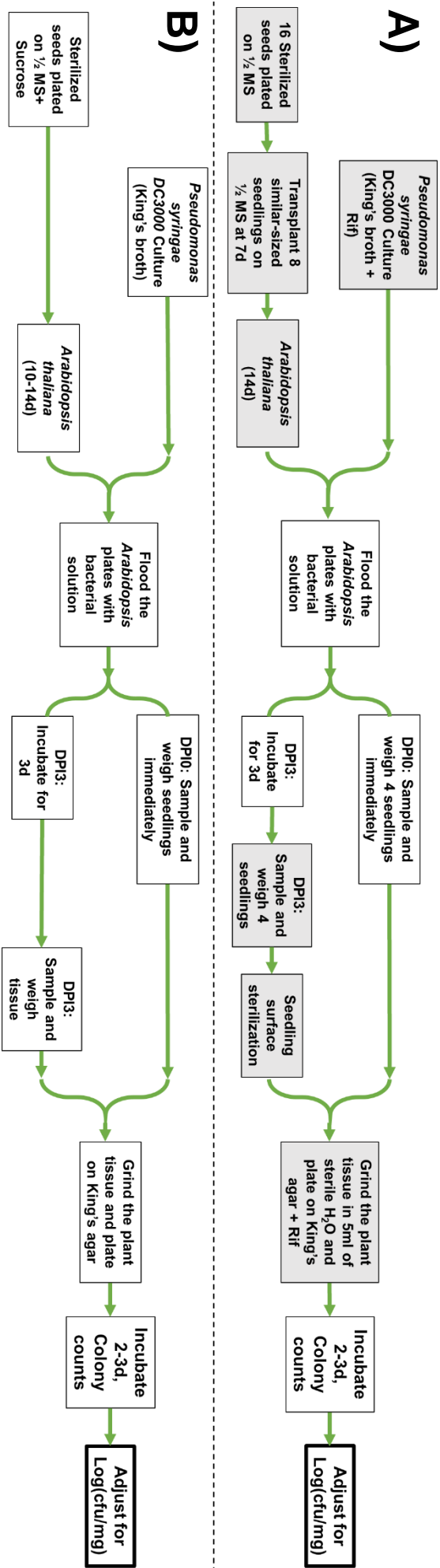


Figure 2.1 Comparison of the old and new flood assay protocols.

A) New protocol on the top, and **B)** Old protocol on the bottom. Steps shaded in grey indicate changes and improvements to the new protocol.

For the new protocol, *Arabidopsis thaliana* seeds, courtesy of Dr. Stuart Sullivan (University of Glasgow), were sterilised and cold-stratified similarly to the seeds in the old protocol. However, the media was changed into the ½ MS medium (see section 2.2 “Sterile Plant Tissue Cultures: ½MS (Murashige-Skoog) Medium”) without sucrose and plated on 12cm x 12cm square Petri dishes (Greiner AG, Kremsmünster, Austria) in a density of 16 seedlings per plate. At the age of 7d, the seedlings were visually assessed for similar size, and similar seedlings were transplanted on round ½ MS medium plates (Ø9cm, Sterilin™ Thermo Fisher Scientific, Massachusetts, US) at a density of 8 seedlings per plate using sterile autoclaved forceps. After this, the seedlings were grown for one more week, so that the flood assay could be performed with exactly 14-day old seedlings.

In the original old protocol, *Pseudomonas syringae* pv. tomato (*Pst*) DC3000 cells (courtesy of Dr. Lingfeng Xia, University of Glasgow) freshly picked from a King’s B agar plate were grown overnight suspended in 10 mL of King’s broth and stored in 30 mL Universal tubes (Sterilin™ Thermo Fisher Scientific, Massachusetts, US), after which the cells were centrifuged in a Sorvall Legend centrifuge (Sorvall Thermo Scientific, Massachusetts, US) for 10 mins at 3500 rpm. The pelleted cells were resuspended in 10 mM MgCl₂ 10 mM MES (pH 5.6) solution, the OD₆₀₀ of the solution was measured using an Eppendorf Biophotometer (Eppendorf, Stevenage, UK) and adjusted to 0.2, corresponding to 1x10⁸ cfu. The final concentration of the flood assay solution was adjusted to 1x10⁶ cfu by further diluting the solution with 10 mM MgCl₂ 10 mM MES (pH 5.6) into 1/100 of OD₆₀₀=0.2 and adding 0.025% Silwet L-77 surfactant (OSI Specialties Inc., Connecticut, US). In contrast to the original protocol, for the new protocol, the *Pst* DC3000 cells were grown overnight suspended in 10 mL of King’s broth + rifampicin antibiotic (50 µg/mL media) in order to ensure the selection of the *Pst* DC3000 cells.

According to the original protocol, the *Pst* DC3000 inoculation of plates was performed inside laminar flow hoods by flooding 10–14-day old WT Col-0, *nch1-1* and *rpt2-3* single mutant and *nch1-1/rpt2-3* double mutant *Arabidopsis thaliana* plants (courtesy of Dr. Stuart Sullivan, University of Glasgow) with the flood assay solution for 1 min without shaking, after which the bacterial suspension was decanted away, and the plates were dried briefly, for about 10 min, inside the laminar flow hood with lids off. After this, plants were either harvested for DPI0 samples, or incubated further in SANYO growth rooms (16h day/ 8h night cycle conditions, with the daytime temperature set to 26°C and humidity to 60%, and night-time temperature to 18°C and 70%) until later harvesting at desired DPI. The new protocol followed this same methodology, except for the age of the *Arabidopsis* plants used, which was always 14d.

In the old method, seedlings were harvested and weighed and lysed in 1.5mL Eppendorf microfuge tubes for the calculation of the logarithm of colony-forming units per mg tissue (cfu/mg). Dilutions up to 10⁻⁹ were made using the 10 mM MgCl₂ 10 mM MES (pH 5.6) buffer and these serial dilutions were plated on King’s B agar plates, with three 10 µl spots of each solution plated per dilution. For DPI0, dilutions of 10⁻¹-10⁻⁴ were plated, whereas for DPI1-6 the dilutions of 10⁻⁴-10⁻⁹ range were plated to acquire a good resolution for colony counts. The resulting inoculated plates were incubated at 28°C for 2-3 days, after which the colonies were counted and recorded. The number of colonies, dilution and the exact weight of the harvested tissue was used to calculate the final logarithm of colony-forming units per milligram of tissue, log₁₀ (cfu/mg).

For the calculation of colony-forming units per mg tissue (cfu/mg) in the new method, the collection of plants for sampling was done similarly to Ishiga et al. (2011). Four similar seedlings per plate were harvested and weighed. For DPI > 0, the harvested plants were surface sterilised with 5% H₂O₂ for 3 min and rinsed with double distilled and autoclaved sterile H₂O, and ground with sterile autoclaved ceramic mortars and pestles until homogenous. The homogenized tissue was resuspended in 5 mL of sterile water, which was used as the initial sample. This sample was then further diluted with 10 mM MgCl₂ 10 mM MES (pH 5.6) buffer as a serial dilution on 96-well plates: Dilutions up to 10⁻⁹ were made and these serial dilutions were plated on King's B agar plates, with three 10 µl spots of each solution plated per dilution. For DPI0, dilutions of 10⁻¹-10⁻⁴ were plated, whereas for DPI1-6 the dilutions of 10⁻⁴-10⁻⁹ range were plated for better resolution. The resulting inoculated agar plates were incubated in 28°C for 2-3 days, after which the colonies were counted and recorded. The number of colonies, dilution of the sample and the exact weight of the harvested tissue was used to calculate the final logarithm of colony-forming units per milligram of tissue, log₁₀(cfu/mg). Each plate and the pooled sample of four seedlings were treated as a single biological replicate, as these plates were independent in terms of the plants and the *Pst* solution used from other plates.

Visual Assessment of *Pst* Infection

For the visual assessment experiment, old protocol flood assay methodology was applied for the inoculation of the full plates of WT *Col-0 Arabidopsis*, courtesy of Dr. Stuart Sullivan. 10-14-day old seedlings were infected with *Pseudomonas syringae* pv. *tomato* DC3000 as per the old protocol, but instead of tissue harvesting, the progression of disease symptoms was followed by taking representative photographs with Canon EOS 1000D digital SLR camera (Canon Inc., Ota, Japan) with manufacturer's standard optics over the course of the infection DPI0 to DPI6. To ensure even photograph quality, a mount was used for the camera, and the distance of the camera was set to 50 cm from the plates.

Statistics: F-test and Student's T-test

To determine whether the differences seen in the flood assay results between WT *Col-0* and *nch1-1/rpt2-3* double mutant *Arabidopsis* plants were statistically significant, Microsoft Excel (Office 365 -version) with additional Analysis Toolpak add-in was used.

Firstly, the "F-test: Two-Sample for Variances" option with a confidence interval (alpha) of 0.05 was applied to find whether the variances of the two flood assay data sets were similar, and to help decide which variation of Student's T-test to use. When the variances of the two data sets were found similar, "Student's T-test for Two Factors Assuming Equal Variances" option with a confidence interval (alpha) of 0.05 was applied. The two-tailed value was then used as the P-value.

3. Biochemical Characterisation of NCH1

3.1. Introduction and Bioinformatic Analysis

As discussed in section 1.4, the key outcomes of this study involved the characterisation NCH1 protein for its biochemical properties, such as subcellular localization and potential dynamic relocalization movement in response to BL stimulus, protein dimerization and phosphorylation. These objectives were achieved using both *in silico* and *in vivo* methodology. This chapter, therefore, presents the work carried out to provide further biochemical background for the studies regarding the role of NCH1 in plant immunity and introduces the potential underlying mechanisms underpinning the NCH1 protein function.

NCH1 is a protein-coding gene located on the *Arabidopsis* chromosome 5 (see **Figure 3.1 A**). The genomic DNA length is 3228 base pairs (bp) of which the coding sequence length is 1815bp, and there are 5 known splice variants of *NCH1*, pictured in **Figure 3.1 B**. Computational crystal structure models predicted with AlphaFold (Senior et al., 2020) suggest the NCH1 protein crystal structure to be globular and characterised by alpha-helices, open loops and disordered regions, with very little beta-pleated sheets, as seen in **Figure 3.1 C**. During *Arabidopsis* development and life cycle, the *NCH1* transcript appears to be the most abundantly transcribed in the seedling hypocotyl during early seedling establishment (Klepikova et al., 2016), as seen in **Figure 3.2**. This is surprising, as one might expect the highest transcript levels in the main photosynthetic tissues, such as leaf lamina, and secondarily in other above ground photosynthetic tissues such as petioles and stems, which would be consistent with the function in chloroplast accumulation movement and photosynthesis maximisation. However, as these are microarray measured mRNA transcript levels, the final functional protein expression levels are unknown.

The functional WT NCH1 protein is 604 aa long, with a molecular weight of 67.6 kDa and an isoelectric point of pI=8.09. Further breakdown of residue characteristics can be seen in **Figure 3.3**, which shows the distribution of different types of amino acid residues throughout the NCH1 protein sequence. The amino acid composition analysis of the NCH1 protein does not appear to highlight any notable features or particular areas of the protein distinctively different from the rest, as regions enriched with hydrophobic residues might suggest the presence of transmembrane domains. As mentioned before and portrayed in **Figure 1.15**, the functional domains of NCH1 are the N-terminal BTB-POZ domain, and the C-terminal NPH3 domain with putative E3 ubiquitin ligase adapter protein function. Phylogenetic analysis of NCH1 performed using PANTHER 16.0 (Mi et al., 2021) and shown in **Figure 3.4** revealed the evolutionary relationships between different NRL proteins. As expected, the analysis returned the 34 members of the NRL subfamily of NCH1 (syn. SR1IP1), RPT2 and NPH3 (syn. RPT3), together with the expected more distant relatives such as NPY proteins and SETH6 and DOT3, as discussed in section 1.3.4 and detailed in the literature previously (Christie et al., 2018). From this data, it is interesting to note how NCH1 settles among the NRL proteins in comparison to NPH3 and RPT2, and how it is more closely related to RPT2 than NPH3. This finding is also confirmed by literature, with analysis by Suetsugu et al. (2016a) finding that NCH1 and RPT2 belong to the same clade of proteins, unlike NPH3.

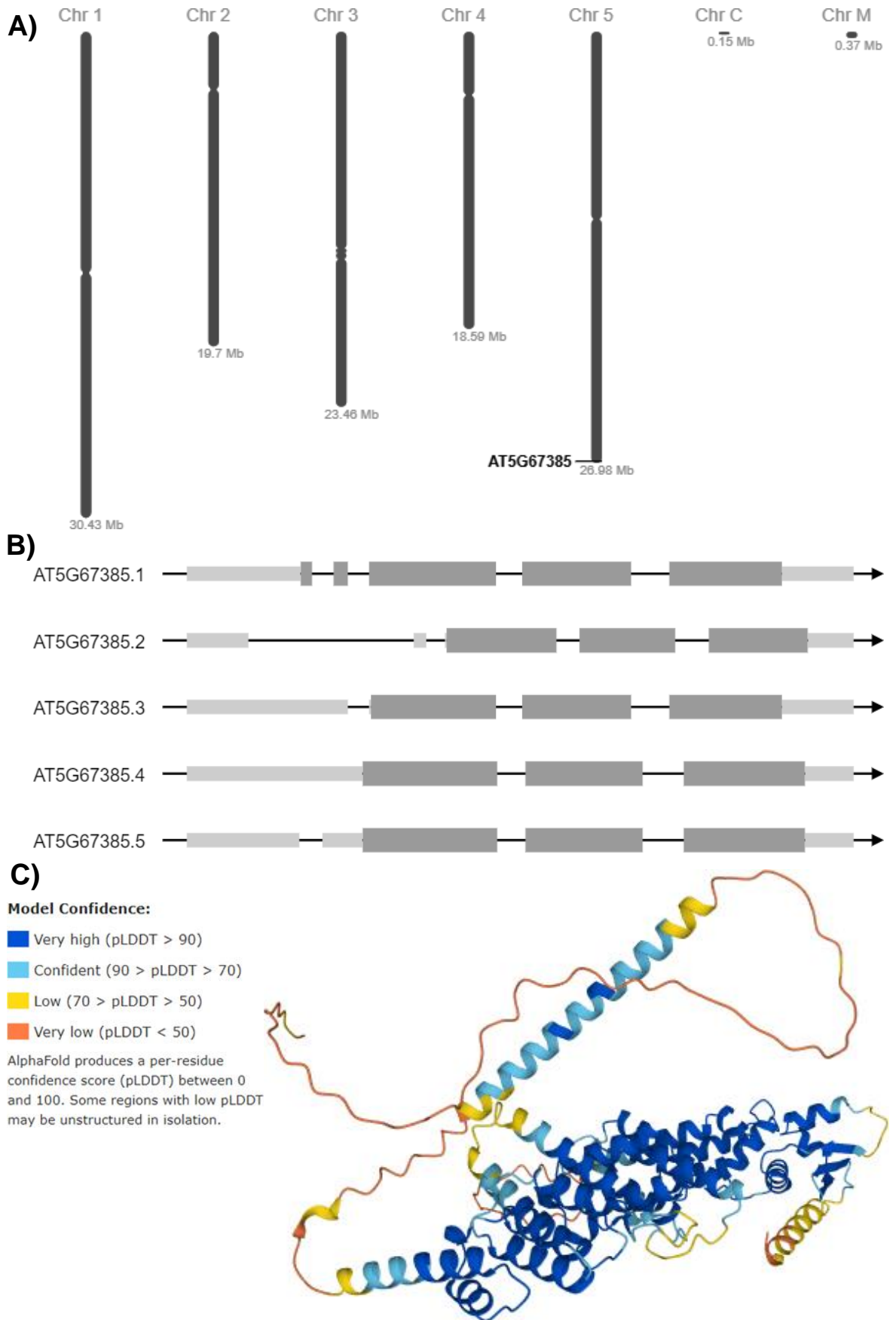


Figure 3.1 Bioinformatic analysis of the NCH1 gene locus, exon structure and protein crystal structure.

A) Location of the *NCH1* locus (AT5G67385) on chromosome 5 of the *Arabidopsis* genome, and **B)** the known *NCH1*-gene alternative splicing patterns recorded on TAIR, with 5' and 3' UTRs marked in light grey and exons in dark grey. Figures generated with the BAR-ePlant browser (Winter et al., 2007).

C) Computational NCH1 crystal structure, predicted using machine learning/AI protein structure prediction tool AlphaFold (Senior et al., 2020).

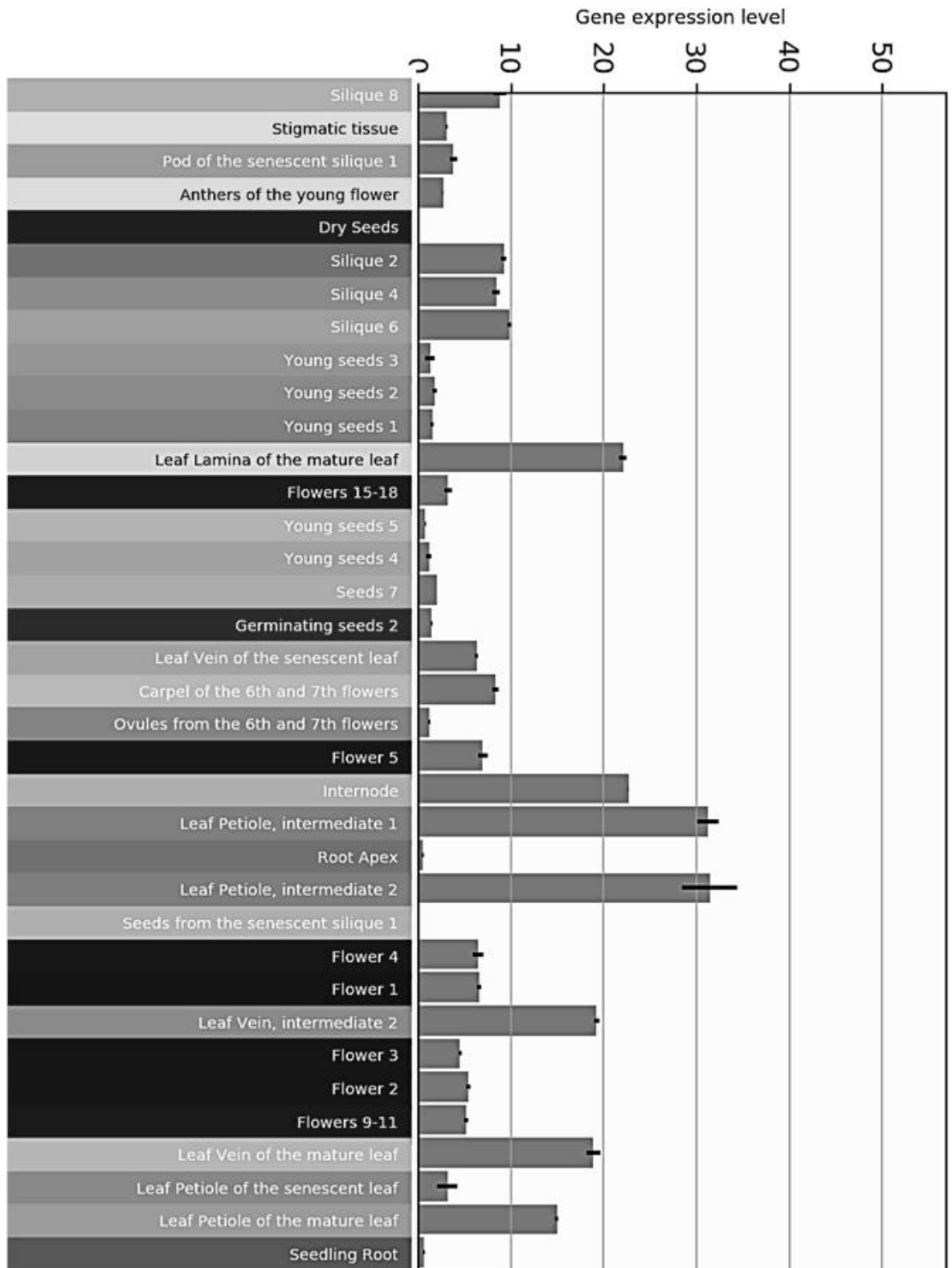


Figure 3.2 NCH1 transcript expression patterns in *Arabidopsis* organs and tissues during development.

Numbers refer to the sample clustering method used in the original literature. Figure constructed from large-scale microarray data by Klepikova et al. (2016) and generated with BAR-*Arabidopsis* eFP Browser (Winter et al., 2007), gene ID AT5G67385.

Figure continues on the next page.

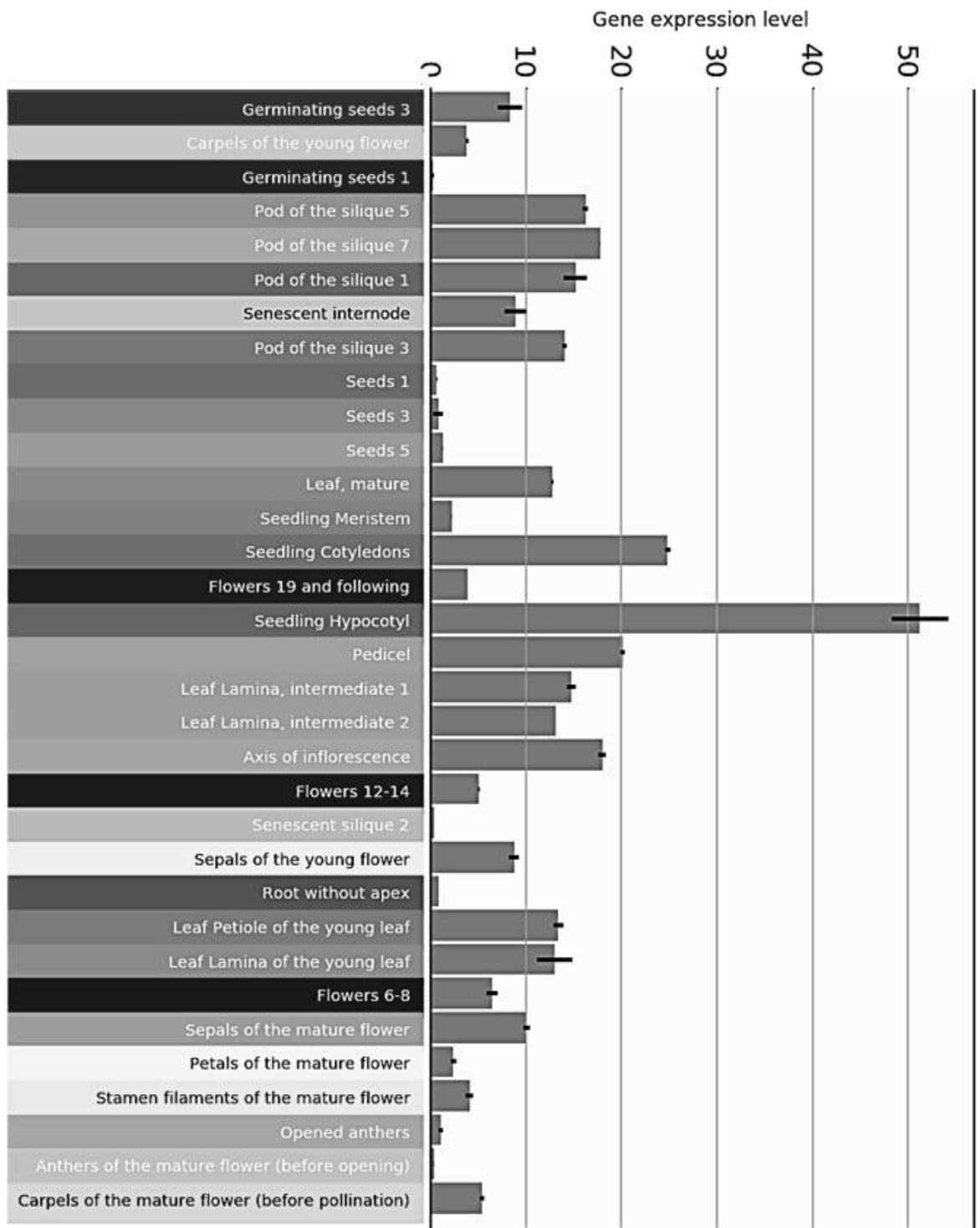


Figure 3.2 (continued)

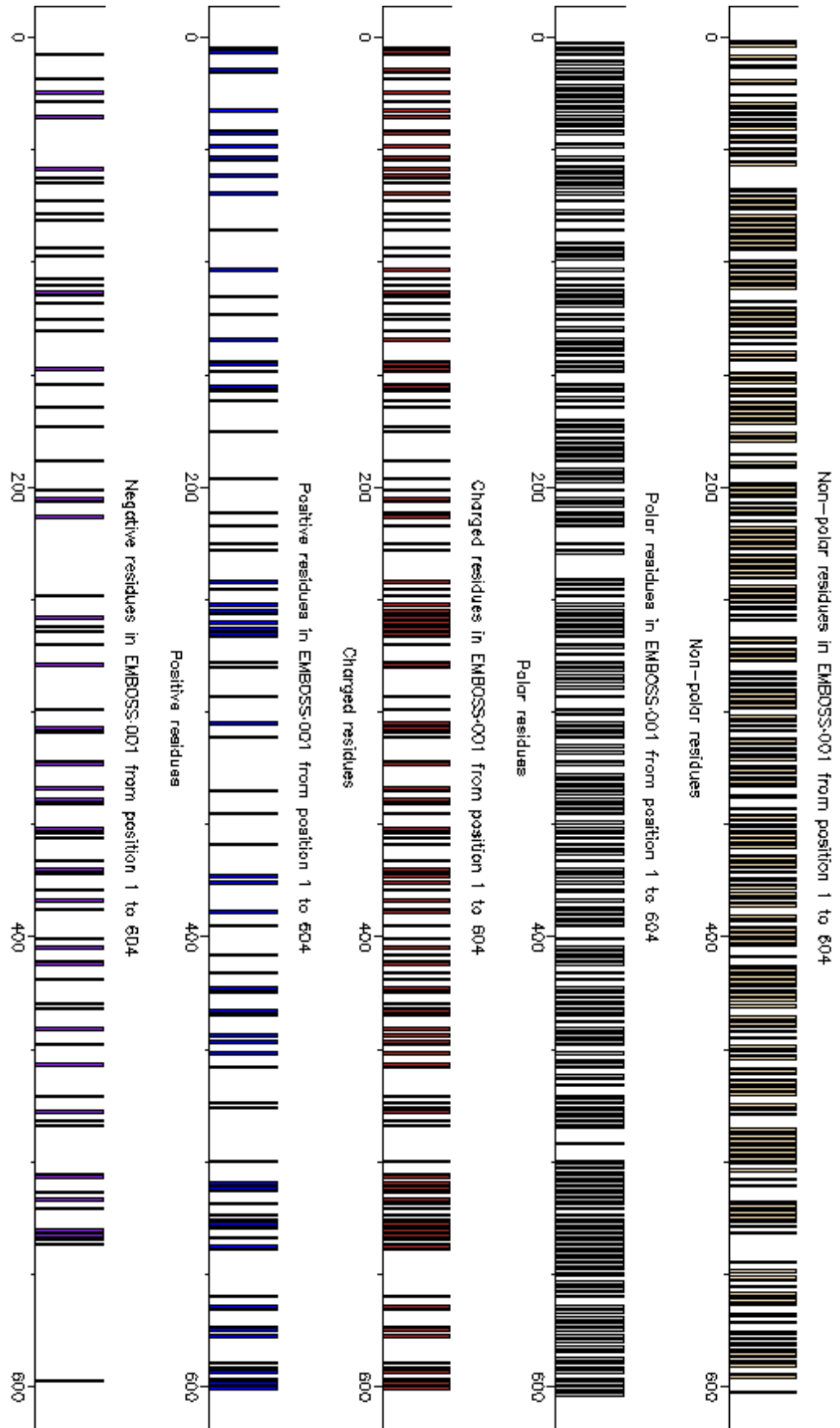


Figure 3.3 Amino acid residue characteristic analysis of AtrNCH1 protein.

Residue analysis was generated with EMBOSS Pepinfo, showing the distribution of different amino acids according to residue characteristics such as polarity (polar and non-polar side chains), and residue charge (charged, positive and negative), and size (tiny, small and large aromatic side chains, on the next page), throughout the NCH1 protein sequence.

Figure continues on the next page.

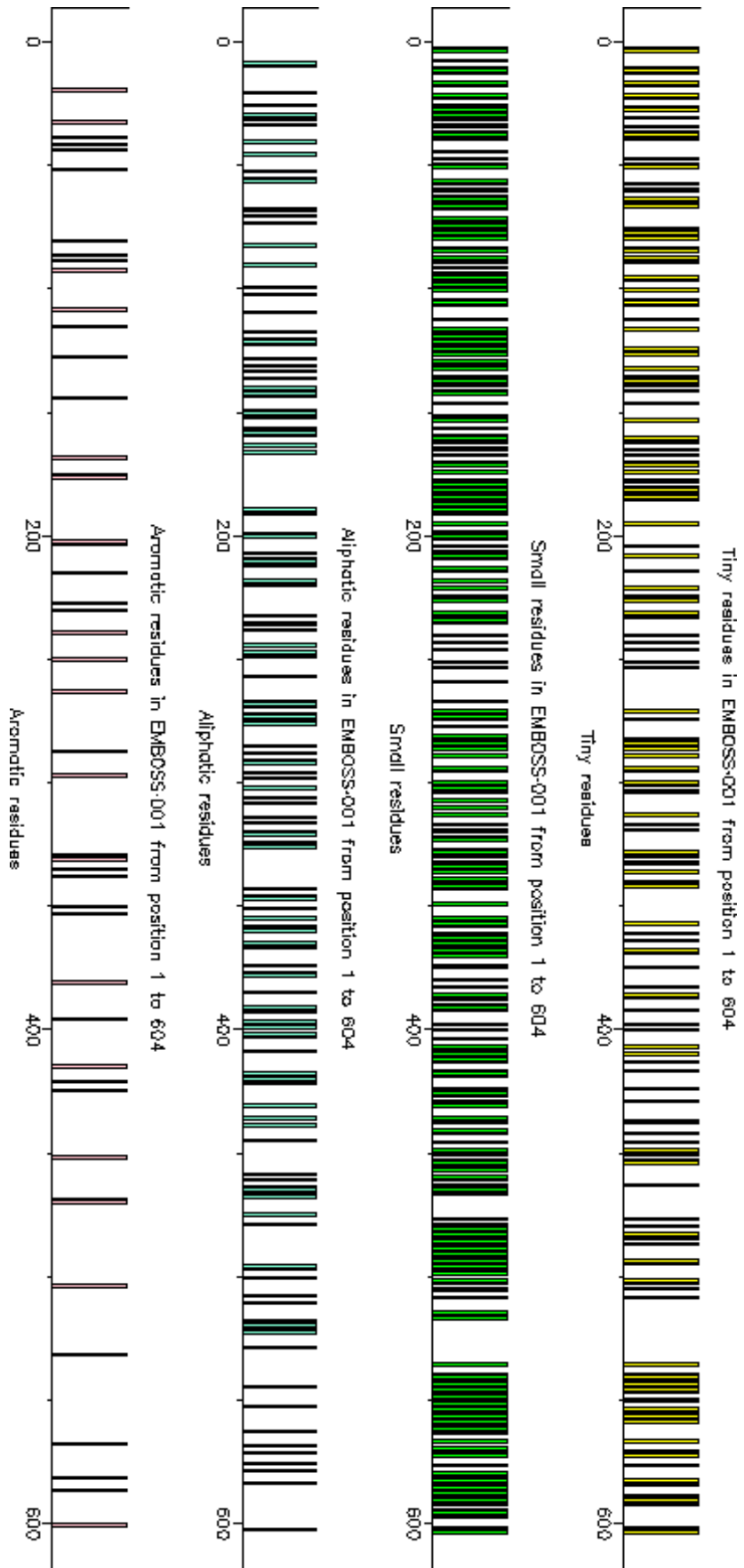


Figure 3.3 (continued)

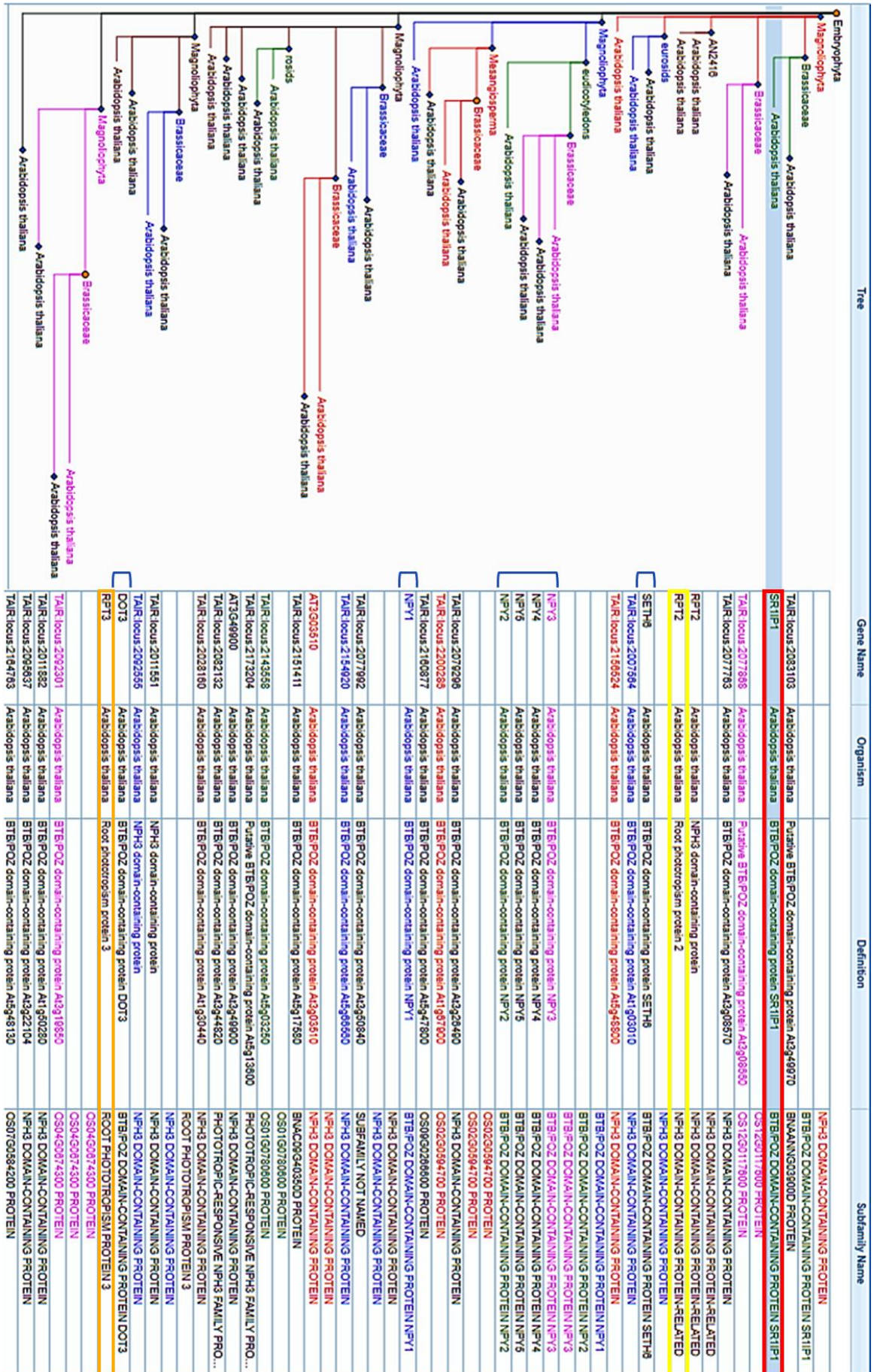


Figure 3.4 Phylogenetic analysis of NCH1.

Phylogenetic tree, showing NCH1 (syn. SR1IP1, highlighted red) and the 34 related Arabidopsis NRL family proteins. Note the positions of the other phot-dependent NRL-subfamily members RPT2 (orange) and NPH3 (syn. RPT3). Other family members with known functions indicated with blue brackets. **Blue Diamond**: Expanded subfamily node; **Orange sphere**: Expanded duplication. Figure generated using PANTHER 16.0 -database (Mi et al., 2021).

3.2. Subcellular Localization of NCH1 *in silico* and *in vivo*

The subcellular localization of NCH1 was studied using both *in silico* and *in vivo* methodology. Firstly, the protein localization was studied *in silico*: BAR eFP ePlant browser (Sullivan et al., 2019; Waese-Perlman et al., 2021; Winter et al., 2007) was used to predict the subcellular localization according to the bioinformatic sequence information, and the computational subcellular prediction algorithm using SUBA4 database (Hooper et al., 2017), pictured in **Figure 3.5 A**, predicted a cytoplasmic (localization score 16) and/or a plasma membrane (localization score 12) localization for the NCH1 protein, with lowest localization scores for the cytoskeleton, the ER, peroxisomes, the vacuole and extracellular matrix (localization score 0 for all). Nuclear localization (score 10), Golgi apparatus (score 10), plastids including the chloroplasts (score 6), and mitochondria (score 4) fall between these extremes. Therefore, a cytoplasmic or plasma membrane-associated localization would be a probable site for the NCH1 protein. Protein-protein interactions map (**Figure 3.5 B**) generated with BAR *Arabidopsis* Interactions viewer database (Geisler-Lee et al., 2007) suggests NCH1 to be a partner in protein-protein interactions with at least three proteins: an immune and stress signalling related serine/threonine kinase *AtSR1* (Lumba et al., 2014; Zhang et al., 2014), ubiquitin E3 ligase component CULLIN3 (CUL3) (Zhang et al., 2014), and surprisingly, a telomere protection protein POT1 homolog POT1A, locus AT5G05210 (Rossignol et al., 2007).

As the photoreceptor phot1 and the related protein NPH3 are membrane-associated, but not transmembrane proteins (Christie et al., 2018), the NCH1 protein sequence was analysed for hydrophathy and potential transmembrane domains. The hydrophathy plot (EMBOSS Pepwindow) for the NRL proteins NCH1, RPT2 and NPH3 protein can be seen in **Figure 3.6**, and a window of 19 amino acids was used as this is recommended as the optimal hydrophathy window for the detection of transmembrane domains according to Kyte and Doolittle (1982). The NCH1 hydrophathy plot has peak values less than 2, and the probability plot marks no potential sites for transmembrane domains, together suggesting that the NCH1 protein does not have any transmembrane domains. However, the related NRL proteins RPT2 and NPH3 show peak values of above 2, which directs attention to these regions. Therefore, a separate probability plot generated using TMHMM 2.0 (Krogh et al., 2001) was performed for the presence of transmembrane domains in **Figure 3.7**. From these two sources of data, it can be deduced, that the NCH1 protein is unlikely to contain any transmembrane regions. Furthermore, the probability plot highlights possible single-pass transmembrane domains for both RPT2 and NPH3: in the N-terminus of NPH3 and in the C-terminus of RPT2. While there is no experimental evidence for membrane-spanning domains nor other means of integral membrane attachment for either of these proteins, there is evidence for membrane association for NPH3 through a positively charged polybasic C-terminal motif. This motif binds plasma membrane phospholipids and becomes displaced by light-dependent phosphorylation and consequent 14-3-3 protein interaction during light activation (Reuter et al., 2021). These charged polybasic motifs might be highlighted in the plot as potential transmembrane domains, and therefore exist for both NPH3 and RPT2. However, the probability of transmembrane domains is difficult to predict accurately, as the results depend on the computational algorithm used and therefore vary depending on the program used, as exemplified by analysis by e.g. Kamano et al. (2015). In addition to this, algorithms such as the one used for TMHMM 2.0 may interpret N-terminal signal peptides erroneously as transmembrane regions.

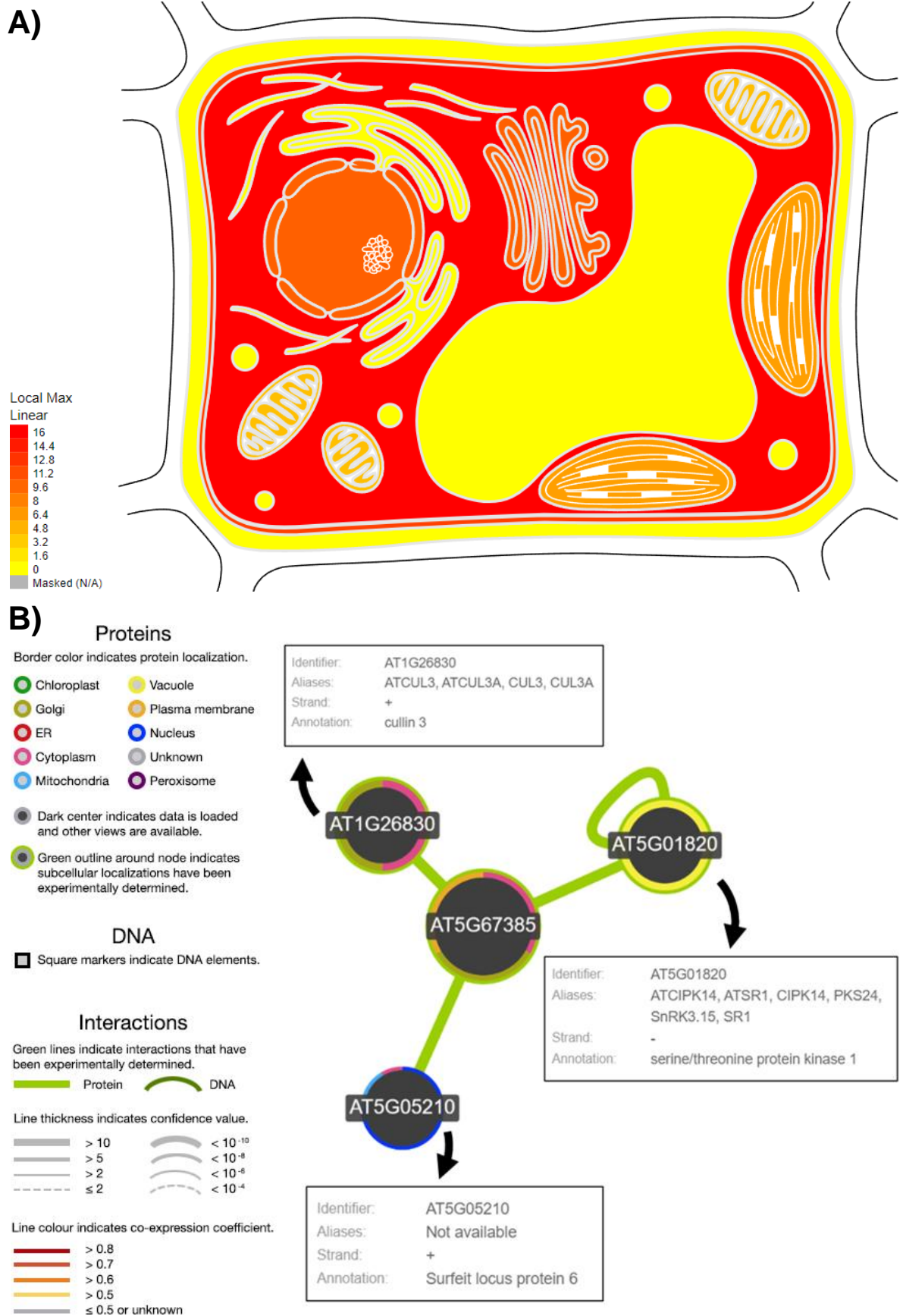


Figure 3.5 NCH1 is predicted to localize into the plasma membrane and/or cytoplasm, and interacts with at least 3 other proteins.

A) Computational prediction of the NCH1 protein localisation inside the *Arabidopsis* cell according to SUBA4-database. Figure generated with BAR-*Arabidopsis* Cell eFP Browser after SUBA4 database by Hooper et al. (2017), gene ID AT5G67385.

B) Protein-protein interaction interactome for NCH1 (AT5G67385, in the centre). Figure modified from BAR *Arabidopsis* Interactions viewer database, originally introduced by Geisler-Lee et al. (2007).

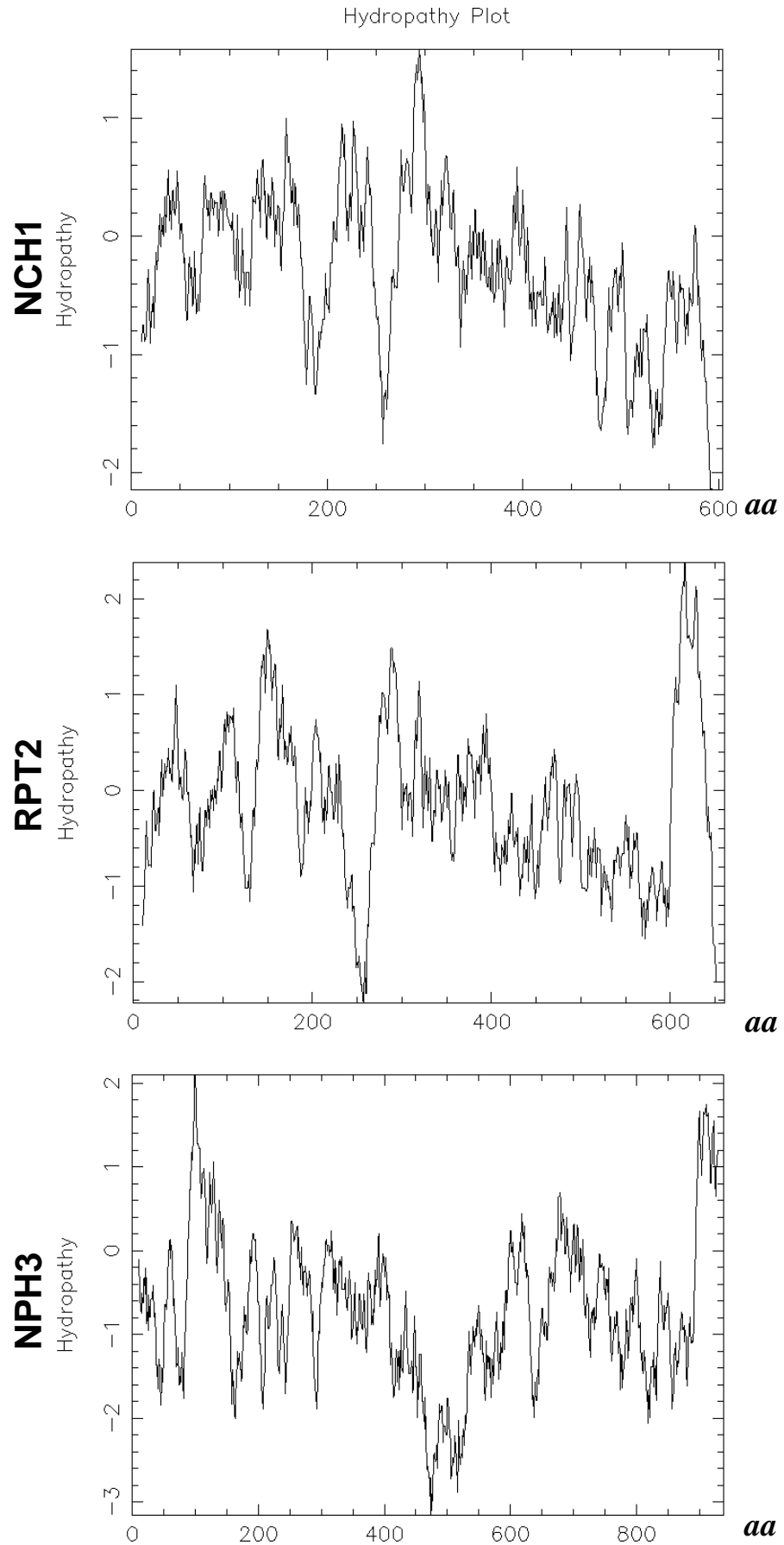


Figure 3.6 Hydropathy plots for the prediction of potential transmembrane domains in three *Arabidopsis* NRL subfamily member proteins, NCH1, RPT2, and NPH3.

The figures were generated using EMBOSS Pepwindow, following the Kyte & Doolittle methodology, with the amino acid residue number reflected on the x-axis and the relative hydropathy parameter on the Y-axis. The window size used is 19 amino acids.

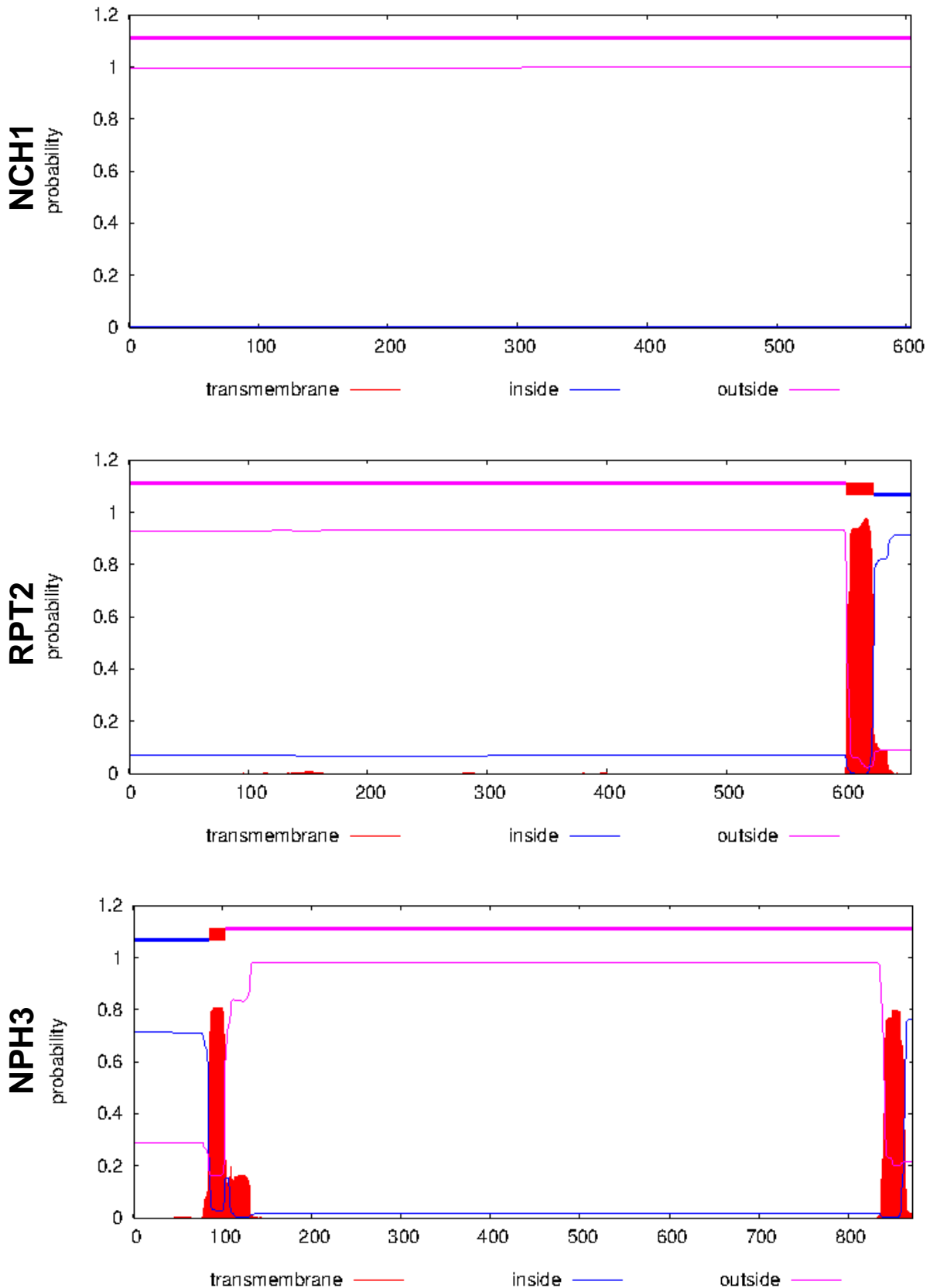


Figure 3.7 Probabilities and placements for potential transmembrane domains in three *Arabidopsis* NRL subfamily proteins NCH1, RPT2, and NPH3, based on protein sequence data.

The figures were generated using TMHMM 2.0 (Krogh et al., 2001), with amino acid residue number reflected on the x-axis and the probability of transmembrane domains on the Y-axis. The plot above the curves (between 1 and 1.2) shows the calculated best prediction. **Red:** Predicted TM domain; **Blue:** Inside the cell; **Pink:** Outside the cell.

The *in vivo* localization and potential movement of NCH1 protein in response to BL was studied using transgenic lines of *Arabidopsis thaliana* expressing mCitrine tagged *NCH1::mCit-NCH1* (pDEST, hygromycin resistant), and treating the 3-day old etiolated seedlings with a confocal laser at 488 nm wavelength to activate phototropin signalling, and consequently, the NRL proteins downstream in the signalling cascade. The related protein NPH3 from the same NRL family of proteins was used as a control and as an example of a protein undergoing dynamic relocalization in response to a BL stimulus (Haga et al., 2015). Based on the results from the bioinformatic analysis, it was hypothesised, that the NCH1 protein would either localize to the cytoplasm or associate with the plasma membrane similarly to the related membrane-associated NRL proteins NPH3 and RPT2. Furthermore, as NPH3 exhibits a dynamic relocalization pattern, the protein movement would be tracked in response to a prolonged BL irradiation stimulus: The experiment was designed so that the same initially etiolated cells could be visualised at multiple time intervals before and during BL irradiation: before irradiation ($t=1$), at 5 min ($t=2$) and at 10 min ($t=3$) intervals, see **Figure 3.8 A**. The use of confocal laser in the excitation of the phot1 photoreceptor has several benefits, such as the precise control of BL wavelength, and the monitoring and visualisation of single cells in real-time, allowing high-quality data gathering. However, a drawback of the method is that the intensity of the irradiation cannot be measured with a conventional light meter.

The results, which were witnessed consistently over three independent repeats, indicated WT NCH1 localizes at the plasma membrane both in BL and darkness (**Figure 3.8 B**) and does not exhibit a dynamic localization pattern in response to BL irradiation. This is important, as this contrasts with its relative protein NPH3, which has a well-characterised movement pattern and was therefore used as a positive control: NPH3 localizes at the plasma membrane in darkness but rapidly concentrates into bright cytoplasmic foci in response to BL (Haga et al., 2015). Overall, the consistent static position at the plasma membrane seen in multiple replicates, including in the dimerization studies in the next section, implies that NCH1 does not require dynamic protein relocalization to mediate its normal function in BL -dependent chloroplast accumulation. It has been suggested that NCH1 protein performs an E3 ubiquitin ligase substrate adapter function (He et al., 2018; Zhang et al., 2014), and therefore, NCH1 protein could mediate the chloroplast accumulation movement through the regulation of other proteins or intermediates, specifically the BL -dependent degradation of targets through the 26S proteasomal system. While unlikely to affect the localization of NCH1 protein, the technical execution of the experiment could be improved by visualising hypocotyl cells of the same cell type: the NCH1-expressing cells in **Figure 3.8 B** are cortical cells, whereas the NPH3 expressing cells are epidermal cells.

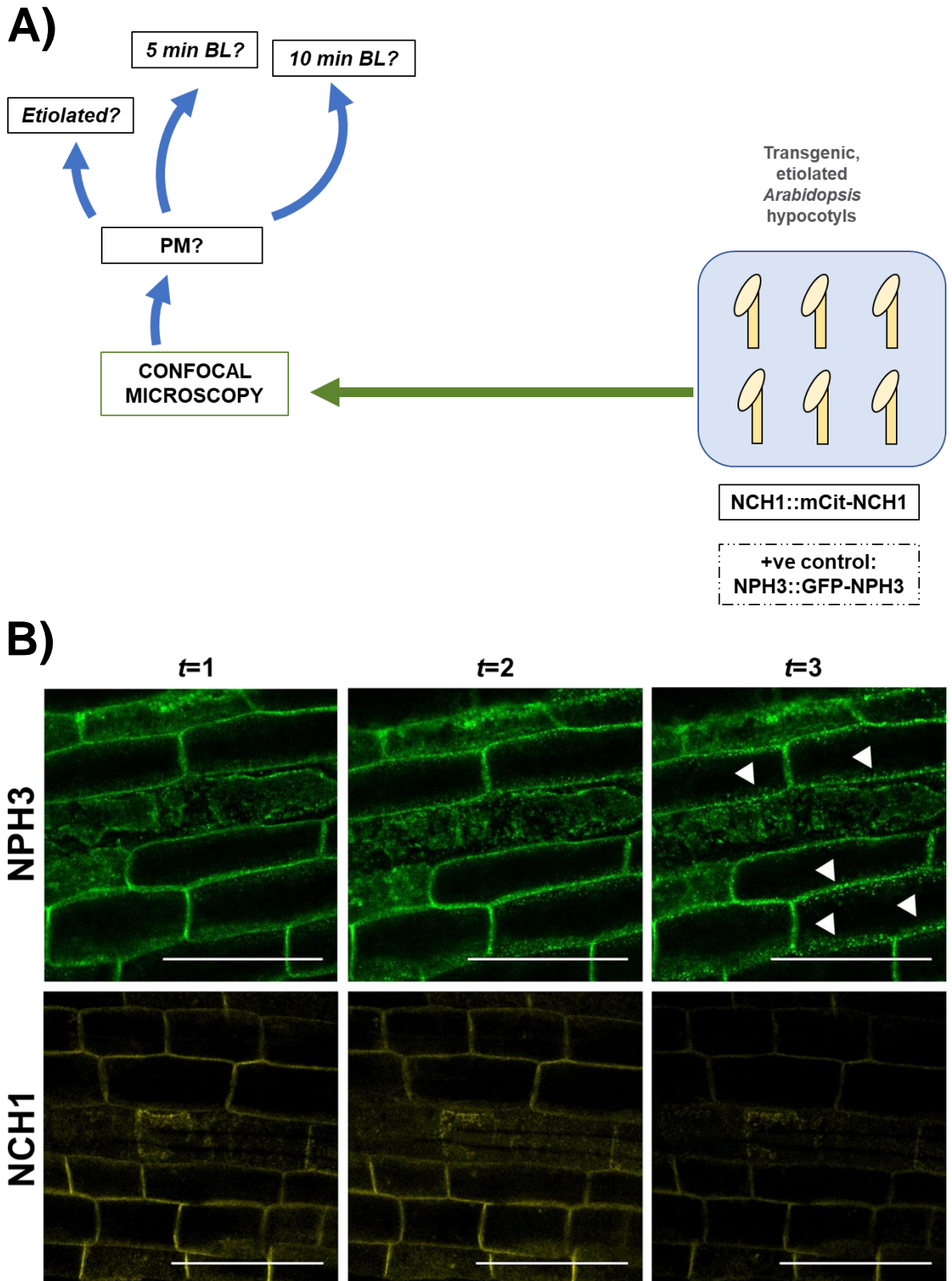


Figure 3.8 NCH1 localization is not influenced by BL.

A) Strategy graph for the study of the localization of WT NCH1 protein in etiolated hypocotyls, and potential relocalization movement in response to prolonged BL stimulus for the time lapse experiment presented in 3.8B. **PM:** Plasma membrane.

B) NCH1 localization does not change in response to blue light. Representative confocal micrographs showing a time lapse series of etiolated transgenic *Arabidopsis* seedlings during irradiation with blue light. These transgenic seedlings express either *NCH1::mCit-NCH1* (*NCH1*) or *NPH3::GFP-NPH3* (*NPH3*). White arrowheads on the *NPH3* sample show the relocalization of *NPH3* protein into bright foci in response to blue light. **T1:** Etiolated state before irradiation, **T2:** After 5 min of BL irradiation, **T3:** After 10 min of BL irradiation. **Scale bar 100 μ m.**

3.3. Site-Directed PCR Mutagenesis: Putative Dimerization Mutant

nch1^{D28N-K42Q}

As He et al. (2018) found putative dimerization sites D28 and K42 forming a salt bridge in the NCH1 potato (*Solanum tuberosum*) ortholog *StNRL1*, a bioinformatics approach was used to compare potato and *Arabidopsis NCH1* sequence data to find the corresponding residues in the *Arabidopsis NCH1* protein. Comparison of the sequence information revealed that the sites were conserved, and therefore, the *Arabidopsis NCH1* protein had the same D28 and K42 amino acid residues at the same positions as the potato ortholog.

The *35S-SPYNE* and *35S-SPYCE* vectors (acronyms for *split YFP N-terminal/C-terminal fragment expression*) are convenient molecular genetic tools used for the study of two interacting proteins, readily visible in real time when visualized with confocal microscopy (Walter et al., 2004). The basic structures of the vectors (see **Figure 3.9**) contain **A**) a cauliflower mosaic virus 35S promoter for the constitutive expression of the target protein, **B**) a multiple-cloning site (MCS), **C**) a protein affinity tag: cMyc in *35S-SPYNE*, and haemagglutinin (HA) in *35S-SPYCE* useful for e.g. detection, purification, and/or Western blotting of the products, **D**) a yellow fluorescent protein (YFP) fluorophore is split into its N-terminal and C-terminal halves, and **E**) *nos*-promoter, a kanamycin resistance gene (*nptII*) as an antibiotic selection marker, and a *nos*-terminator in the C-terminus of the vector. The most important feature of the vector is its split YFP fluorophore: the *35S-SPYNE* vector has the N-terminal half of the YFP fluorophore, whereas the *35S-SPYCE* contains the C-terminal half of the YFP. Therefore, these vectors are specifically made to study protein dimerization, as the split halves of the fluorophore reconstitute the functional YFP, and consequently emit a fluorescent signal only when the halves would come sufficiently close together, such as during protein dimerization. The gene of interest (e.g. *NCH1*, *nch1*^{D28N-K42Q}) is ligated to the N-terminal side of the split YFP fluorophore inside the MCS (Walter et al., 2004).

To make the BiFC constructs for co-infiltrations and dimerization experiments, the original pDONR WT *NCH1* template had to be mutagenized to contain the D28N-K42Q double mutations and combined with the empty BiFC vectors *35S-SPYNE* and *35S-SPYCE*. To introduce the corresponding dimerization mutations into the *Arabidopsis NCH1* gene, site-directed PCR mutagenesis approach utilising mismatch primers was used to perform the residue changes at the dimerization sites D28 and K42 to make the putative dimerization deficient mutant *nch1*^{D28N-K42Q} construct. The mutations were introduced one at a time on the template WT *NCH1*

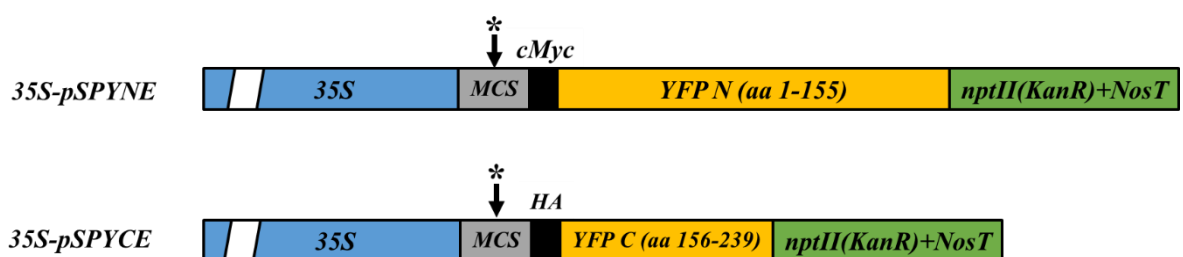


Figure 3.9 The schematic structure of the *35S-SPYNE* and *35S-SPYCE* BiFC vectors used in this study.

Note the site for the placement of the gene of interest (*) inside the multiple cloning site.

35S: Cauliflower mosaic virus promoter; **MCS**: Multiple cloning site; **cMyc**: cMyc tag; **HA**: Haemagglutinin tag; **YFP**: Yellow fluorescent protein; **NosT**: Nos-terminator; **nptII**: Kanamycin resistance for selection. Figure after Walter et al. (2004).

sequence contained in a pDONR plasmid, courtesy of Dr. Noriyuki Suetsugu University of Tokyo, and the resulting mutations were confirmed by sequencing (see red branch on **Figure 3.10**).

As the particular 35S-SPYNE and 35-SPYCE vector constructs used came with a *PHOT1* gene fragment ligated in them (see blue branch on **Figure 3.10**), the *PHOT1* fragments were removed by digesting the vector using *Bam*HI and *Sma*I restriction enzymes, yielding the separate vector and *PHOT1* insert fragments. These were then separated using gel electrophoresis and subsequent gel extraction to choose only the empty vector, ready to be ligated with the *nch1*^{D28N-K42Q} double mutation fragment.

After the desired fragments, i.e., WT *NCH1* and the double mutant *nch1*^{D28N-K42Q} were successfully made, these fragments were combined with the empty BiFC vectors 35S-SPYNE and 35S-SPYCE using NEBuilder Hi-Fi Assembly (New England Biolabs, Massachusetts, US). This yielded the WT *NCH1* BiFC constructs 35S-SPYNE WT *NCH1* and 35S-SPYCE WT *NCH1*, and the double mutant constructs 35S-SPYNE *nch1*^{D28N-K42Q} and 35S-SPYCE *nch1*^{D28N-K42Q}, seen as band shifts on DNA gel electrophoresis as the ligated product appears heavier than the non-ligated vector (**Figure 3.11**). These constructs were used for *Agrobacterium* transformations and co-infiltrations, detailed in the next section. For the plasmid maps of the 35S-SPYNE *nch1*^{D28N-K42Q} and 35S-SPYCE *nch1*^{D28N-K42Q} plasmids, see **Figure 3.12**. For BiFC experiments, the empty 35S-SPYNE and 35S-SPYCE vectors were kept for negative controls, and *NPH3* BiFC constructs 35S-SPYNE *NPH3* and 35S-SPYCE *NPH3*, courtesy of Mr. Franco Vegliani (University of Glasgow), were used for positive controls.

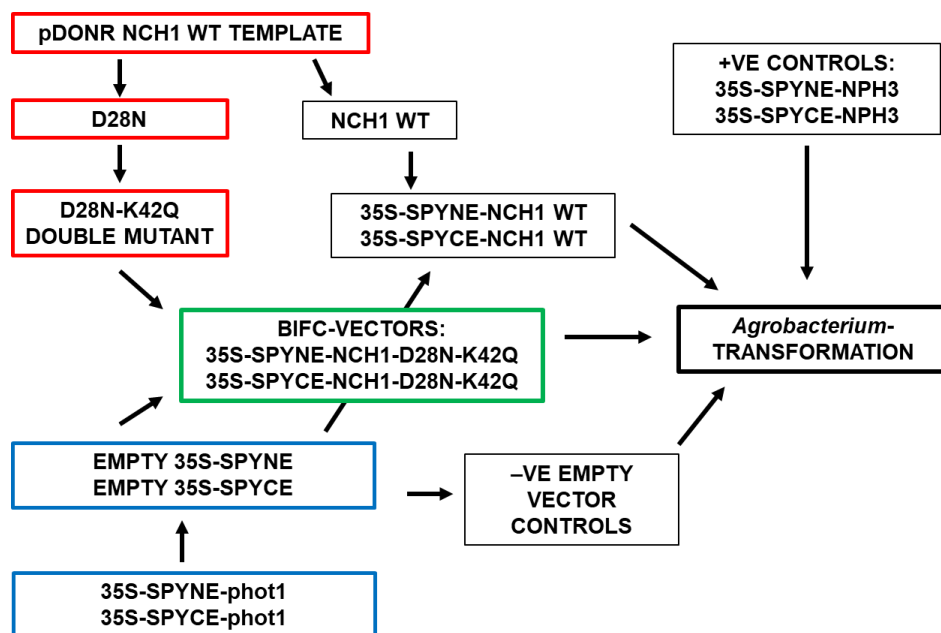


Figure 3.10 Cloning strategy for the BiFC vectors used in this study.

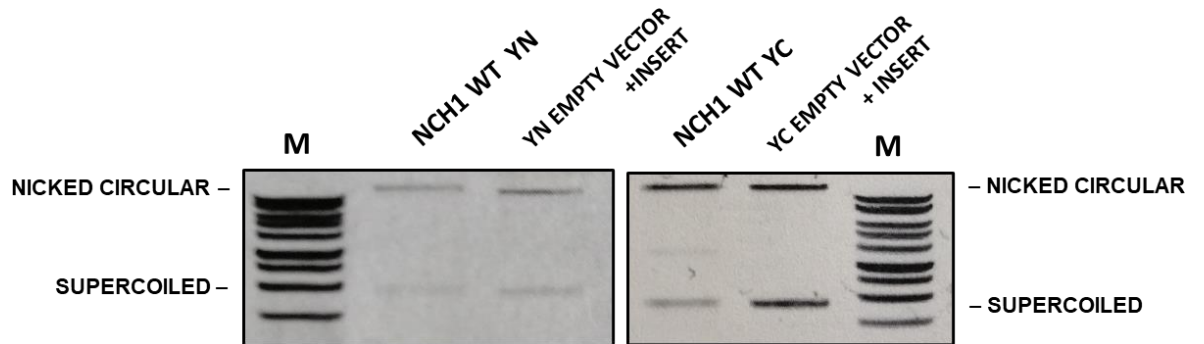
Strategy graphs for the creation of the BiFC constructs 35S-SPYNE-*nch1* D28N-K42Q, 35S-SPYNE-*nch1* D28N-K42Q.

Red: Site-directed mutagenesis of the WT *NCH1* pDONR template for point mutations D28N and K42Q, and the creation of the double mutant *nch1* D28N-K42Q.

Blue: Preparation of empty 35S-SPYNE and 35S-SPYCE vectors from a 35S-SPYNE-*PHOT1* constructs by removal of the *PHOT1* fragment by double-digestion, gel electrophoresis and gel extraction of the empty vector to be used for the creation of both the WT *NCH1* and the double-mutant *nch1* BiFC constructs.

Green: The completed *nch1* D28N-K42Q BiFC vectors created from the double-digestion of both the fragment and the vector, and combination by Gibson assembly into *Agrobacterium* transformation-ready BiFC constructs.

A)



B)

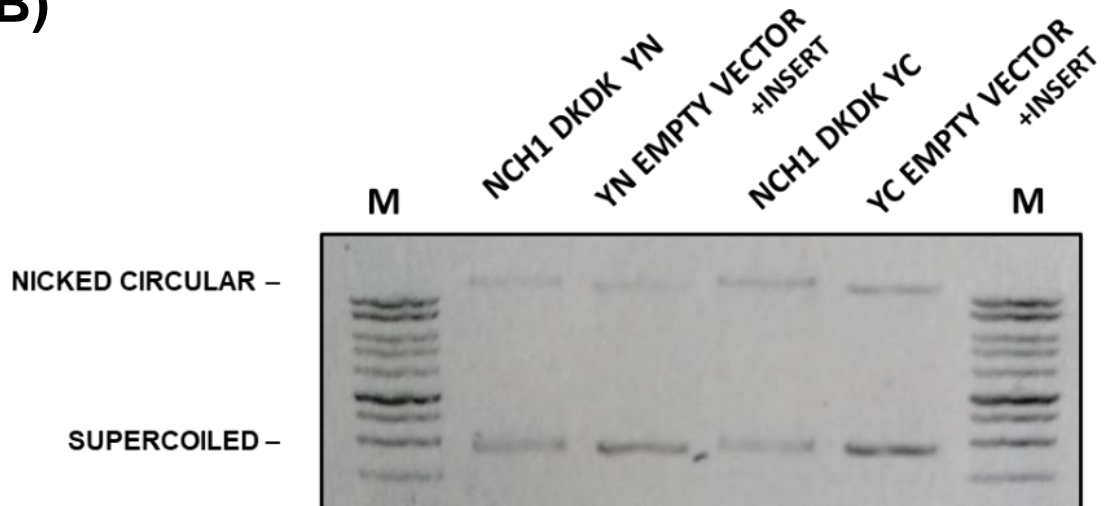


Figure 3.11 Results of the Gibson assembly reaction can be visualised as an electrophoretic mobility shift in the DNA gel electrophoresis.

a) Pre- and **b)** post- Gibson assembly BiFC plasmids, *35S-SPYNE* WT *NCH1* and *35S-SPYCE* WT *NCH1*, and the double mutant constructs *35S-SPYNE nch1 D28N-K42Q* and *35S-SPYCE nch1 D28N-K42Q* were visualised using DNA gel electrophoresis on a 0.8% agarose gel. The "Empty vector + Insert" -controls were taken before the Gibson Assembly reaction, containing only vector + insert in dH₂O. As the plasmids are mostly in circular and in nicked circular (single-stranded break) configuration, the markers are not representative of their true size, and been omitted.

M: Marker ladder, **YN:** *35S-SPYNE*; **YC:** *35S-SPYCE*, **DKDK:** *nch1 D28N-K42Q*

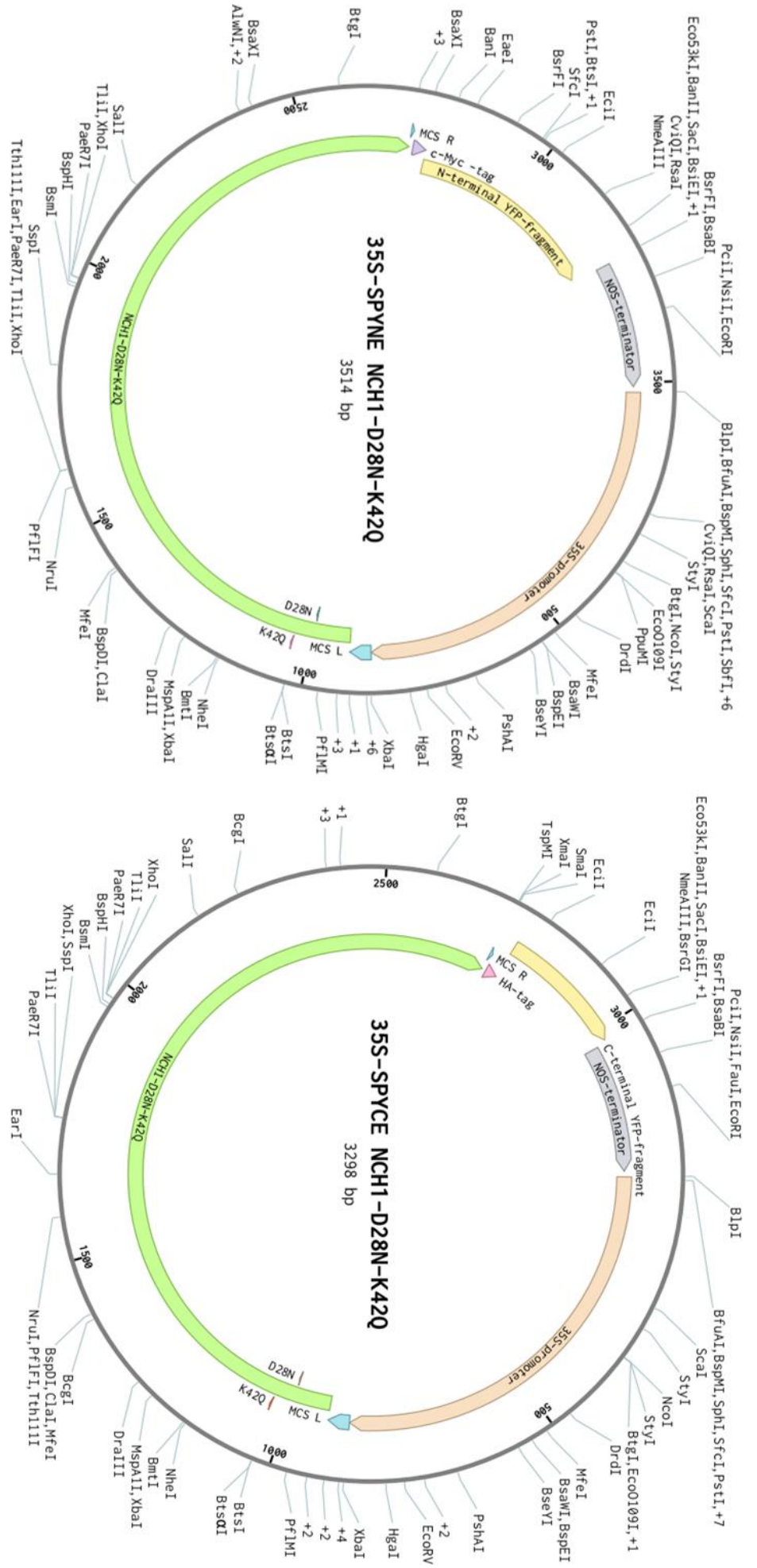


Figure 3.12 Plasmid maps for 35S-SPYCE *nch1* D28N-K42Q and 35S-SPYNE *nch1* D28N-K42Q.

The bifluorescence complementation (BiFC) vectors 35S-SPYNE and 35S-SPYCE with the putative dimerization mutant *nch1* D28N-K42Q made using NEB HiFi Assembly. Dimerization of the target protein brings the N- and C-terminal halves of the yellow fluorescent protein (YFP) together, resulting in a fluorescence signal during confocal microscopy. MCS: Multiple cloning site, left and right borders.

3.4. NCH1 protein Homodimerization

Previous studies by He et al. (2018) have reported the NCH1 ortholog protein to dimerize in potato (*Solanum tuberosum*). To investigate the dimerization of *Arabidopsis* protein AtNCH1 utilising transient expression in *Nicotiana benthamiana* model system, BiFC experiments were performed on plants infiltrated with BiFC constructs (35S-SPYNE and 35S-SPYCE) of wild type NCH1 and putative dimerization deficient NCH1^{D28N-K42Q}. BiFC is based on the assumption, that a yellow fluorescent signal is produced, when the two halves of the YFP chromophore, attached to the ends of two NCH1 proteins (35S-SPYNE-NCH1 and 35S-SPYCE-NCH1), come to close proximity as during protein dimerization, reconstituting the functional fluorescent protein.

Gene constructs containing both the desired *Arabidopsis*-derived N-terminal translational fusions of the WT NCH1 gene to the two halves of the YFP segment in the corresponding BiFC compatible vectors, 35S-SPYNE and 35S-SPYCE, reconstituting the functional YFP fluorophore during the protein interaction were prepared, using the site directed mutagenesis approach detailed in the previous section. Populations of *Agrobacterium* carrying both vectors were co-infiltrated in *Nicotiana benthamiana* leaves in 1:1 ratio, and visualised using confocal microscopy, as summarised in **Figure 3.13**. The results can be seen in **Figure 3.14 A-B**. The positive NPH3 control in **Figure 3.14 A** proved to give a strong positive dimerization signal, whereas both empty vector combinations used as negative controls were successful, with only sporadic background signal visible. In comparison to the positive NPH3 signal, 35S-SPYNE-NCH1 + 35S-SPYNE-NCH1 co-infiltration gave at least an equal level of fluorescence, providing strong evidence for the homodimerization of NCH1 proteins. In addition, the presence and estimated molecular weight of N-YFP or C-YFP fused proteins in tissue samples were confirmed using Western blot analysis for cMyc and HA tags (see **Figure 3.14 B**), which are the tags

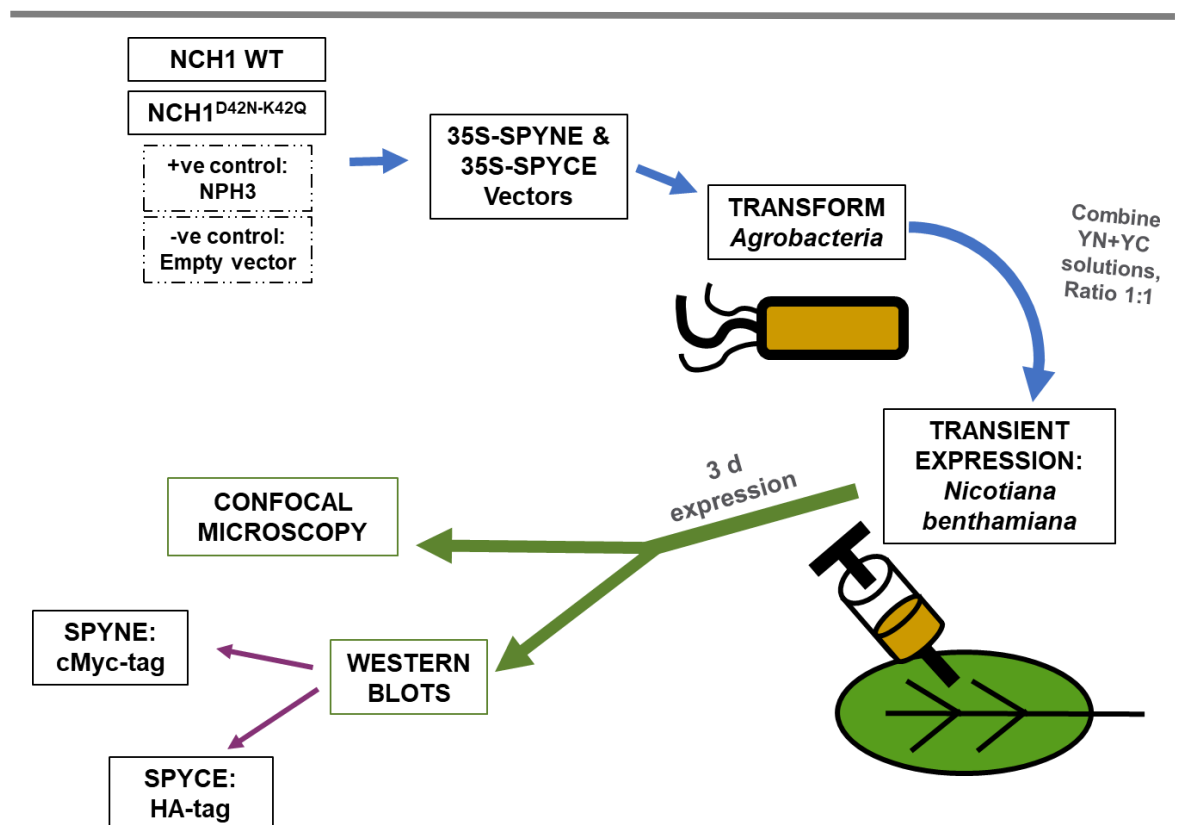


Figure 3.13 Schematic overview of the BiFC method used in this study.

See the previous section for the detailed construction of the BiFC constructs. Note the protein tags contained by the 35S-SPYNE and 35S-SPYCE BiFC vectors, that can be detected by antibodies in Western blots. **YN**: 35S-SPYNE; **YC**: 35S-SPYCE.

belonging to *35S-SPYNE* and *35S-SPYCE* plasmids, respectively. The anti-cMYC antibody sometimes gave a low signal, but it was always detectable when the *35S-SPYNE* vector contained an insert. The approximate molecular weights of the fusions were as expected.

The NCH1 homodimer is predicted to be held together by putative salt bridge sites at D28 and K42, which are therefore likely to contribute to the stability of the NCH1 homodimer. To test the ability of the mutant to dimerise, the *nch1*^{D28N-K42Q} mutant was made using site-directed PCR mutagenesis and introduced into the BiFC vector plasmids, similarly to the WT *NCH1*. Whereas wild type NCH1 protein produces a strong yellow positive dimerization signal (**Figure 3.15 A “NCH1 WT”**) at the plasma membrane, this signal is diminished in the mutant (**Figure 3.15 A “NCH1 DKDK”**), providing strong evidence for the contribution of these salt bridge-forming residues to the stability and inter-molecular integrity of the homodimer. The empty vector control E YN- E YC appeared to show more residual signal than usually, but the level was still clearly lower than the positive NPH3 control and WT NCH1 samples. Western blots (**Figure 3.15 B**) were performed from *N. benthamiana* leaf tissue samples, collected from the same leaves that were imaged for the figures using confocal microscopy, to confirm the protein expression in the visualised tissues. Antibodies recognising the cMyc and HA protein tags included in the *35S-SPYNE* and *35S-SPYCE* BiFC vectors were used, confirming the presence of these fusion proteins in the co-infiltrated leaf tissue.

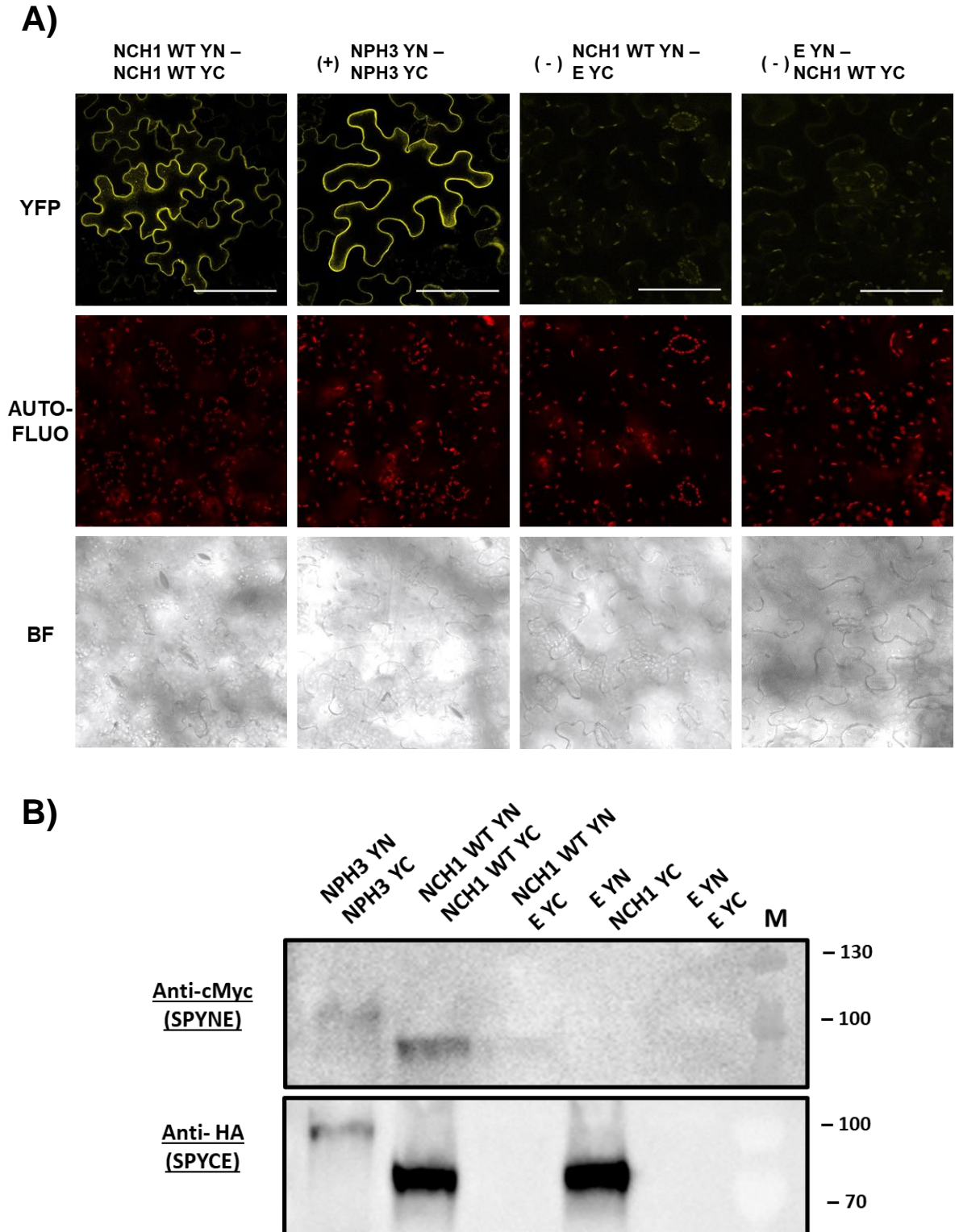


Figure 3.14 WT A α NCH1 forms dimers in planta.

A) Confocal micrographs showing dimerization of two WT NCH1 protein monomers during bimolecular fluorescence complementation (BiFC) experiment in *Nicotiana benthamiana*. Yellow signal is produced, when the two halves of the YFP chromophore, attached to the ends of two WT NCH1 proteins, come together and reconstitute the functional fluorescent protein. NPH3 is a positive control (+), whereas combinations with empty vectors, NCH1 YN-E YC, E YN-NCH1 YC and EYN-EYC are negative controls (-). **Autofluo**: Autofluorescence signal; **BF**: Brightfield image. **Scale bar** 100 μ m.

B) Western blot from the same tissues visualized in A. NPH3 is a positive control, whereas combinations with empty vectors, such as NCH1 YN-E YC, E YN-NCH1 YC and EYN-EYC are negative controls. Anti-cMyc antibody recognizes SPYNE fragment of YFP, whereas anti-HA recognizes the SPYCE fragment. **E**: Empty vector, **YN**: 35S-SPYNE BiFC vector, **YC**: 35S-SPYCE BiFC vector.

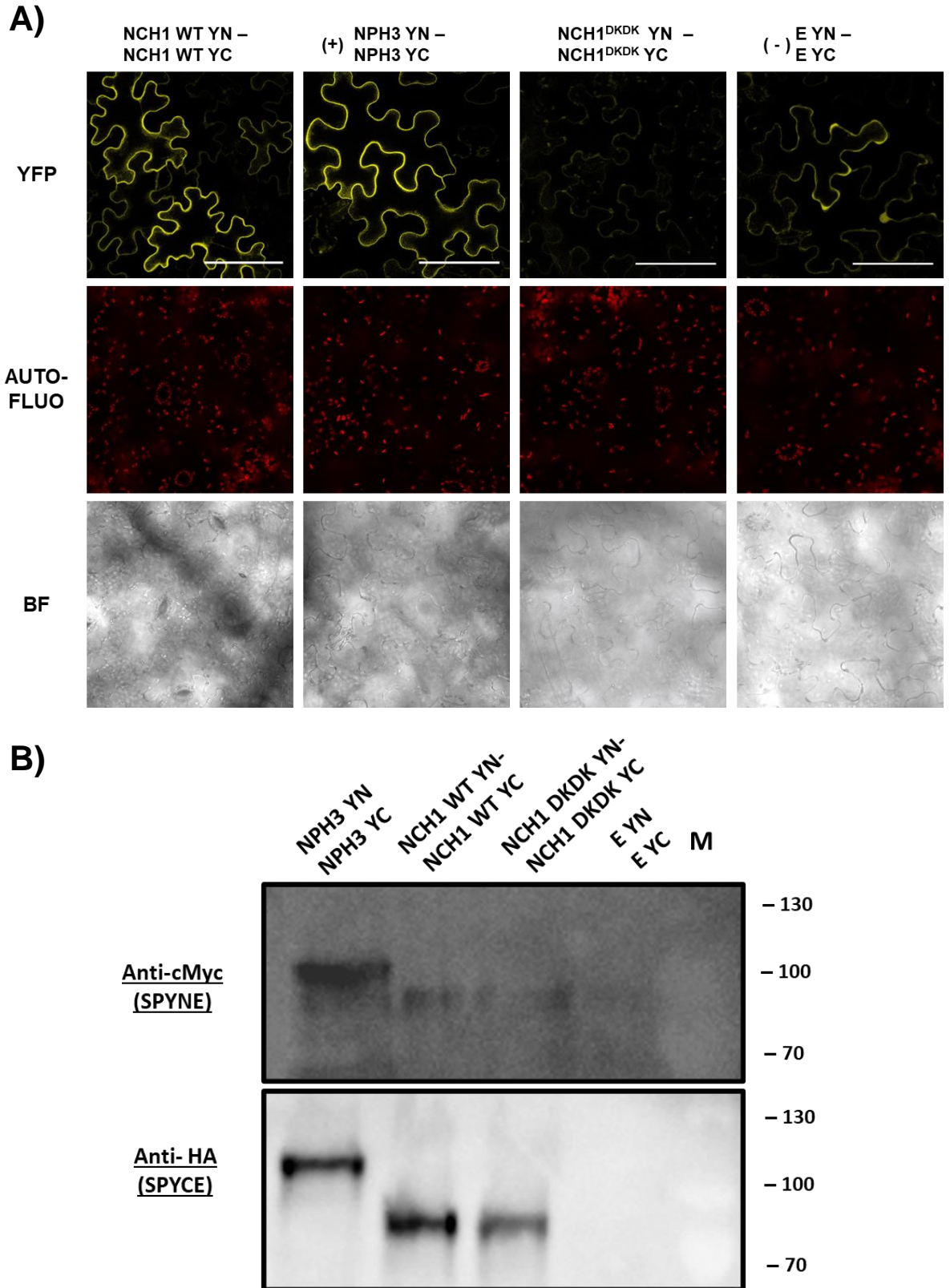


Figure 3.15 Mutagenesis of salt bridge residues D28N and K42Q prevents AtNCH1 dimerization in *Nicotiana benthamiana*.

A) Confocal micrographs showing dimerization of WT AtNCH1 and the putative dimerization-mutant NCH1-D28N-K42Q (DKDK) proteins during bimolecular fluorescence complementation (BiFC) experiment in *Nicotiana benthamiana*. NPH3 is a positive control (+), whereas the combination with empty vectors EYN and EYC function as a negative control (-). **Scale bar 100µm**. **YFP**: Yellow fluorescent protein, **Autofluo**: autofluorescence, **BF**: Brightfield image, **NCH1 WT**: Wild type AtNCH1 protein, **NCH1 DKDK**: Mutant NCH1-D28N-K42Q protein, **E**: Empty vector, **YN**: 35S-SPYNE-BiFC vector, **YC**: 35S-SPYCE-BiFC vector.

B) Western blot from the same tissues visualized in A. NPH3 is a positive control, whereas combinations with the empty vectors, EYN-EYC, are negative controls. Anti-cMyc antibody recognizes SPYNE fragment of YFP, whereas anti-HA recognizes the SPYCE fragment.

3.5. The Effect of NCH1 Phosphorylation Status on NCH1 Localization

As mentioned in Section 1.3.4, the NRL protein NPH3 is subject to regulation by phosphorylation (Christie et al., 2018). This raises the question of whether the closely related NCH1 is also phosphorylated and, if so, whether this affects its activity. Examination of the NCH1 protein sequence in the PhosPhAt database, which identifies putative phosphorylation sites in *Arabidopsis thaliana* proteins, revealed 52 potential target sites (**Figure 3.16 A**). Preliminary research in the supervisor's laboratory, recently published in the preprint (Sullivan et al., 2021) suggested that phots phosphorylate NPH3 at key RXS phosphorylation sites located at the extreme C-terminus, at residues S744 and S746. Out of these two, the S744 site appears to be crucial for protein function, localization and 14-3-3 interaction, as S744A mutation abolishes these NPH3 protein functions *in vivo*. A scan of the NCH1 sequence reveals several RXS motifs (**Figure 3.16 B**), including the C-terminal sites identified in NPH3, which are also conserved in other NRL proteins in multiple sequence alignment data (**Figure 3.16 C**). Interestingly, these conserved serine residues in NCH1, S602 and S604, are not identified as probable phosphorylation sites in the PhosPhAt database (**Figure 3.16 A**).

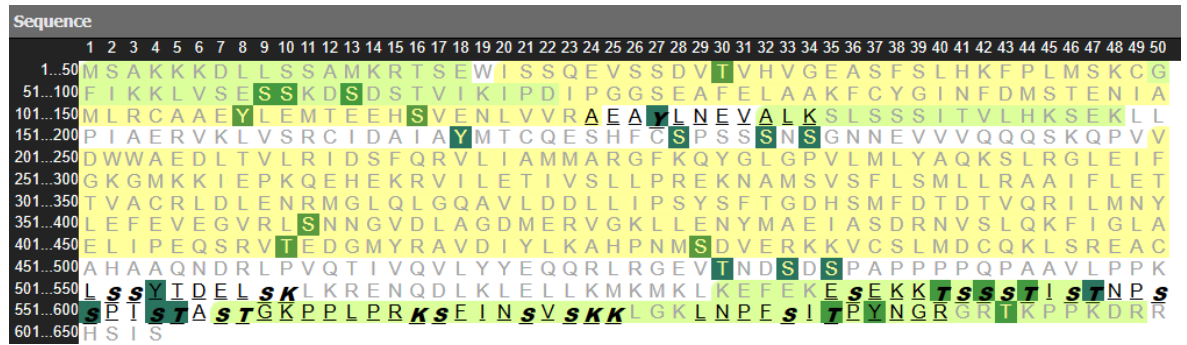
Preliminary data from a previous project by Dr. Noriyuki Suetsugu (University of Tokyo) had indicated that NCH1 C-terminal serine residues S602 and S604 could become phosphorylated by *Arabidopsis* kinases, potentially including phots. Therefore, to investigate the effect of phosphorylation of these residues on the localization of NCH1, putative phosphorylation deficient mutant *NPH3::GFP-nch1^{S602A-S604A}* was made for transient expression in *Nicotiana benthamiana*. The mutant was made in a *pEZR(K)LC* binary vector, see **Figure 3.17 A**. The binary vector *NPH3::GFP-nch1^{S602A-S604A}* was made by combining a *nch1^{S602A-S604A}* template with the GFP binary vector *pEZR(K)LC*, both courtesy of Dr. Noriyuki Suetsugu, University of Tokyo. The *nch1^{S602A-S604A}* insert was first mutagenized with restriction site overhang primers using PCR mutagenesis, which would produce both the *KpnI* and *BamHI* restriction sites in the forward and reverse strands, respectively, and include the desired S602A and S604A mutations in the coding sequence. Both *nch1^{S602A-S604A}* PCR fragment and the *NPH3::GFP-NCH1* vector were double digested with *KpnI* and *BamHI*, restriction enzymes (New England Biolabs, Massachusetts, US), and ligated together using T4 ligase (New England Biolabs, Massachusetts, US). The resulting construct was amplified in NEB 5α High Efficiency *E. coli* cells (New England Biolabs, Massachusetts, US), purified using a Miniprep kit (Qiagen, Hilden, Germany) and subsequently used to transform *Agrobacteria* for transient protein expression in *N. benthamiana*. A preliminary experiment was undertaken to test expression and localisation in darkness; the confocal micrographs were gathered from different *N. benthamiana* plants expressing *NPH3::GFP-WT NCH1*, putative phosphorylation deficient mutant *NPH3::GFP-nch1^{S602A-S604A}*, and positive *NPH3::GFP-NPH3* control.

The experiment was undertaken only once. The preliminary results (**Figure 3.18**) indicated that the putative phosphorylation mutant variant of NCH1, *NPH3::GFP-NCH1^{S602A-S604A}*, localized to the plasma membrane and exhibited similar localization to the WT NCH1 protein expressed in the transgenic *Arabidopsis* (**Figure 3.8 B**) or the *Nicotiana benthamiana* transient expression system expressing *AtNCH1* in BiFC constructs (**Figure 3.14**). The *NPH3::GFP-WT NCH1* samples also exhibited a plasma membrane localization in the present experiment (**Figure 3.18**), but some of the GFP-WT NCH1 appeared to exhibit an aberrant localisation behaviour that was not seen often in other experiments with different WT NCH1 constructs. This observed 'sock-like' expression pattern (marked in **Figure 3.18** with white arrowheads) could be a result of protein

(mis)localization in the cytoplasm and around the vacuole and appear as shading in the extremities of the cell as the large central vacuole pushes the cytoplasm against the plasma membrane. Other explanations for the changed appearance of the cell include overexpression artefacts or mislocalisation due to the use of non-native *NPH3* promoter. The positive *NPH3* control was successful, exhibiting the typical localization to the plasma membrane.

However, major drawbacks to the preliminary experimental design included the use of the non-native promoter from *NPH3*, which was used due to its ready availability at the time, since the native *NCHI* promoter was not present in the desired template. Therefore, the next proposed step for the experiment included the cloning of both the *NCHI* fragments, WT and S602A-S604A, under the control of the native *NCHI* promoter fusions. In addition to this, due to logistic constraints, the confocal images were taken before the sequencing results had arrived and were analysed, and the later analysis of the sequences indicated the plasmid sequence information to be ambiguous and require re-sequencing. In addition to this issue, the experiment was done only once. Due to these issues, the results of the preliminary experiment cannot be generalised, and the experiment should be repeated multiple times for better reproducibility and with the native *NCHI* promoter for all *NCHI* fusions. In addition to this, Western blots could be incorporated into the experimental design to monitor protein abundance in the desired tissues.

A)



B)



C)

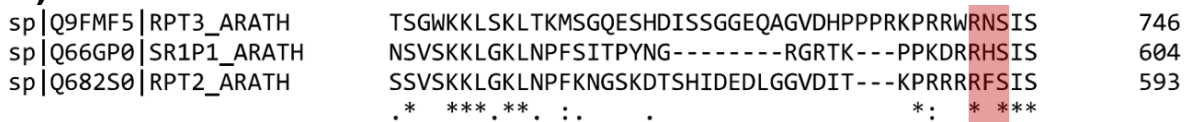


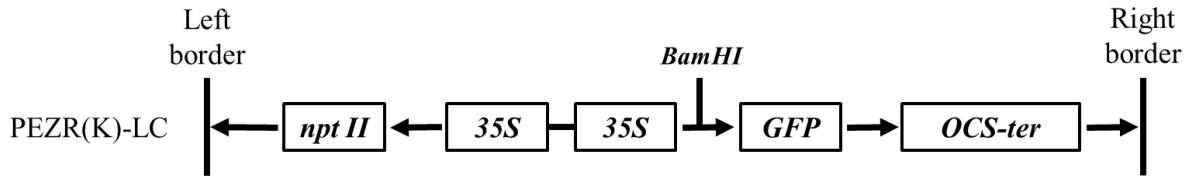
Figure 3.16 NCH1 protein contains multiple putative phosphorylation sites.

A) Predicted phosphorylation sites in NCH1 protein sequence, 52 in total. Dark teal colour signifies sites with higher probability scores, whereas lighter green sites with lower probability scores, and lightest green background phosphorylation hotspots. Yellow colour signifies protein domains. Bold letter signifies a site for which experimental data exists. Figure generated from PhosPhAt 4.0 -database (Heazlewood et al., 2008).

B) Presence of AGCVIII kinase target RXS motifs on the NCH1 protein sequence, marked with yellow bolded highlights. Note the location of the last RXS motif in the very C-terminus of the NCH1 coding sequence. Image generated according to query on Benchling to the translated coding sequence from Genbank -sequence database, ID EU796372.1.

C) Multiple sequence alignment of the C-termini of the NRL-subfamily of proteins, consisting of NCH1 (syn. SR1P1, centre), NPH3 (syn. RPT3, top) and RPT2 (bottom). C-terminal RXS motif is highlighted in red. Figure generated using Clustal Omega (Sievers et al., 2011), using protein sequence data from Uniprot database. Asterisk (*): Single fully conserved residue; Colon (:): Conservation between residues of similar property; Period (.) : Conservation between groups of weakly similar property.

A)



B)

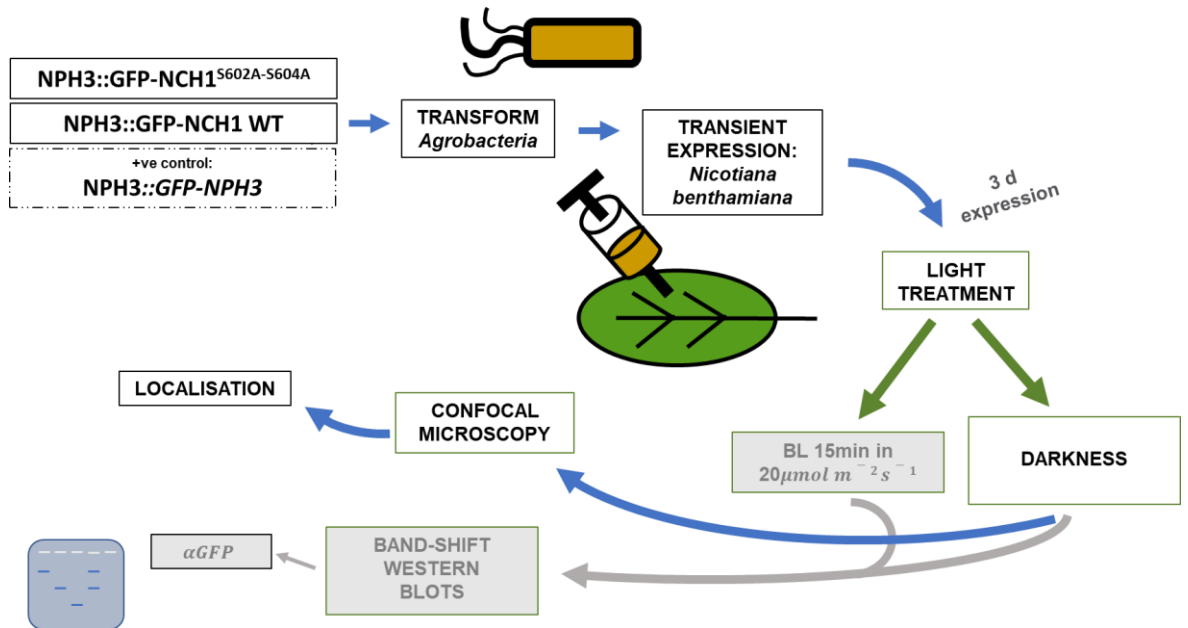


Figure 3.17 Expression of GFP-containing binary vectors in *N. benthamiana*.

A) Schematic representation of the *pEZR(K)LC* binary vector. *BamHI* restriction site indicates the restriction site used for the ligation of the gene fragment of interest in place. **npt II**: neomycin phosphotransferase (antibiotic resistance); **35S**: cauliflower mosaic virus 35S-promoter; **GFP**: Green fluorescent protein; **OCS-ter**: octopine synthase gene terminator. **Left and right border** refer to the sides of the T-DNA. Figure modified from Zhang et al. (2018)

B) Schematic overview of the experimental strategy. Items on the grey background were planned as a part of the experiment but not executed during the preliminary stage.

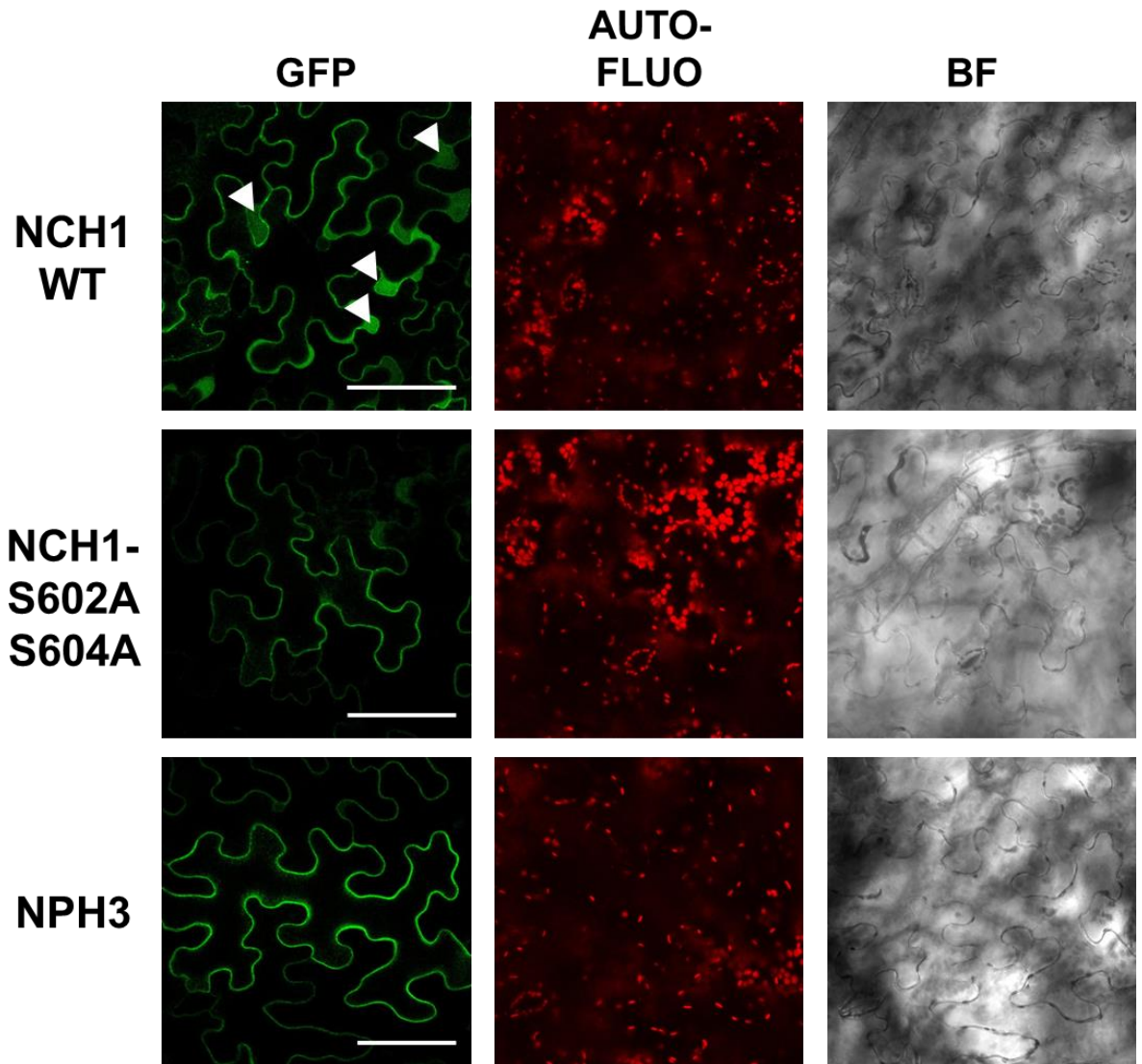


Figure 3.18 Preliminary confocal micrograph data on the subcellular localisation of the *At*NCH1 putative phospho-mutant NCH1^{S602A-S604A} suggests NCH1 localization is not determined by its phosphorylation status.

The pictures were gathered from *Nicotiana benthamiana* leaves treated with *Agrobacterium* infiltration method, transiently expressing *NCH1::NCH1-GFP*, *NCH1::NCH1^{S602A-S604A}-GFP* and *NPH3::NPH3-GFP*. The bright expression patterns of WT NCH1 (marked with white arrowheads) were thought to be overexpression artefacts. **Scale bar 50 μ m.**

3.6. Discussion of Findings

As stated before in the section 1.4, the aims of the biochemical characterisation branch of the investigation included: **a)** studies on the subcellular localization of *At*NCH1 in response to light, by utilising fluorescent protein mCit tagging and time-lapse confocal microscopy in stable *Arabidopsis* expression systems, and following the localization of the mCit-NCH1 from dark-grown etiolated seedlings to sustained 10 minute BL irradiation; **b)** investigation of NCH1 dimerization based on the studies of its potato ortholog *S*tNRL1 (He et al., 2018), the introduction of synonymous mutations to the *At*NCH1 protein by mutagenesis PCR to create functional *nch1*^{D28N-K42Q} BiFC vectors; **c)** use of the constructed BiFC vectors in the dimerization studies of NCH1, and to study the effects of dimerization mutations D28N and K42Q on NCH1 localization; **d)** investigation of the NCH1 phosphorylation status by the introduction of putative phosphorylation site mutations *nch1*^{S602A-S604A} to produce an initial binary vector construct for the future study of the roles of C-terminal phospho-mutations on the NCH1 phosphorylation status, intracellular localization and dimerization.

In the localization experiments, the mCit-tagged WT *At*NCH1 protein was found to localize to the plasma membrane and/or be a membrane-associated protein *in planta* when visualised in transgenic *Arabidopsis* hypocotyls (section 3.2). This is in line with the hypothesis formulated based on the bioinformatic data (section 3.1 and 3.2) and literature regarding the related proteins (Haga et al., 2015; Reuter et al., 2021), suggesting NCH1 to be a putative membrane-associated protein similarly to its related NRL proteins, NPH3 and RPT2. However, from the hydropathy analysis, it is very unlikely that NCH1 would contain transmembrane regions or be a single-pass transmembrane protein, and therefore it is more likely, that the membrane association would be through other means than by integral membrane domains. For example, Reuter et al. (2021) suggested that the NPH3 C-terminal positively charged motif could bind membrane phospholipids by electrostatic interactions, while a C-terminal amphipathic helix is embedded into the cytosolic leaflet of the plasma membrane, interacting with the hydrophobic membrane core. Polybasic motifs and electrostatic interactions are known to facilitate membrane attachment and play a role in lipid modifications facilitating membrane tethering and targeting, such as myristoylation: This is known to be the case e.g. with G α proteins (Crouthamel et al., 2008). While NCH1 does not appear to contain such a charged polybasic motif in its C-terminus according to bioinformatic analysis, it is likely to be a peripheral membrane protein and associate with the membrane through other mechanisms, for example, by associating with other transmembrane or peripheral membrane proteins, or anchors.

The difference in membrane association between NPH3 and NCH1 could also be reflected in the different subcellular localization patterns: unlike the NPH3 protein that was used as a positive control in the localization experiment, NCH1 does not exhibit dynamic relocalization patterns in response to light. Instead, the NCH1 signal was found to be constant and static at all points of the time course experiment, from etiolated seedlings to sustained irradiation with BL up to 10 min. Protein-protein interactions may underpin different localization patterns in addition to the mechanism of membrane association. NPH3 requires RPT2 for its re-association with the plasma membrane in darkness after initial light-dependent relocalization from the plasma membrane to the cytoplasmic foci (Reuter et al., 2021). In contrast, other proteins might play a role in the membrane association of NCH1, and NCH1 might dissociate from the plasma membrane in other conditions modulating protein-protein interactions. Therefore, the investigation of NCH1 phosphorylation patterns is important, as phosphorylation might function as a switch for possible interacting protein partners: out of the three NCH1

interacting proteins found in the *in silico* analysis, *AtSR1* is an immunity-related serine/threonine kinase (Zhang et al., 2014), which might modulate NCH1 phosphorylation status in response to immune cues. Other proteins of interest for NCH1 interactions would be other proteins associated with chloroplast movement, such as CHUP1 and KAC1/2, in addition, keeping in mind that NCH1 is also a E3 ubiquitin ligase, it might negatively regulate proteins that mediate chloroplast accumulation movement.

The dimerization status of *AtNCH1* was studied using BiFC methodology, with dimerization reconstituting a split YFP chromophore. It was found that *AtNCH1* samples exhibited a bright YFP signal at the expected location at the plasma membrane, providing strong evidence that the protein is a dimer. As it was hypothesised, that the protein would be held together by salt bridges forming at residues D28 and K42. The putative dimerization mutant NCH1^{D28N-K42Q} indeed exhibited a reduced YFP dimerization signal, supporting the hypothesis for NCH1 dimerization. The data on the homodimerization ability of NCH1 also raises other questions of interest, namely whether NCH1 homodimerization status changes in response to light or during immune challenge. Preliminary BiFC studies on the heterodimerization of the WT *AtNCH1* protein and its relative *AtNPH3* suggested that there are no hetero interactions between these two under normal conditions in light-grown *N. benthamiana*, but further investigation of this is required. In addition to NCH1-NPH3 hetero interactions, it would also be important to study heterodimerization between NCH1 and NCH1's most closely related protein RPT2, with which NCH1 is partially functionally redundant, along with other members of NRL family proteins and the chloroplast movement machinery. In addition, the dimerization status and protein partners might change during pathogen challenge.

According to the current models, NPH3 localization is thought to be dependent on the interacting protein RPT2, the phosphorylation status of the third last C-terminal residue S744 and association with 14-3-3 protein -- especially ϵ and ω isoforms (Reuter et al., 2021) -- at the NPH3 C-terminus: BL irradiation initiates the net dephosphorylation reaction yet simultaneous phosphorylation of the residue S744, which in turn triggers the subsequent 14-3-3 protein association with the C-terminus and the consequent NPH3 release from the plasma membrane to the cytoplasm (Reuter et al., 2021). This raises the possibility that the phosphorylation status of NCH1 has the theoretical potential to affect its localization and possibly initiate subcellular relocation. To provide insight into this matter, the subcellular localization of the putative phosphorylation deficient mutant was investigated in preliminary experiments using the transiently expressed *AtNCH1* protein and confocal microscopy of *Nicotiana benthamiana* leaves. Initial results from the confocal microscopy and comparison of the *NPH3::GFP-WT NCH1* and putative phosphorylation mutant *NPH3::GFP-nch1^{S602A-S604A}*, alongside with the positive control *NPH3::GFP-NPH3*, suggested the phosphorylation mutant to localize to the plasma membrane. However, the critical weaknesses in the experimental design, including that only one experiment was performed, the requirement for further validation of the construct sequence and the use of a non-native promoter mean that the preliminary results have limited value and further experimentation with larger sample sizes and native promoter constructs is required to investigate whether phosphorylation has a role in NCH1 function.

4. The Effect of NCH1 on Immunity in *Arabidopsis*

4.1. Introduction

NCH1 is a multifunctional protein with links to both plant blue light signalling (Christie et al., 2018) and immunity (He et al., 2018; Zhang et al., 2014). While the BL signalling functions of NCH1 have been connected to chloroplast movement – and specifically, the chloroplast accumulation response – the known immune functions of NCH1 have so far been independent of chloroplast movement. Instead, they have been found to be connected to the function of NCH1 as a ubiquitin E3 ligase substrate acceptor for SCF (Skp1–Cullin–F-box) E3 ubiquitin ligase family proteins CULLIN3A (CUL3A) and 3B (CUL3B) (Choi et al., 2014; Gingerich et al., 2005; He et al., 2018; Willems et al., 2004; Zhang et al., 2014). However, studies by He et al. (2018) and Zhang et al. (2014) found contrasting functions for NCH1, as both a positive and a negative regulator of immunity: He et al. (2018) found NCH1 to be a negative regulator of immunity in potato, while Zhang et al. (2014) considered it a positive one in *Arabidopsis*. As these two examples form the main body of experimental evidence on the role of NCH1 on plant immunity, their findings shall be reviewed in detail in this section.

In potato (*Solanum tuberosum*), NCH1 ortholog *StNRL1* appears to promote the proteasomal degradation of a positive immune regulator *StSWAP70* (He et al., 2018), as shown in **Figure 4.1 A**. NCH1, therefore, forms a part of the plant homeostasis in the absence of pathogen challenge: SWAP70 is a component of plant pathogen recognition machinery during the immune response, and promotes a type of plant hypersensitive reaction/programmed cell death called INF1 triggered cell death (ICD) in response to the *P. infestans* protein INF1 to limit the spread of the oomycete in the plant tissues. However, as a part of the homeostasis and prevention of autoimmunity, NCH1, therefore, discourages unnecessary SWAP70-mediated ICD through negative regulation and ubiquitin-dependent SWAP70 turnover in the absence of immunological challenge as an E3 ubiquitin ligase substrate acceptor for CUL3 (He et al., 2018). As pathogen effectors interfere with the normal plant signalling and ubiquitination and proteasomal protein degradation pathways can be readily targeted by plant pathogens, NCH1 is not an exception: potato NCH1 was found to be targeted by *P. infestans* RLXR effector Pi02860 (syn. SRE1), which appeared to function by enhancing the interaction between NCH1 and SWAP70, which in turn promoted the degradation of SWAP70, downregulating the hypersensitive response and allowing the pathogen to colonise plant tissues more efficiently (He et al., 2018; Naveed et al., 2020).

In addition to its ortholog in potato, there is also evidence for NCH1 mediated immune functions in *Arabidopsis* dependent on its E3 ubiquitin ligase substrate adapter function yet as a positive regulator of plant defence in contrast to the findings in potato. As rapid Ca²⁺ uptake response is a typical signalling event in infected cells during both MTI and ETI signalling yet appears to suppress SA mediated immunity and SAR in plants, the additional layers of signalling must overcome the negative effect of Ca²⁺ on SAR (Zhang et al., 2014). Therefore, the intracellular calcium spike forms an important signalling cue that activates calcium-dependent proteins, such as the calmodulin-binding calcium-dependent transcription factor and plant immune defence suppressor SR1 (syn. CAMTA3) (Zhang et al., 2014). As SR1 is a transcriptional repressor of SA mediated immunity in immunologically unchallenged *Arabidopsis* plants, and a negative regulator of the positive ETI marker and plant SA mediated immunity protein EDS1, NCH1 (syn. *AtSR1IP1*) was found to target SR1 for degradation under high intracellular Ca²⁺ conditions during *Pst* DC3000 challenge (Zhang et al., 2014). This regulatory feedback loop is pictured in **Figure 4.1 B**. NCH1 was found to interact with SR1's TIG domain

from its NPH3 domain in Cytotrap two-hybrid screens, and further to ubiquitinate SR1 for targeted degradation as a substrate adapter of plant CULLIN 3 (CUL3) E3 ligase in response to *Pst* DC3000 challenge (Zhang et al., 2014). Therefore, NCH1 was found to be a positive regulator of the SAR and SA mediated immunity, further ensuring, that the negative regulation of the intracellular Ca^{2+} influx is overcome and the transcriptional repression by SR1 removed despite the Ca^{2+} influx (Zhang et al., 2014). Accordingly, Zhang et al. (2014) found *Arabidopsis nch1-1* mutants to have a reduced resistance against *Pst* DC3000 as SR1 turnover and SAR was prevented, while *NCH1* over-expressing plants contrastingly had more robust disease resistance than wild type plants. Negative *sr1* mutant plants similarly had a constitutive SAR and autoimmune phenotype, as SR1 was proposed to be a negative regulator of immunity and would therefore repress *EDS1* transcription in the absence of immunological challenge. *nch1/sr1* double mutant *Arabidopsis* plants had stunted growth and enhanced disease resistance phenotype due to the constitutive defence and *PR* gene expression, revealing SR1 and NCH1 to be on the same immunity pathway, and NCH1 being epistatic to SR1. In addition to immunity and biotic stress, the SR1 transcription factor appears to underlie also other environmental stresses, such as freezing and salt tolerance (Prasad et al., 2016).

These findings form the theoretical background for the studies on the role of NCH1 in plant immunity. For this thesis, the plant pathology branch of the investigation was started by utilising the flood assay method to inoculate *Arabidopsis* plants with *Pst* DC3000. This method was used to visually examine the course of bacterial *Pst* DC3000 infection on WT *Arabidopsis* and the quantification of the bacterial titre in the WT plants from the day of inoculation up to 6 days post-inoculation (DPI6). After this, the role of NCH1 on plant immunity was studied in transgenic *Arabidopsis* plants (courtesy of Dr. Noriyuki Suetsugu, University of Tokyo) by subjecting *nch1-1 / rpt2-3* double mutant *Arabidopsis* plants to the flood assay. The double mutant plants were chosen to reduce the effect of functional redundancy between these two proteins. The flood assay method was also further developed into a new version to include both transplantation for more uniform sampling and surface sterilization for higher resolution.

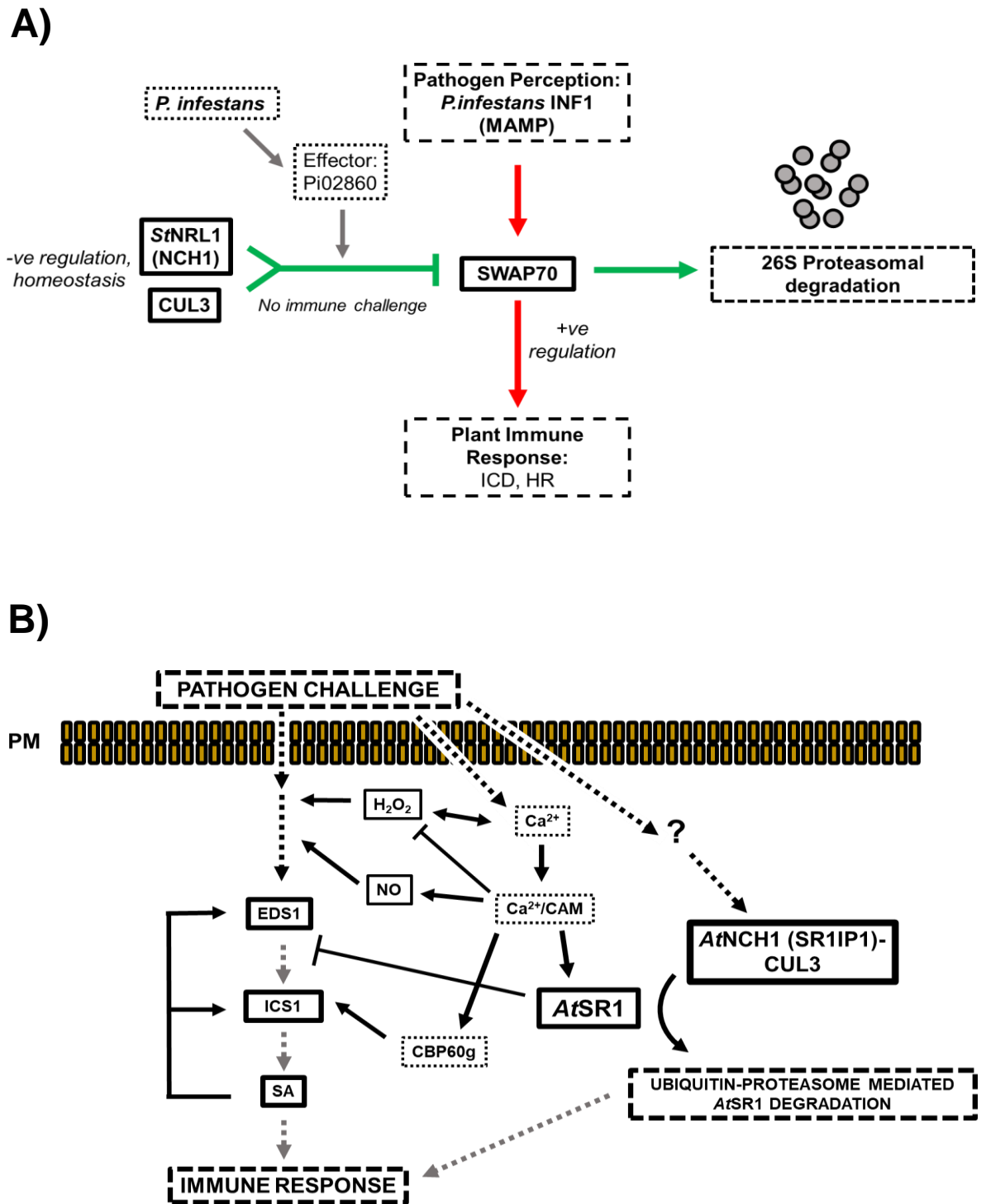


Figure 4.1 Models of NCH1 function in plant immunity.

A) Model of the function of *P. infestans* effector Pi02860 in down-regulating the plant susceptibility factor StNRL1 (NCH1 ortholog) through SWAP70, leading to unregulated proteolysis of SWAP70 and down-regulation of plant immune response. Figure modified after He et al. (2018).

B) NCH1 (syn. SR1IP1) functions in the SA-mediated branch in the plant defence pathway by modulating AtSR1 concentration and activity. Therefore, NCH1 overcomes the negative regulation on immunity by high intracellular Ca^{2+} concentration, releasing transcriptional repression from the key SA immunity gene *EDS1*, and promoting SA-biosynthesis and SA-mediated defence responses. Potential alternative links between NCH1 and immunity against biotic stresses such as pathogen challenge are unknown. Figure after Zhang et al. (2014).

4.2. *Pst* DC3000 Time course Experiment: Visual Assessment of the Infection Cycle

The visual symptoms of a compatible infection between *Pst* DC3000 and *Arabidopsis thaliana* depend on the phase of the infection: in the epiphytic phase when the bacteria have not entered the plant tissues but secrete effectors and phytotoxins to facilitate invasion and force the stomata open (Geng et al., 2012; Toum et al., 2016), the plants may appear visually normal as the bacterial titre is low and they are in the lag phase of population growth. However, as the motile pathogens will enter the plant, the endophytic phase is characterised by rapid pathogen multiplication in the apoplast and the consequential appearance of chlorosis on the leaves, characteristic of the coronatine phytotoxin secreted by the bacteria (Xin and He, 2013). As *Pst* DC3000 is a hemibiotroph, the normal infection cycle also involves the death of the healthy host plant tissue, which manifests in *Arabidopsis* as necrotic, water-filled lesion spots (Xin and He, 2013).

To study the course and follow the progression of the disease symptoms of *Pst* DC3000 infection in 10-14d old wild type (WT) *Arabidopsis* seedlings grown on ½ MS + Sucrose medium, the plants were *Pst* inoculated using the flood inoculation method (old protocol) adapted from Ishiga et al., 2011 and described earlier in **Figure 2.1** and reviewed in **Figure 4.2**. The progression of disease symptoms was followed by taking representative photographs of the same plate of WT *Arabidopsis* seedlings, using a mounted Canon EOS 1000D digital SLR camera (Canon Inc., Ota, Japan) every day over the course of the infection up to 6 days post-inoculation (DPI). The manufacturer's standard optics and settings were used and the distance from the plates was maintained at 50 cm. Images can be seen in **Figure 4.3**, where the plants can be seen following the typical course of the hemibiotrophic *Pseudomonas* infection: the plants appear relatively healthy for the first two days before starting to exhibit hallmarks of endophytic infection and the exponential bacterial growth phase, such as visible chlorosis, liquid-filled lesions and tissue necrosis from DPI3 onwards. In the end at DPI6, the severity of disease symptoms appears visually worse than even DPI4, with chlorosis affecting practically all photosynthetic leaf area. While literature did not mention root phenotypes for the *Pst* infection, and instead, described *Pst* infection as a condition affecting the phyllosphere, the roots were witnessed to accumulate a white coloured coat of unknown physiological or immunological relevance.

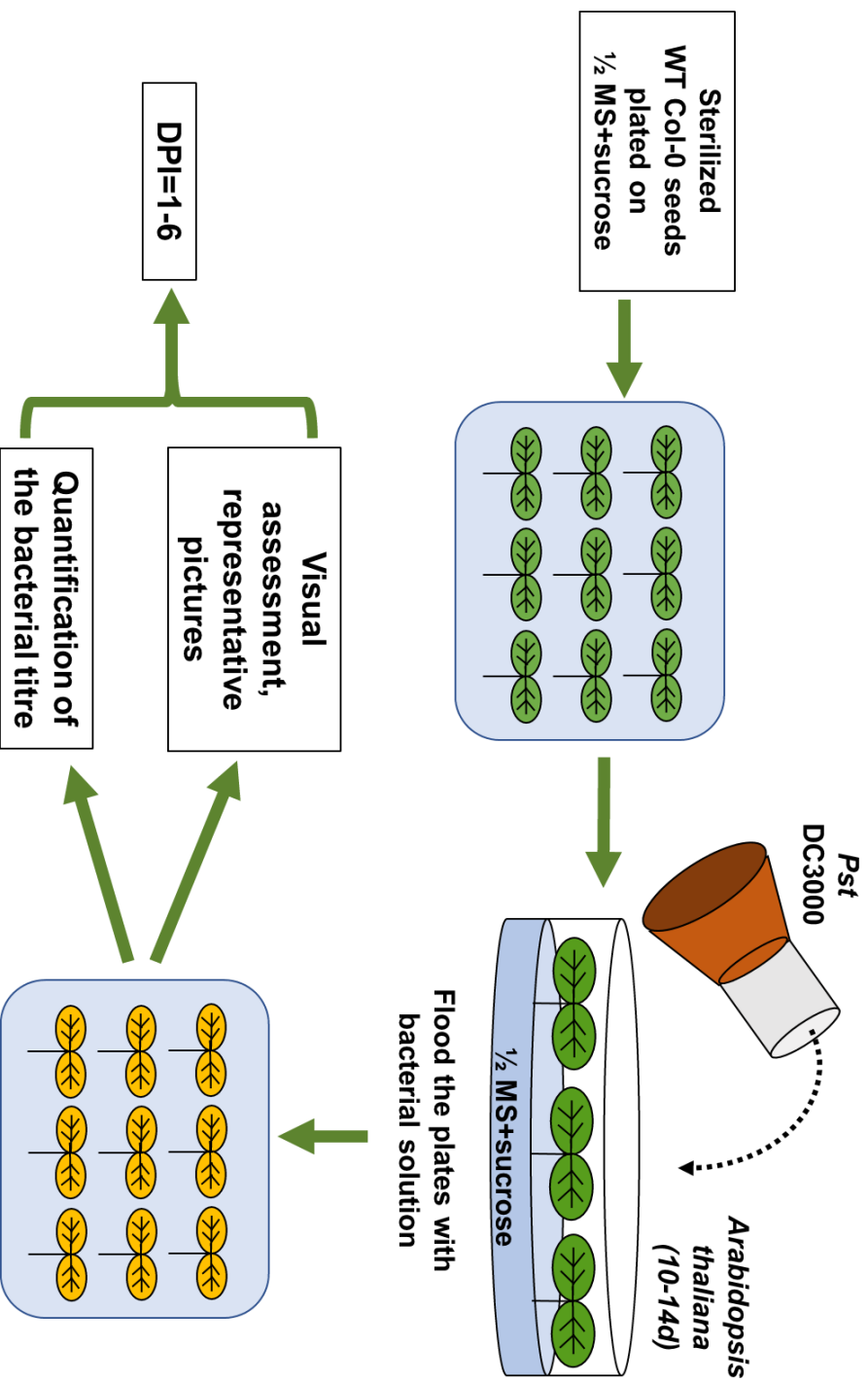


Figure 4.2 Schematic overview for the time course experiment methodology.

A flow chart presenting the general steps of the flood assay method and the two assessment methods of the infection, visual and bacterial quantification. The flood assay was done according to the 'old protocol' described in "Materials and Methods" section 2.5.

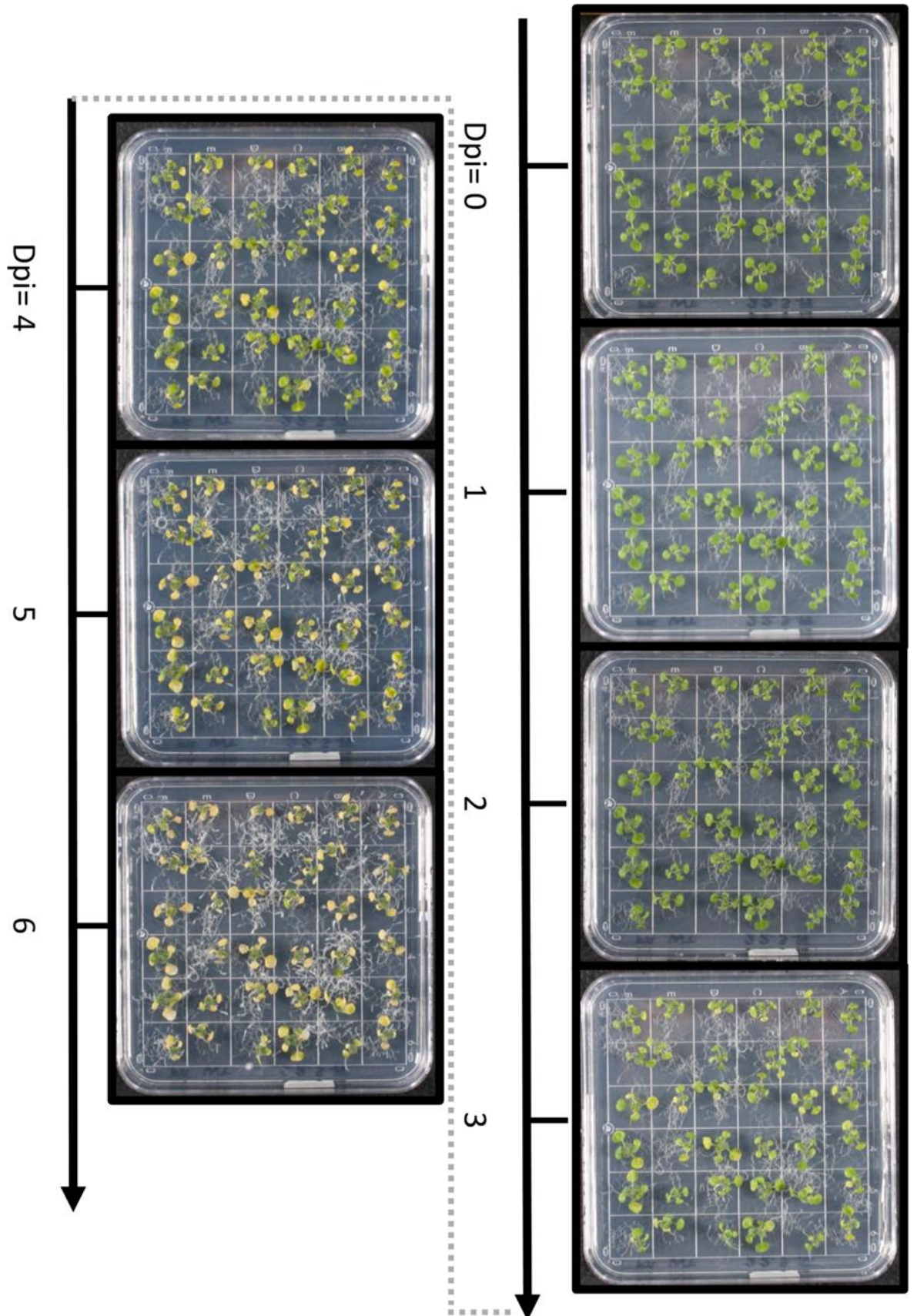


Figure 4.3 Visual assessment of *Pst* DC3000 Infection in WT *Arabidopsis*.

Plants were infected using the flood assay method at the age of 14 days and representative pictures taken every day of the same plate between DPI0 and DPI6. **DPI**: Day(s) post-inoculation.

4.3. *Pst* DC3000 Time Course Experiment: Bacterial Titre in WT *Arabidopsis*

To provide an exact quantification of the bacterial titre in WT *Arabidopsis* tissue over the course of the *Pst* DC3000 infection and to relate the visual time course data with the quantified live bacterial titre inside the leaf tissue in colony-forming units per millilitre, $\log_{10}(\text{cfu/mL})$, *Pst* flood-inoculated plants were weighed (sample weight between 20-100 mg), surface sterilized, and lysed, and the resulting *Pst*-infected cell lysate was diluted in 10 mM MgCl_2 10 mM MES (pH 5.6) buffer to construct a dilution series. The resulting serial dilutions were plated on King's B agar plates with rifampicin antibiotic (50 $\mu\text{g/mL}$) specific for the *Pst* DC3000, with three 10 μl spots of each solution plated per dilution. For DPI0, dilutions of 10^{-1} - 10^{-4} were plated on King's B agar plates, whereas for DPI1-6 the dilutions of 10^{-4} - 10^{-9} range were plated to acquire a good resolution for colony counts. The resulting inoculated plates were incubated at 28°C for 2-3 days, after which the colonies were counted and recorded. The number of colonies, dilution, and the exact weight of the harvested tissue was used to calculate the final logarithm of colony-forming units per milligram of tissue, $\log_{10}(\text{cfu/mg})$.

The results, shown in **Figure 4.4**, exhibit a somewhat typical bacterial growth curve from DPI1 to DPI6. The initial bacterial inoculum from the flood assay method at DPI0 without surface sterilization was found to be $2.55 \log_{10}(\text{cfu/mL})$, from which the bacterial population would start their lag phase. However, the data would indicate that the flood inoculation method gives high enough initial bacterial inoculum, that the initial lag phase is minimal in duration, only hours. Therefore, the bacterial growth reaches an exponential growth phase very quickly, by 1 DPI. Furthermore, the bacterial population appears to reach its peak and plateau between DPI3-4 at population between 7-8 $\log_{10}(\text{cfu/mL})$, which was expected from the literature (see Ishiga et al. (2011)). However, while there were more samples for DPI0 and DPI3 than for the other days' samples, it is unclear why the WT bacterial titres seemed to dip at DPI3. As DPI0 and DPI3 had more biological replicates than the other reference points, the unexpected result might indicate stochastic differences in the data points other than

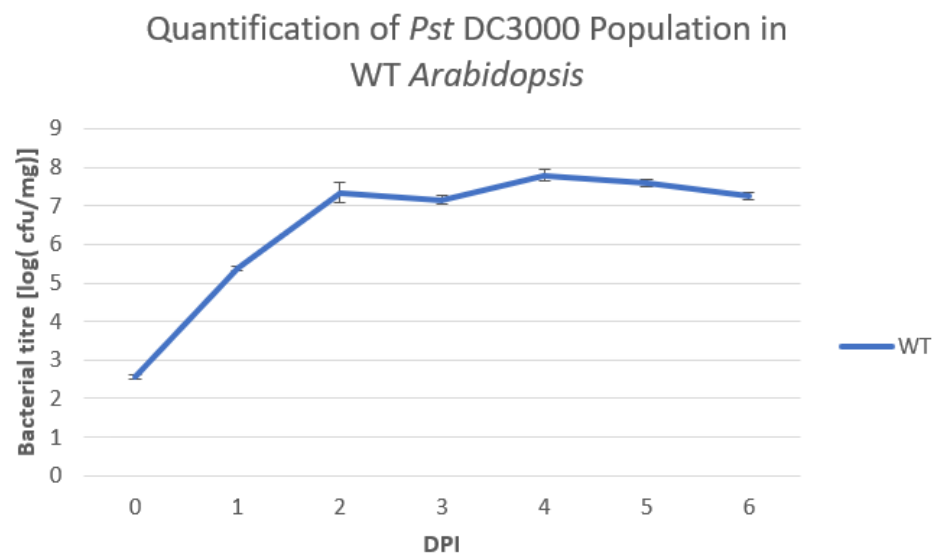


Figure 4.4 *Pst* DC3000 population growth curve in WT *Arabidopsis*.

Pst DC3000 population growth curve from DPI0 (the day of inoculation) to DPI6, measured in the logarithm of colony-forming units per milligram of plant tissue, $\log_{10}(\text{cfu/mg})$. Data are the mean of samples collected from separate Petri dishes for each genotype from which independent tissue samples were assayed for bacterial titre and adjusted for the logarithm of cfu/mg of plant tissue. Replicates as follows: DPI0 (n=24); DPI1(n=12); DPI2(n=4); DPI3(n=13); DPI4(n=4); DPI5(n=8); DPI6(n=4). Error bars represent the standard error.

DPI3, and the fact these samples were inoculated each time with one single *Pst* flood inoculation solution coming from a single picked *Pst* colony.

4.4. Quantification of Bacterial Titre in NRL Mutant Plants

To determine whether *NRL* mutant plants are more susceptible to the *Pst* DC3000 infection than WT plants, the data from the WT Col-0 plants and the time course experiment was used as a baseline for the *Pst* bacterial titre comparisons in transgenic *NRL* mutant plants. The comparisons were done in two branches: Firstly, the comparison of bacterial titres in WT, *nch1-1* and *rpt2-3* single mutants, and *nch1-1/rpt2-3* double mutants at DPI0 and DPI3, and secondly, a similar 7-day time course experiment for *nch1-1/rpt2-3* double mutant as was done for the WT Col-0 *Arabidopsis*. Therefore, the hypotheses formulated according to the literature were, that **a)** the inoculum at DPI0 should be roughly similar in all genotypes, **b)** at DPI3 timepoint, *nch1-1/rpt2-3* double mutant would be expected to be more susceptible than WT plants and the single mutants due to the partial functional redundancy between NCH1 and RPT2, and **c)** for this reason, the single mutants would land between the double mutant and WT Col-0 plants in terms of bacterial titres at DPI3. To test these hypotheses, *Pst* DC3000 was used in flood assays to determine the susceptibility of 10-14-day old *Arabidopsis* seedlings against bacterial infection. Bacterial titres were quantified by lysing plant tissue samples (sample weight between 20-100 mg) from infected WT Col-0, *nch1-1* and *rpt2-3* single mutants and *nch1-1/rpt2-3* double mutant plants and spreading the diluted lysate on King's B agar plates. For DPI0, lysate dilutions of 10^{-1} - 10^{-4} were plated on King's B agar plates, whereas for DPI1-6 the dilutions of 10^{-4} - 10^{-9} range were plated to acquire a good resolution for colony counts. The resulting inoculated plates were incubated at 28°C for 2-3 days, after which the colonies were counted and recorded. The number of colonies, dilution and the exact weight of the harvested tissue was used to calculate the final logarithm of colony-forming units per milligram of tissue, \log_{10} (cfu/mg).

In the first experiment, data were collected both for DPI0 and DPI3 to determine the effect of genotype on the immunity of the WT and mutant *Arabidopsis* plants. DPI3 was chosen as the date of sampling as a result of literature search, as many papers recommend either DPI3 or DPI4 as the preferred sampling date (e.g., Khare et al., (2016); Sohn et al., (2012); de Torres Zabala et al. (2015)). Indeed, the results from the initial WT time-course experiment (**Figure 4.4**) suggested the bacterial titre to plateau between 3-4 DPI, as the bacterial population transitions from the exponential phase to the stationary phase. Moreover, since other studies (e.g. Ishiga et al. (2017a,b) have successfully used DPI0 and DPI3 as the time points for quantifying the effects of mutations on plant immunity, they were chosen for comparison of WT and *nch1-1/rpt2-3* double mutant plants.

The results (**Figure 4.5 A**) on the effects of *NRL* family (*nch1-1*, *rpt2-3*, *nch1-1/rpt2-3*) mutations on the disease resistance in *Arabidopsis* suggested *nch1-1* and *rpt2-3* single mutants, and *nch1-1/rpt2-3* double mutants had decreased disease resistance against *Pseudomonas syringae* in comparison to the wild type. This *Pst* flood assay data suggests *nch1-1/rpt2-3* double mutants may exhibit slightly impaired disease resistance against *Pst* in comparison to the WT Col-0, as the bacterial titres in \log_{10} (cfu/mg) seem slightly higher in double mutants ($7.71 \log_{10}$ (cfu/mg)) than in WT Col-0 plants ($7.15 \log_{10}$ (cfu/mg)). The result for the *nch1-1/rpt2-3* double mutant was found to be statistically significant at $P \leq 0.05$ with Student's T-test (two samples with equal variances, tested beforehand with an F-test), but not at a lower confidence interval of 0.01 (ie. $P \geq 0.01$). For the statistics breakdown, see **APPENDIX 2: *Pst* DC3000 Flood Assay Data Statistics (DPI3)**.

In addition to the comparison of DPI0 and DPI3 results, a time-course experiment from DPI0 to DPI6 was done for the double mutant to provide a comparison for the WT Col-0 plant data. For the time course data regarding the double mutants, see **Figure 4.5 B**. As it can be seen from the graph, the bacterial populations in

the double mutant plants appeared to be very similar to the WT Col-0 plants, with similar curve shape and overall titres – apart from the WT DPI3 sample, which appears to be significantly lower in comparison to the other data points. Overall, this raises the question, whether the external flood inoculation method would leave a high enough inoculum on the plant surface that would persist on the epiphytic surfaces, if not necessarily multiply. Therefore, this provided a further idea for method optimization and would support the addition of an additional surface sterilization step for the plant tissue sampling. However, the sample sizes, especially on the single mutants and DPI on days other than DPI0 and DPI3, were small. Therefore, the results may be explained by low initial sample sizes of 3-4 replicates per day, which should be increased to minimise random stochastic effects and for performing thorough statistical analysis. Therefore, it is unclear whether the statistically significant difference between WT Col-0 and *nch1-1/rpt2-3* double mutant plants at DPI3 is enough to conclude there to be a clear impairment of immunity.

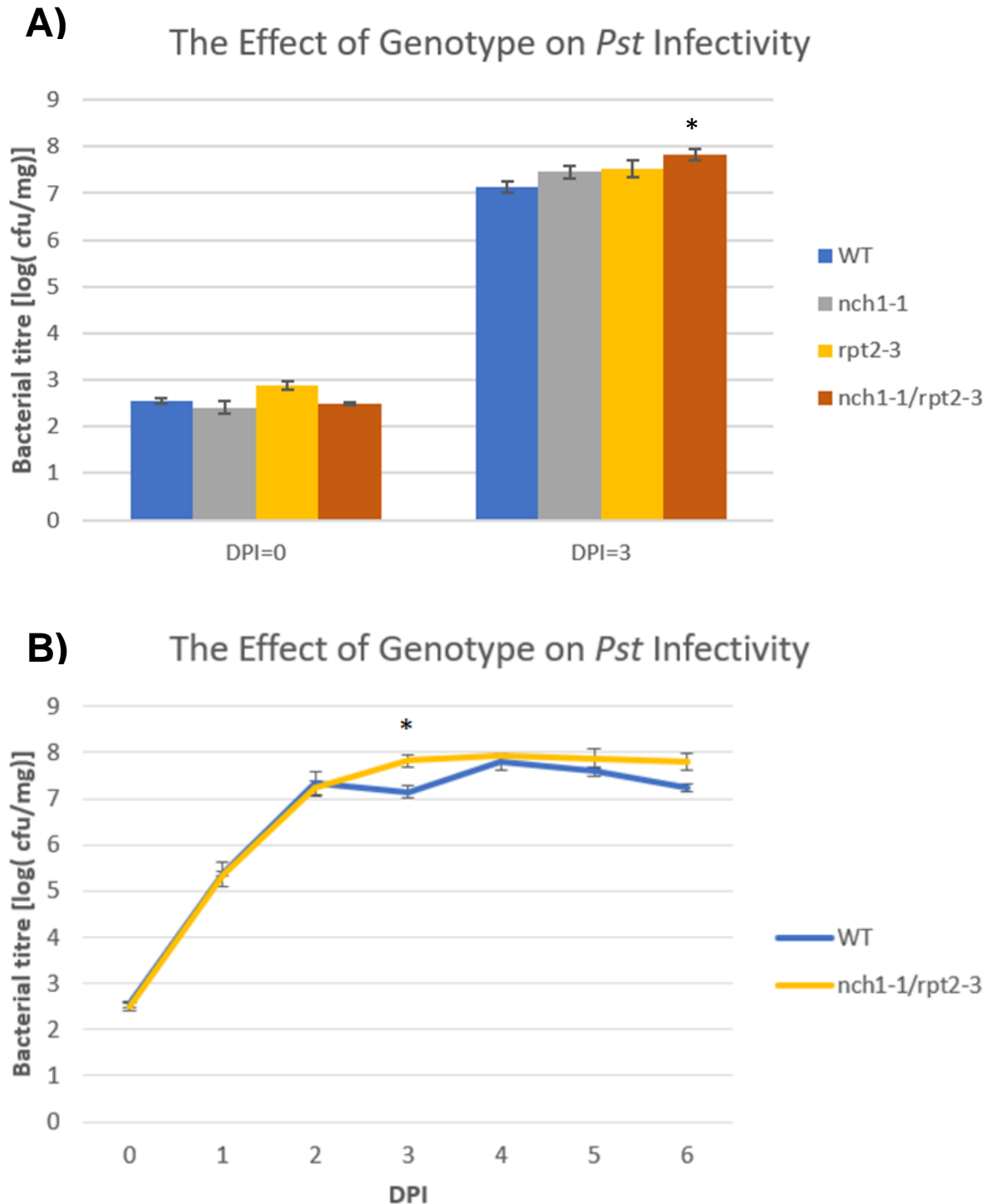


Figure 4.5 The effect of *NCH1* genotype on *Pst* DC3000 infectivity in *Arabidopsis*.

A) Flood assay data on *Pst* DC3000 infected *Arabidopsis* plants. Plants were infected at the age of 10-14 days, and plant tissue was harvested on the same day (DPI0) and 3 days (DPI3) post-inoculation. Each replicate represents at least one independent Petri dish of plants, from which 20-100 mg samples were taken. The lysed tissue was diluted using serial dilutions up to 10^{-9} , and the dilutions were plated on King's B agar media plates. After 2 days, colonies were counted to determine the logarithm of colony-forming units per mg of lysed tissue $\log_{10}(\text{cfu}/\text{mg})$. Error bars represent the standard error. For DPI3, N = 12 in WT and N = 13 for nch1-1/rpt2-3 double-mutant, N=1 in nch1 and rpt2 single mutants. *: Significant difference from the WT DPI3 sample, $P \leq 0.05$.

B) Time course experiment, following the changes in bacterial titres from the day of the inoculation (DPI0) to DPI6. Each point represents at least one independent Petri dish of plants, from which 20-100 mg samples were taken. The lysed tissue was diluted using serial dilutions up to 10^{-9} , and the dilutions were plated on King's B agar media plates. After 2 days, bacterial colonies were counted to determine the number of colony-forming units per mg of lysed tissue. Data are the mean of samples collected from separate Petri dishes for each genotype from which independent tissue samples were assayed for bacterial titre and adjusted for $\log_{10}(\text{cfu}/\text{mg})$. Replicates for WT samples as in **Figure 4.4**, and replicates for the double mutant samples as follows: DPI0 (n=6); DPI1(n=4); DPI2(n=3); DPI3(n=12); DPI4(n=3); DPI5(n=4); DPI6(n=4). Error bars represent the standard error. *: Significant difference from WT DPI3 sample, $P \leq 0.05$.

4.5. Flood Assay Method Optimization

While the bacterial titre did not appear significantly higher in the samples treated with the old protocol than what was reported in the literature for the method (see Ishiga et al. (2011), where bacterial $\log_{10}(\text{cfu}/\text{mg})$ for flood treated plants was found to be roughly 3.2 cfu/mg for DPI0 and 8.0 cfu/mg for DPI3), there was an impression from the data, that the effect of the *NCHI* genotype could be small and therefore masked by the epiphytic bacteria remaining on the plant surfaces from the flood inoculation, as the initial inoculum by flood assay method seemed to affect mainly the epiphytic parts of the plant. Therefore, it was considered beneficial to optimise the protocol by introducing further steps to the technique to enhance the sensitivity and specificity of the data for future experiments.

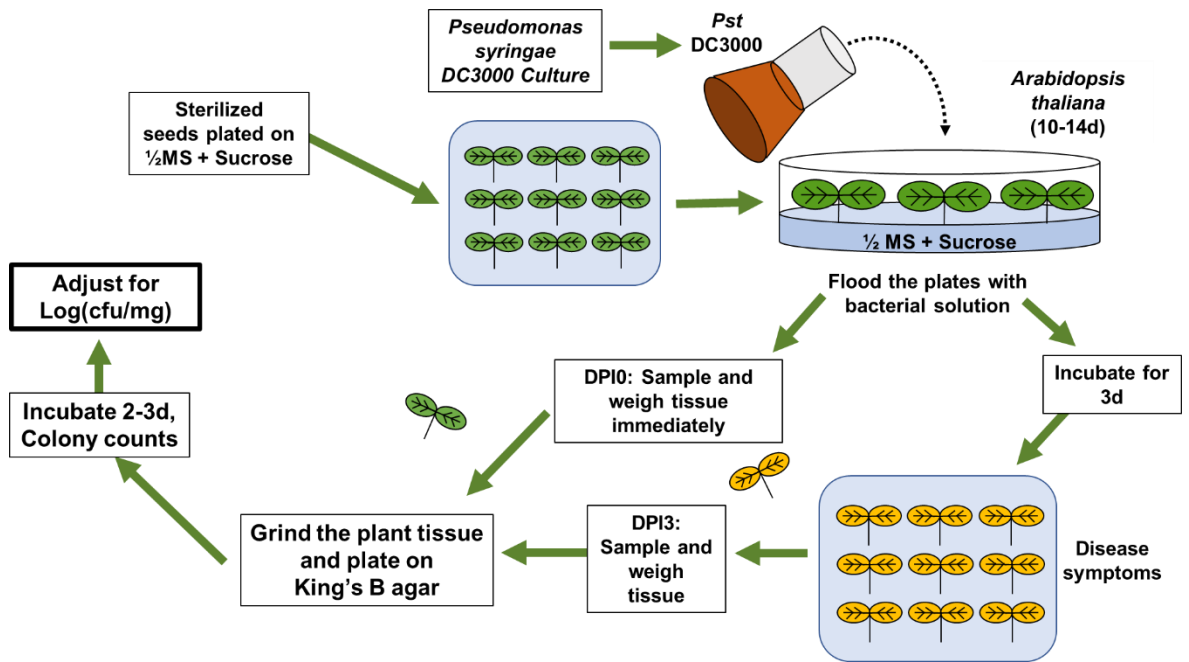
As there were several weaknesses in the original old flood assay experimental design, a new protocol was developed to address these issues with reproducibility, which can be seen in **Figure 4.6**. The first one was the problem of variable tissue weight instead of sampling of a fixed number of seedlings: the old protocol was changed to define the sample as a defined number of seedlings -- 4 per plate -- instead. In contrast to the older protocol, seedlings of similar sizes were now transplanted at 1 week's age on fresh $\frac{1}{2}$ MS medium plates to promote the synchrony of growth. Furthermore, the addition of antibiotic 50 $\mu\text{g}/\text{mL}$ rifampicin to the King's B agar media was introduced to minimise and discourage bacterial growth of species and strains other than *Pst* DC3000. The most significant determinant on the bacterial titre would be expected to come from the introduction of the surface sterilization procedure to limit the bacterial colony count to the bacteria only in the endophytic tissues of the plant, and not the bacteria growing epiphytically. Therefore, the harvested plants were surface-sterilized with 5% H_2O_2 before grinding the tissue for the determination of the bacterial titre. In addition to this, the sucrose present in the $\frac{1}{2}$ MS media was found to promote fungal contamination on the *Arabidopsis* plates, which would spread from one plate to another via the *Pst* solution during flood inoculation, leading to significant losses of research plants. Sucrose was therefore removed from the subsequent $\frac{1}{2}$ MS tissue culture plates.

The new flood assay protocol including the surface sterilisation and the use of rifampicin on King's B agar plates (see "Materials and Methods", section 2.5) was applied on $n=4$ DPI0 independent biological replicates and $n=3$ DPI3 biological replicates of WT *Col-0* plants. The comparison experiment between the new and old protocols revealed that there was a major difference in bacterial titres between the surface-sterilized and non-surface sterilized plants, as seen in **Figure 4.7**. It appears, that the transplantation, addition of 50 $\mu\text{g}/\text{mL}$ rifampicin on the overnight cultures and to the King's B agar media, plant surface sterilization, and the plant tissue lysate resuspension step reduced the bacterial titre by 1 log value. As the plants were not surface-sterilized at the initial DPI0 sampling, as suggested in the protocol by Ishiga (2011), it is likely, that the changed tissue lysate resuspension regime as per the protocol by (Ishiga et al., 2017a), and secondarily, the addition of the antibiotic to the *Pst* media together have the largest effect on the bacterial titre out of all the new steps introduced in the improved protocol. Therefore, while the reduced bacterial titre would suggest the improved protocol to be more sensitive, specific and better-suited for the analysis of small changes in plant immune phenotype than the old protocol, due to the changed dilution system during the resuspension step, the results of the old and new protocols would not be directly comparable.

Overall, the new protocol would be expected to yield more specific and sensitive results, as these would be assumed to be beneficial for studying the role of *nchl* mutations in plant immunity. For a polygenic and

quantitative trait such as plant immunity, the effect of *nch1* and *rpt2* mutations would be expected to be small, and therefore more likely to be detected with a protocol that reduces the background bacterial concentration as much as possible. While *Pst* DC3000 is an obligate plant parasite that should not be able to multiply on the plant or ½ MS plant tissue culture agar surface, the laboratory conditions using sealed and environmentally controlled Petri plates and artificial LED lights without bactericidal UV radiation present in nature could change this, enhancing the survival and viability of bacteria residing on the surfaces of the plant. This is crucial, as the flood inoculation technique itself administers and potentially preserves the initial bacterial inoculum on the plant surfaces in a way that could increase the background level of the bacterial population counts, especially at earlier DPIs. Therefore, to reduce this possibility, the introduction of the additional measures was considered successful and recommended for future investigations.

A) Old method



B) New method

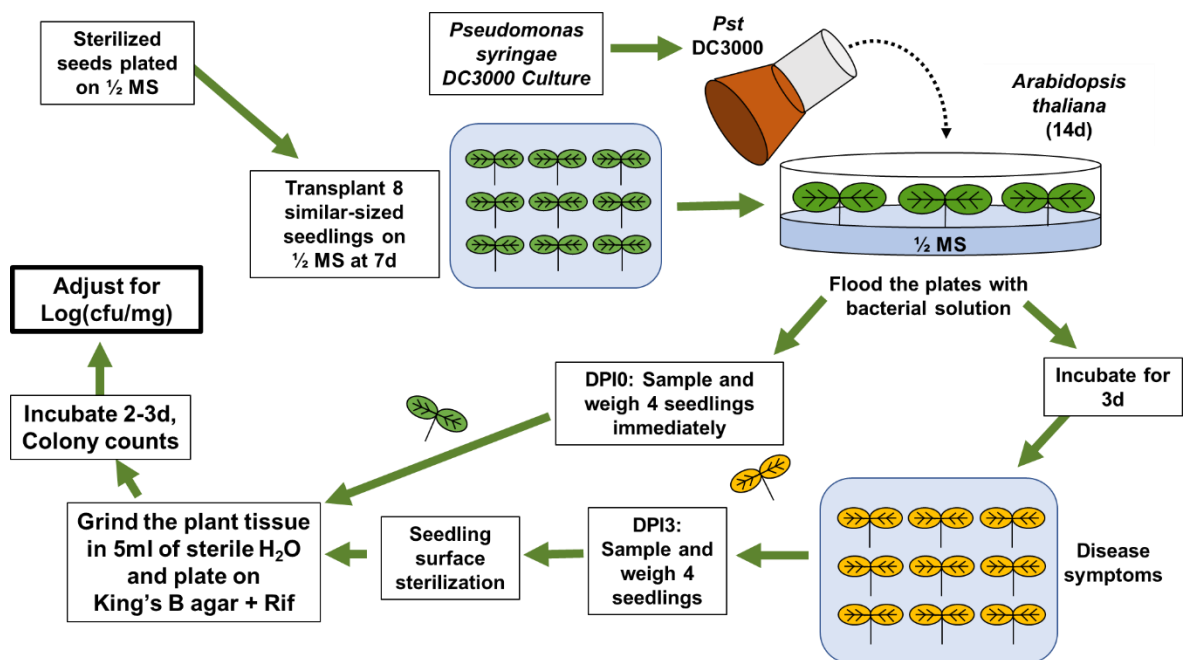


Figure 4.6 Visual comparison of the old and the new flood assay methods.

Schematic diagram showing the general workflow of the two flood assay methods, the old (A, top) and improved new B, (bottom) method. Note the additional steps and other adjustments done for the new method, i.e., the addition of seedling transplantation, surface sterilization, tissue dilution, rifampicin antibiotic on King's B media (agar and broth), and the removal of sucrose from *Arabidopsis* $\frac{1}{2}$ MS media.

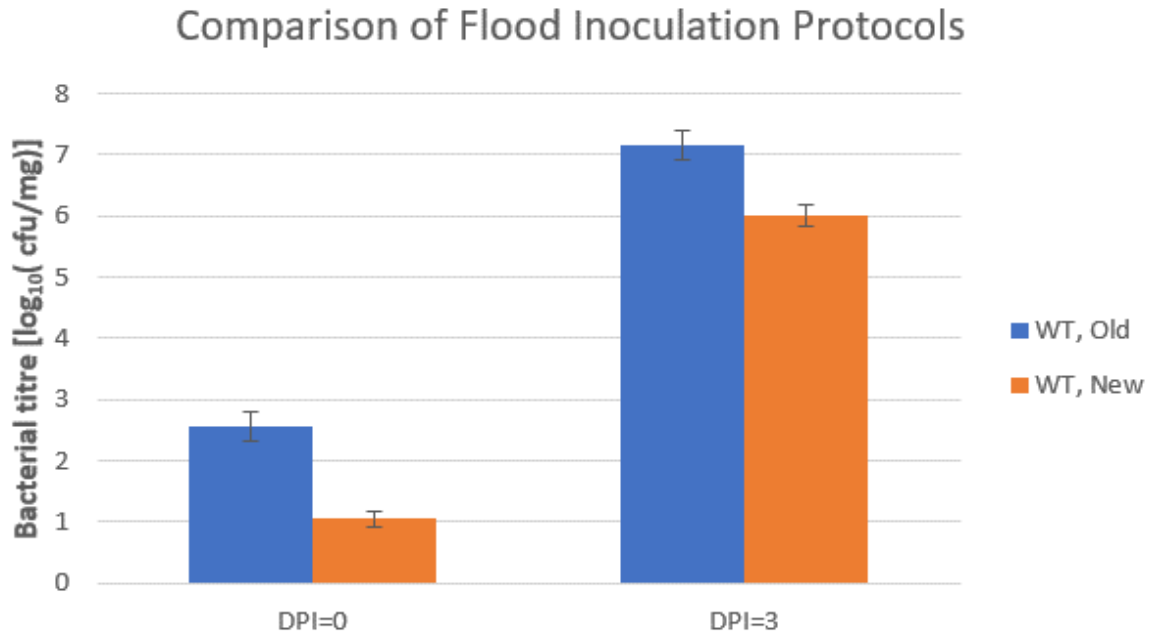


Figure 4.7 Comparison of the old flood assay method and the new one developed after optimization.

The difference between the old and new (i.e., the addition of seedling transplantation, surface sterilization, tissue dilution, rifampicin antibiotic on King's B agar media, and removal of sucrose from *Arabidopsis* ½ MS media) flood assay protocols on *Pst* bacterial titre in *Arabidopsis* WT Col-0 plants, with the comparison of the *Pst* log₁₀(cfu/mg) of tissue values. Error bars portray the standard error. N (New protocol) = 9, N (Old protocol) = 13

4.6. Discussion of Findings

In conclusion, the second main branch of this investigation focused on the immunological relevance of NCH1 on the immunity in *Arabidopsis thaliana*, and to study the effects of plant BL signalling NRL subfamily mutations, namely the *nch1-1* and *rpt2-3* single and the *nch1-1/rpt2-3* double mutations, on the plant disease resistance. In the literature, authors Zhang et al. (2014), He et al. (2018) and Yang et al. (2016) have previously reported the relevance of the target protein NCH1 in plant immunity, both in *Arabidopsis* and potato (*Solanum tuberosum*) pathosystems, respectively: in *Arabidopsis*, the role of NCH1 in plant immunity was shown against the bacterial pathogen *Pst* DC3000 (Zhang et al., 2014b), whereas in potato, the oomycete pathogen *P. infestans* was demonstrated to target NCH1 with its effector Pi02860 (syn. SRE1) (He et al., 2018; Yang et al., 2016). To replicate the findings regarding the role of NCH1 in plant immunity, phytoimmunological studies were conducted using the *Arabidopsis* - *Pst* DC3000 model pathosystem, utilising two modified flood assay protocols by Ishiga et al. (2011) and (Ishiga et al., 2017a). These assays were conducted with Columbia ecotype (Col-0) *Arabidopsis* plants on *rpt2* mutant background to prevent potential functional redundancy between NCH1 and RPT2 proteins.

Firstly, a reference bacterial growth curve was done by determining the bacterial titre at different time points of the *Pst* infection in WT Col-0 *Arabidopsis*: the old flood assay protocol (modified from Ishiga et al. (2011) was applied to flood inoculate the Petri plates of 10-14 day old *Arabidopsis* seedlings with the *Pst* DC3000 bacterial solution. After this, the course of the infection was followed from immediately after the inoculation (DPI0) to up to 6 days post-inoculation (DPI6). Both a visual reference and a bacterial quantification of the logarithm of colony-forming units per milligram of infected plant tissue were done. Time-course experiments (**Figure 4.4**) following the course of *Pseudomonas syringae* pv. *tomato* in *Arabidopsis thaliana* showed that the bacterial titre increased rapidly after the inoculation and stayed on a constant high level even at DPI6 when the plants were visibly chlorotic and dying (**Figure 4.3**). This was interpreted to portray the hemibiotrophic lifestyle of the pathogen, consisting of both the epiphytic and endophytic phases. While the effect of NCH1 on the plant immunity appeared to be statistically significant in *nch1-1/rpt2-3* double mutant plants when a direct comparison between the DPI0 and DPI3 samples of mutant and WT Col-0 plants was performed (**Figure 4.5 A**), this did not appear to be necessarily the case in the time-course experiment. The comparison of DPI3 WT and *nch1-1/rpt2-3* double mutant plants yielded statistically significant results (**APPENDIX 2: Pst DC3000 Flood Assay Data Statistics (DPI3)**), but the time-course growth curves from DPI0 to DPI6 between WT Col-0 and *nch1-1/rpt2-3* double mutant plant did not appear to be significantly different -- apart from this single DPI3 result -- raising a question whether the finding was genuine or a sporadic event. Therefore, the previous findings of the role of NCH1 in plant immunity using the same *Pst* DC3000 – *Arabidopsis* pathosystem as Zhang et al. (2014) could not be fully replicated. However, the time-course and flood assay experiments had a limited number of replicates, and inaccuracies in the bacterial titre arising from flaws in the experimental design left room for improvement. Therefore, more rigorous testing in terms of replicates is required to provide convincing data and to determine whether the postulated effect of NCH1 in plant immunity is real.

To address the weaknesses in the original flood assay method experimental design and to provide preliminary insight into the effects of the technical improvements on the bacterial titre data, a new improved protocol, based on a synthesis of the flood assay protocols described in Ishiga et al. (2011, 2017a), was tested on WT *Arabidopsis* (**Figure 4.6** to determine the bacterial titre in log₁₀(cfu/mg) tissue). This new protocol also

included the transplantation of 1-week old *Arabidopsis* seedlings on fresh ½ MS plates, the addition of 50 µg/mL rifampicin on the King's B agar and King's broth media, the surface sterilization of the harvested seedlings before tissue homogenisation, and the grinding and resuspension of the harvested *Arabidopsis* tissue in 5 mL of double-distilled and autoclaved H₂O. These changes appeared to reduce the bacterial titre of the resulting samples by about 1 log value in both DPI0 and DPI3 samples (**Figure 4.7**), which is assumed to be attributed mainly to the post-sterilization tissue lysate resuspension step, the standardization of the plant tissue quantity/quality, and the addition of the rifampicin antibiotic into the bacterial cultures in addition to the surface sterilization, as the effect is visible in both DPI0 and DPI3 plants. While the changes in the protocol mean the results between the old and new protocols are not directly comparable between each other, overall, the introduction of the new steps would be expected to have a positive effect on the sensitivity and specificity of the data. As the study was investigating the effect of genes of a relatively small overall effect on plant immunity, such as the NRL subfamily proteins including NCH1 and RPT2, these measures would reduce the background bacterial population levels and therefore allow the detection of smaller changes in the plant immunity phenotype.

5. Conclusion & Discussion

NCH1 (NRL PROTEIN FOR CHLOROPLAST MOVEMENT) is a plant protein postulated to play a role in plant immunity, in addition to being a component of the plant blue light signalling pathway directly downstream of phototropin 1 BL receptor. The interplay between plant immunity and BL sensing has not been studied until recently. The potential links between plant light sensing and immunity are currently unknown, but postulated to lie in the central photosynthetic organelles and systems: Chloroplasts form an ideal microbial target due to their central role in the plant life cycle and biomass synthesis, key bioenergetic pathways and their roles in plant hormone -- including key defence hormone -- synthesis (Kangasjärvi et al., 2012; de Torres Zabala et al., 2015). Therefore, pathways controlling chloroplast function and movement, such as ones regulated by BL and phototropin photoreceptors, add further complexity and points of interaction for pathogen effectors. Furthermore, the endosymbiotic origin of chloroplasts requires them to co-operate seamlessly with the host cells' nuclei for nuclear-encoded chloroplast gene expression, making the cellular trafficking and cytoskeletal contacts between these organelles also a lucrative target (Sowden et al., 2018). Consequently, it is likely, that pathogens aim to indirectly down-regulate plant immune response by affecting all these vital processes to re-route plant energy use and resources away from the immune system (Park et al., 2018). Indeed, by manipulating only a few key cellular events, pathogens may actively affect the whole status of the cell, or even the plant itself for their benefit.

As NCH1 protein is assumed to play a multifaceted role in blue light signalling, chloroplast movement and as an intracellular immunity-related homeostatic protein with a ubiquitin E3 ligase substrate acceptor function, the immunomodulatory role of the protein could be related to **a)** chloroplasts and the chloroplast movement, **b)** the function of the NCH1 protein as a ubiquitin E3 ligase as postulated by He et al., (2018) and Zhang et al. (2014), **c)** both of the above, **d)** a BL and phot signalling-related functions, or **e)** an unknown mechanism. While the ubiquitin E3 ligase function of the NCH1 is documented in previous research (He et al., 2018; Zhang et al., 2014), it is unknown whether it is linked to the other pathways involving NCH1, namely chloroplast movement under phot and BL-signalling. The chloroplast-related function would be immunologically feasible, as chloroplasts are central to the plant immunity through the synthesis of plant immunity hormones SA and JA, and the generation of ROS (Ishiga et al., 2017b). Recent evidence also suggests that physical chloroplast movement would also play a direct role in plant immunity, with impairment of chloroplast movement through mutations negatively affecting the plant immunity (Savage et al., 2021).

The localization and possible dynamic movement patterns of NCH1 in response to blue light irradiation were studied using confocal microscopy. The results indicated that the localization of the protein is plasma membrane-bound, with no dynamic relocalization behaviour nor any other visible movements, therefore ruling out the light-dependent relocalization as a potential mode of action. However, even though the localization of the protein does not change in response to light signals, there are other potential triggers that could alter the subcellular localization of the protein, including binding partners such as 14-3-3 proteins and pathogen challenge, which could be studied next. Furthermore, the dimerization status of the protein was studied using bimolecular fluorescence complementation BiFC and site-directed mutagenesis, which suggested NCH1 to homodimerize, and this dimerization to be dependent on the formation of salt bridges at residues D28 and K42, as nonsynonymous mutations of D28N and K42Q in the mutant form of NCH1 (NCH1^{D28N-K42Q}) abolish the dimerization signal almost completely. While the homodimerization of NCH1 can be determined using BiFC

experiments, the functional significance of this finding is unknown. Many NRL proteins also undergo light-dependent phosphorylation, and the C-termini of proteins such as NPH3, RPT2 and NCH1 contain an AGCVIII kinase phosphorylation consensus sequence RXS (Sullivan et al., 2021). More importantly, these proteins appear to share the RXS motif in the very C-terminus of the protein (Sullivan et al., 2021), which is postulated to be the target for phot1 phosphorylation, also additionally allowing the subsequent 14-3-3 protein interaction and initiation of the NRL protein downstream signalling (Sullivan et al., 2021). Therefore, this information raises the question of whether this would be true for NCH1 and whether NCH1 would be a potential phot1 substrate.

Potential reasons for the seen low effect of *nch1/rpt2* mutations may lay in the way plant immunity is organised: quantitative immunity would mean individual genetic components would weigh reasonably little if measured individually, but might still have a part in the plant immune reaction as a part of the overall coordinated immune reaction (Corwin and Kliebenstein, 2017). While the potential functional redundancy between NCH1 and RPT2 was taken into account in this study, it is still possible that some of the other NRL family members detailed in the phylogenetic analysis (seen in **Figure 3.4**) could also exhibit further functional redundancy with NCH1. This is the case for example with the related protein NPH3 where less closely related proteins outside the immediate NRL subfamily (including NCH1 and RPT2), namely DOT3 and MAB4, still exhibit functional redundancy (Furutani et al., 2007; Reuter et al., 2021). These could include proteins that can exhibit similar functions as a ubiquitin E3 ligase substrate acceptor protein, such as NRL proteins with BTB-POZ domains (see **Figure 3.4**). While the function of the NPH3 domain is still unknown at present, further studies on its functional relevance could also provide clues to the potential functional redundancy. It's also important to note, that NCH1 has 3 known splice variants, as seen in **Figure 3.1**, of which significance is unknown.

Additional perspectives to the immunity investigation would include the studies on the hetero interactions of NCH1 with related NRL subfamily proteins NPH3 and RPT2, and the potential 14-3-3 protein association and its effect on NCH1 phosphorylation status and localization. Further work could also involve providing more both biological and technical replicates for the flood assay time course experiment, with both wild type *Arabidopsis thaliana* Col-0 plants and *nch1/rpt2* double mutant plants, to construct a profile of the course of the infection and to find further evidence for the dip in the $\log_{10}(\text{cfu/mg})$ values witnessed in the experiment. The infection could also be monitored more closely in single mutants *nch1-1* and *rpt2-3* at DPI0 and DPI3, in addition to time course studies to determine the individual roles of *nch1* and *rpt2*. The molecular basis of the disease symptoms and progress in the mutants could also be investigated by monitoring the well-characterised defence indicators, such as PR-gene transcript levels, by quantitative RT-PCR (RT-qPCR) at different points of the infection. To bridge the structure and function of NCH1 together in the context of protein biochemistry, signalling and plant immunity, preliminary tests were performed to determine whether *Pst* treated plant tissue can be mounted on microscope slides for studies on a confocal microscope. It appears, that mounting single *Arabidopsis* leaves in the same way as *N. benthamiana* leaf discs is possible, at least in the early stages of infection: namely DPI1-2. This can ultimately allow more detailed confocal microscopy studies to determine NCH1 protein localization, abundance, and dimerization status in *Pst* infected tissues when the infection is studied in fluorescent protein-tagged *Arabidopsis* lines.

REFERENCES

- Backer, R., Naidoo, S., and van den Berg, N. (2019). The NONEXPRESSOR OF PATHOGENESIS-RELATED GENES 1 (NPR1) and Related Family: Mechanistic Insights in Plant Disease Resistance. *Front. Plant Sci.* *10*. <https://doi.org/10.3389/fpls.2019.00102>.
- Bae, G., and Choi, G. (2008). Decoding of Light Signals by Plant Phytochromes and Their Interacting Proteins. *Annu. Rev. Plant Biol.* *59*, 281–311. <https://doi.org/10.1146/annurev.arplant.59.032607.092859>.
- Barrett, L.G., and Heil, M. (2012). Unifying concepts and mechanisms in the specificity of plant–enemy interactions. *Trends Plant Sci.* *17*, 282–292. <https://doi.org/10.1016/j.tplants.2012.02.009>.
- Ben Khaled, S., Postma, J., and Robatzek, S. (2015). A Moving View: Subcellular Trafficking Processes in Pattern Recognition Receptor–Triggered Plant Immunity. *Annu. Rev. Phytopathol.* *53*, 379–402. <https://doi.org/10.1146/annurev-phyto-080614-120347>.
- Birch, P.R.J., Armstrong, M., Bos, J., Boevink, P., Gilroy, E.M., Taylor, R.M., Wawra, S., Pritchard, L., Conti, L., Ewan, R., et al. (2009). Towards understanding the virulence functions of RXLR effectors of the oomycete plant pathogen *Phytophthora infestans*. *J. Exp. Bot.* *60*, 1133–1140. <https://doi.org/10.1093/jxb/ern353>.
- Blanco, L.P., Payne, B.L., Feyertag, F., and Alvarez-Ponce, D. (2018). Proteins of generalist and specialist pathogens differ in their amino acid composition. *Life Sci. Alliance* *1*, e201800017. <https://doi.org/10.26508/lsa.201800017>.
- Boller, T., and Felix, G. (2009). A Renaissance of Elicitors: Perception of Microbe-Associated Molecular Patterns and Danger Signals by Pattern-Recognition Receptors. *Annu. Rev. Plant Biol.* *60*, 379–406. <https://doi.org/10.1146/annurev.arplant.57.032905.105346>.
- Botero, K., Restrepo, S., and Pinzón, A. (2018). A genome-scale metabolic model of potato late blight suggests a photosynthesis suppression mechanism. *BMC Genomics* *19*, 863. <https://doi.org/10.1186/s12864-018-5192-x>.
- Bozkurt, T.O., Belhaj, K., Dagdas, Y.F., Chaparro-Garcia, A., Wu, C.-H., Cano, L.M., and Kamoun, S. (2015). Rerouting of Plant Late Endocytic Trafficking Toward a Pathogen Interface. *Traffic* *16*, 204–226. <https://doi.org/10.1111/tra.12245>.
- Bradbury, J.F. (1983). The New Bacterial Nomenclature -- What to Do. *Phytopathology* *73*, 1349. <https://doi.org/10.1094/Phyto-73-1349>.
- Brutus, A., Sicilia, F., Macone, A., Cervone, F., and De Lorenzo, G. (2010). A domain swap approach reveals a role of the plant wall-associated kinase 1 (WAK1) as a receptor of oligogalacturonides. *Proc. Natl. Acad. Sci.* *107*, 9452–9457. <https://doi.org/10.1073/pnas.1000675107>.
- Buell, C.R., Joardar, V., Lindeberg, M., Selengut, J., Paulsen, I.T., Gwinn, M.L., Dodson, R.J., Deboy, R.T., Durkin, A.S., Kolonay, J.F., et al. (2003). The complete genome sequence of the Arabidopsis and tomato pathogen *Pseudomonas syringae* pv. tomato DC3000. *Proc. Natl. Acad. Sci.* *100*, 10181–10186. .
- Burgh, A.M. van der, and Joosten, M.H.A.J. (2019). Plant Immunity: Thinking Outside and Inside the Box. *Trends Plant Sci.* *24*, 587–601. <https://doi.org/10.1016/j.tplants.2019.04.009>.
- Caplan, J.L., Mamillapalli, P., Burch-Smith, T.M., Czymmek, K., and Dinesh-Kumar, S.P. (2008). Chloroplastic protein NRIP1 mediates innate immune receptor recognition of a viral effector. *Cell* *132*, 449–462. <https://doi.org/10.1016/j.cell.2007.12.031>.
- Caplan, J.L., Kumar, A.S., Park, E., Padmanabhan, M.S., Hoban, K., Modla, S., Czymmek, K., and Dinesh-Kumar, S.P. (2015). Chloroplast Stromules Function during Innate Immunity. *Dev. Cell* *34*, 45–57. <https://doi.org/10.1016/j.devcel.2015.05.011>.
- Celaya, R.B., and Liscum, E. (2005). Phototropins and Associated Signaling: Providing the Power of Movement in Higher Plants. *Photochem. Photobiol.* *81*, 73–80. <https://doi.org/10.1111/j.1751-1097.2005.tb01524.x>.
- Chaparro-Garcia, A., Schwizer, S., Sklenar, J., Yoshida, K., Petre, B., Bos, J.I.B., Schornack, S., Jones, A.M.E., Bozkurt, T.O., and Kamoun, S. (2015). *Phytophthora infestans* RXLR-WY Effector AVR3a Associates with Dynamin-Related Protein 2 Required for Endocytosis of the Plant Pattern Recognition Receptor FLS2. *PLOS ONE* *10*, e0137071. <https://doi.org/10.1371/journal.pone.0137071>.
- Choi, C.M., Gray, W.M., Mooney, S., and Hellmann, H. (2014). Composition, Roles, and Regulation of Cullin-Based Ubiquitin E3 Ligases. *Arab. Book Am. Soc. Plant Biol.* *12*, e0175. <https://doi.org/10.1199/tab.0175>.

- Christie, J.M., Arvai, A.S., Baxter, K.J., Heilmann, M., Pratt, A.J., O'Hara, A., Kelly, S.M., Hothorn, M., Smith, B.O., Hitomi, K., et al. (2012). Plant UVR8 Photoreceptor Senses UV-B by Tryptophan-Mediated Disruption of Cross-Dimer Salt Bridges. *Science* *335*, 1492–1496. <https://doi.org/10.1126/science.1218091>.
- Christie, J.M., Blackwood, L., Petersen, J., and Sullivan, S. (2015). Plant Flavoprotein Photoreceptors. *Plant Cell Physiol.* *56*, 401–413. <https://doi.org/10.1093/pcp/pcu196>.
- Christie, J.M., Suetsugu, N., Sullivan, S., and Wada, M. (2018). Shining Light on the Function of NPH3/RPT2-Like Proteins in Phototropin Signaling. *Plant Physiol.* *176*, 1015–1024. <https://doi.org/10.1104/pp.17.00835>.
- Cook, D.E., Mesarich, C.H., and Thomma, B.P.H.J. (2015). Understanding Plant Immunity as a Surveillance System to Detect Invasion. *Annu. Rev. Phytopathol.* *53*, 541–563. <https://doi.org/10.1146/annurev-phyto-080614-120114>.
- Corwin, J.A., and Kliebenstein, D.J. (2017). Quantitative Resistance: More Than Just Perception of a Pathogen. *Plant Cell* *29*, 655–665. <https://doi.org/10.1105/tpc.16.00915>.
- Couto, D., and Zipfel, C. (2016). Regulation of pattern recognition receptor signalling in plants. *Nat. Rev. Immunol.* *16*, 537–552. <https://doi.org/10.1038/nri.2016.77>.
- Crouthamel, M., Thiagarajan, M.M., Evanko, D.S., and Wedegaertner, P.B. (2008). N-terminal polybasic motifs are required for plasma membrane localization of Gas AND Gαq. *Cell. Signal.* *20*, 1900–1910. <https://doi.org/10.1016/j.cellsig.2008.06.019>.
- Cuppels, D.A. (1986). Generation and Characterization of Tn5 Insertion Mutations in *Pseudomonas syringae* pv. tomato. *Appl. Environ. Microbiol.* *51*, 323–327. .
- Elizabeth, S.V., and Bender, C.L. (2007). The phytotoxin coronatine from *Pseudomonas syringae* pv. tomato DC3000 functions as a virulence factor and influences defence pathways in edible brassicas. *Mol. Plant Pathol.* *8*, 83–92. <https://doi.org/10.1111/j.1364-3703.2006.00372.x>.
- Erb, M., Meldau, S., and Howe, G.A. (2012). Role of phytohormones in insect-specific plant reactions. *Trends Plant Sci.* *17*, 250–259. <https://doi.org/10.1016/j.tplants.2012.01.003>.
- Fantini, E., and Facella, P. (2020). Cryptochromes in the field: how blue light influences crop development. *Physiol. Plant.* *169*, 336–346. <https://doi.org/10.1111/ppl.13088>.
- Feil, H., Feil, W.S., Chain, P., Larimer, F., DiBartolo, G., Copeland, A., Lykidis, A., Trong, S., Nolan, M., Goltsman, E., et al. (2005). Comparison of the complete genome sequences of *Pseudomonas syringae* pv. *syringae* B728a and pv. *tomato* DC3000. *Proc. Natl. Acad. Sci.* *102*, 11064–11069. <https://doi.org/10.1073/pnas.0504930102>.
- Flor, H.H. (1971). Current Status of the Gene-For-Gene Concept. *Annu. Rev. Phytopathol.* *9*, 275–296. <https://doi.org/10.1146/annurev.py.09.090171.001423>.
- Folta, K.M., and Carvalho, S.D. (2015). Photoreceptors and Control of Horticultural Plant Traits. *HortScience* *50*, 1274–1280. <https://doi.org/10.21273/HORTSCI.50.9.1274>.
- Furutani, M., Kajiwara, T., Kato, T., Trembl, B.S., Stockum, C., Torres-Ruiz, R.A., and Tasaka, M. (2007). The gene MACCHI-BOU 4/ENHANCER OF PINOID encodes a NPH3-like protein and reveals similarities between organogenesis and phototropism at the molecular level. *Development* *134*, 3849–3859. <https://doi.org/10.1242/dev.009654>.
- Gao, M., Zhang, C., and Lu, H. (2020). Coronatine is more potent than jasmonates in regulating Arabidopsis circadian clock. *Sci. Rep.* *10*, 12862. <https://doi.org/10.1038/s41598-020-69627-2>.
- Geisler-Lee, J., O'Toole, N., Ammar, R., Provart, N.J., Millar, A.H., and Geisler, M. (2007). A Predicted Interactome for Arabidopsis. *Plant Physiol.* *145*, 317–329. <https://doi.org/10.1104/pp.107.103465>.
- Geng, X., Cheng, J., Gangadharan, A., and Mackey, D. (2012). The Coronatine Toxin of *Pseudomonas syringae* Is a Multifunctional Suppressor of Arabidopsis Defense. *Plant Cell* *24*, 4763–4774. <https://doi.org/10.1105/tpc.112.105312>.
- Gingerich, D.J., Gagne, J.M., Salter, D.W., Hellmann, H., Estelle, M., Ma, L., and Vierstra, R.D. (2005). Cullins 3a and 3b Assemble with Members of the Broad Complex/Tramtrack/Bric-a-Brac (BTB) Protein Family to Form Essential Ubiquitin-Protein Ligases (E3s) in *Arabidopsis*. *J. Biol. Chem.* *280*, 18810–18821. <https://doi.org/10.1074/jbc.M413247200>.
- Gutiérrez-Barranquero, J.A., Cazorla, F.M., and de Vicente, A. (2019). *Pseudomonas syringae* pv. *syringae* Associated With Mango Trees, a Particular Pathogen Within the “Hodgepodge” of the *Pseudomonas syringae* Complex. *Front. Plant Sci.* *10*, 570. <https://doi.org/10.3389/fpls.2019.00570>.

- Haga, K., Tsuchida-Mayama, T., Yamada, M., and Sakai, T. (2015). Arabidopsis ROOT PHOTOTROPISM2 Contributes to the Adaptation to High-Intensity Light in Phototropic Responses. *Plant Cell* 27, 1098–1112. <https://doi.org/10.1105/tpc.15.00178>.
- Han, G.-Z. (2019). Origin and evolution of the plant immune system. *New Phytol.* 222, 70–83. <https://doi.org/10.1111/nph.15596>.
- He, Q., Naqvi, S., McLellan, H., Boevink, P.C., Champouret, N., Hein, I., and Birch, P.R.J. (2018). Plant pathogen effector utilizes host susceptibility factor NRL1 to degrade the immune regulator SWAP70. *Proc. Natl. Acad. Sci.* 115, E7834–E7843. <https://doi.org/10.1073/pnas.1808585115>.
- Heazlewood, J.L., Durek, P., Hummel, J., Selbig, J., Weckwerth, W., Walther, D., and Schulze, W.X. (2008). PhosPhAt: a database of phosphorylation sites in Arabidopsis thaliana and a plant-specific phosphorylation site predictor. *Nucleic Acids Res.* 36, D1015–D1021. <https://doi.org/10.1093/nar/gkm812>.
- Hooper, C.M., Castleden, I.R., Tanz, S.K., Aryamanesh, N., and Millar, A.H. (2017). SUBA4: the interactive data analysis centre for Arabidopsis subcellular protein locations. *Nucleic Acids Res.* 45, D1064–D1074. <https://doi.org/10.1093/nar/gkw1041>.
- van der Hoorn, R.A.L., and Kamoun, S. (2008). From Guard to Decoy: A New Model for Perception of Plant Pathogen Effectors. *Plant Cell* 20, 2009–2017. <https://doi.org/10.1105/tpc.108.060194>.
- Huang, J., Zhao, X., Cheng, K., Jiang, Y., Ouyang, Y., Xu, C., Li, X., Xiao, J., and Zhang, Q. (2013). OsAP65, a rice aspartic protease, is essential for male fertility and plays a role in pollen germination and pollen tube growth. *J. Exp. Bot.* 64, 3351–3360. <https://doi.org/10.1093/jxb/ert173>.
- Ishiga, Y., Ishiga, T., Uppalapati, S.R., and Mysore, K.S. (2011). Arabidopsis seedling flood-inoculation technique: a rapid and reliable assay for studying plant-bacterial interactions. *Plant Methods* 7, 32. <https://doi.org/10.1186/1746-4811-7-32>.
- Ishiga, Y., Ishiga, T., Ichinose, Y., and Mysore, K. (2017a). Pseudomonas syringae Flood-inoculation Method in Arabidopsis. *BIO-Protoc.* 7. <https://doi.org/10.21769/BioProtoc.2106>.
- Ishiga, Y., Watanabe, M., Ishiga, T., Tohge, T., Matsuura, T., Ikeda, Y., Hoefgen, R., Fernie, A.R., and Mysore, K.S. (2017b). The SAL-PAP Chloroplast Retrograde Pathway Contributes to Plant Immunity by Regulating Glucosinolate Pathway and Phytohormone Signaling. *Mol. Plant. Microbe Interact.* 30, 829–841. <https://doi.org/10.1094/MPMI-03-17-0055-R>.
- Janeway, C.A. (1989). Approaching the asymptote? Evolution and revolution in immunology. *Cold Spring Harb. Symp. Quant. Biol.* 54 Pt 1, 1–13. <https://doi.org/10.1101/sqb.1989.054.01.003>.
- Jenkins, G.I. (2014). The UV-B Photoreceptor UVR8: From Structure to Physiology. *Plant Cell* 26, 21–37. <https://doi.org/10.1105/tpc.113.119446>.
- Jones, J.D.G., and Dangl, J.L. (2006). The plant immune system. *Nature* 444, 323–329. <https://doi.org/10.1038/nature05286>.
- Jones, J.D.G., Vance, R.E., and Dangl, J.L. (2016). Intracellular innate immune surveillance devices in plants and animals. *Science* 354. <https://doi.org/10.1126/science.aaf6395>.
- Joshi, V., Joshi, N., Vyas, A., and Jadhav, S.K. (2021). Pathogenesis-related proteins: Role in plant defense. In *Biocontrol Agents and Secondary Metabolites*, (Elsevier), pp. 573–590.
- Judelson, H.S., and Blanco, F.A. (2005). The spores of Phytophthora: weapons of the plant destroyer. *Nat. Rev. Microbiol.* 3, 47–58. <https://doi.org/10.1038/nrmicro1064>.
- Kachroo, A., and Kachroo, P. (2020). Mobile signals in systemic acquired resistance. *Curr. Opin. Plant Biol.* 58, 41–47. <https://doi.org/10.1016/j.pbi.2020.10.004>.
- Kachroo, A., and Robin, G.P. (2013). Systemic signaling during plant defense. *Curr. Opin. Plant Biol.* 16, 527–533. <https://doi.org/10.1016/j.pbi.2013.06.019>.
- Kamano, S., Kume, S., Iida, K., Lei, K.-J., Nakano, M., Nakayama, Y., and Iida, H. (2015). Transmembrane Topologies of Ca²⁺-permeable Mechanosensitive Channels MCA1 and MCA2 in Arabidopsis thaliana. *J. Biol. Chem.* 290, 30901–30909. <https://doi.org/10.1074/jbc.M115.692574>.
- Kamoun, S. (2006). A Catalogue of the Effector Secretome of Plant Pathogenic Oomycetes. *Annu. Rev. Phytopathol.* 44, 41–60. <https://doi.org/10.1146/annurev.phyto.44.070505.143436>.
- Kangasjärvi, S., Neukermans, J., Li, S., Aro, E.-M., and Noctor, G. (2012). Photosynthesis, photorespiration, and light signalling in defence responses. *J. Exp. Bot.* 63, 1619–1636. <https://doi.org/10.1093/jxb/err402>.

- Katsir, L., Schilmiller, A.L., Staswick, P.E., He, S.Y., and Howe, G.A. (2008). COI1 is a critical component of a receptor for jasmonate and the bacterial virulence factor coronatine. *Proc. Natl. Acad. Sci.* *105*, 7100–7105. <https://doi.org/10.1073/pnas.0802332105>.
- Khare, E., Kim, K., and Lee, K.-J. (2016). Rice OsPBL1 (ORYZA SATIVA ARABIDOPSIS PBS1-LIKE 1) enhanced defense of Arabidopsis against *Pseudomonas syringae* DC3000. *Eur. J. Plant Pathol.* *146*, 901–910. <https://doi.org/10.1007/s10658-016-0968-9>.
- Kim, J.Y., Song, J.T., and Seo, H.S. (2017). COP1 regulates plant growth and development in response to light at the post-translational level. *J. Exp. Bot.* *68*, 4737–4748. <https://doi.org/10.1093/jxb/erx312>.
- Kimura, S., Waszczak, C., Hunter, K., and Wrzaczek, M. (2017). Bound by Fate: The Role of Reactive Oxygen Species in Receptor-Like Kinase Signaling. *Plant Cell* *29*, 638–654. <https://doi.org/10.1105/tpc.16.00947>.
- Klepikova, A.V., Kasianov, A.S., Gerasimov, E.S., Logacheva, M.D., and Penin, A.A. (2016). A high resolution map of the Arabidopsis thaliana developmental transcriptome based on RNA-seq profiling. *Plant J.* *88*, 1058–1070. <https://doi.org/10.1111/tpj.13312>.
- Kong, S.-G., and Wada, M. (2014). Recent advances in understanding the molecular mechanism of chloroplast photorelocation movement. *Biochim. Biophys. Acta BBA - Bioenerg.* *1837*, 522–530. <https://doi.org/10.1016/j.bbabi.2013.12.004>.
- Kong, S.-G., Suzuki, T., Tamura, K., Mochizuki, N., Hara-Nishimura, I., and Nagatani, A. (2006). Blue light-induced association of phototropin 2 with the Golgi apparatus. *Plant J.* *45*, 994–1005. <https://doi.org/10.1111/j.1365-313X.2006.02667.x>.
- Kong, S.-G., Shimada, A., Kijima, S.T., Hirose, K., Katoh, K., Ahn, J., Higa, T., Takano, A., Nakamura, Y., Suetsugu, N., et al. (2020). CHLOROPLAST UNUSUAL POSITIONING 1 is a new type of actin nucleation factor in plants. *BioRxiv* 2020.01.14.905984. <https://doi.org/10.1101/2020.01.14.905984>.
- Konold, P.E., Mathes, T., Weißenborn, J., Groot, M.L., Hegemann, P., and Kennis, J.T.M. (2016). Unfolding of the C-Terminal α Helix in the LOV2 Photoreceptor Domain Observed by Time-Resolved Vibrational Spectroscopy. *J. Phys. Chem. Lett.* *7*, 3472–3476. <https://doi.org/10.1021/acs.jpcclett.6b01484>.
- Krogh, A., Larsson, B., von Heijne, G., and Sonnhammer, E.L.L. (2001). Predicting transmembrane protein topology with a hidden markov model: application to complete genomes. Edited by F. Cohen. *J. Mol. Biol.* *305*, 567–580. <https://doi.org/10.1006/jmbi.2000.4315>.
- Kubicek, C.P., Starr, T.L., and Glass, N.L. (2014). Plant Cell Wall-Degrading Enzymes and Their Secretion in Plant-Pathogenic Fungi. *Annu. Rev. Phytopathol.* *52*, 427–451. <https://doi.org/10.1146/annurev-phyto-102313-045831>.
- Kumar, A.S., Park, E., Nedo, A., Alqarni, A., Ren, L., Hoban, K., Modla, S., McDonald, J.H., Kambhamettu, C., Dinesh-Kumar, S.P., et al. (2018). Stromule extension along microtubules coordinated with actin-mediated anchoring guides perinuclear chloroplast movement during innate immunity. *ELife* *7*, e23625. <https://doi.org/10.7554/eLife.23625>.
- Kutschera, U., and Briggs, W.R. (2016). Phototropic solar tracking in sunflower plants: an integrative perspective. *Ann. Bot.* *117*, 1–8. <https://doi.org/10.1093/aob/mcv141>.
- Kyte, J., and Doolittle, R.F. (1982). A simple method for displaying the hydropathic character of a protein. *J. Mol. Biol.* *157*, 105–132. [https://doi.org/10.1016/0022-2836\(82\)90515-0](https://doi.org/10.1016/0022-2836(82)90515-0).
- Łabuz, J., Sztatelman, O., Banaś, A.K., and Gabryś, H. (2012). The expression of phototropins in Arabidopsis leaves: developmental and light regulation. *J. Exp. Bot.* *63*, 1763–1771. <https://doi.org/10.1093/jxb/ers061>.
- Lee, J., He, K., Stolc, V., Lee, H., Figueroa, P., Gao, Y., Tongprasit, W., Zhao, H., Lee, I., and Deng, X.W. (2007). Analysis of Transcription Factor HY5 Genomic Binding Sites Revealed Its Hierarchical Role in Light Regulation of Development. *Plant Cell* *19*, 731–749. <https://doi.org/10.1105/tpc.106.047688>.
- Lindeberg, M. (2012). Genome-Enabled Perspectives on the Composition, Evolution, and Expression of Virulence Determinants in Bacterial Plant Pathogens. *Annu. Rev. Phytopathol.* *50*, 111–132. <https://doi.org/10.1146/annurev-phyto-081211-173022>.
- Liu, P.-P., von Dahl, C.C., and Klessig, D.F. (2011). The Extent to Which Methyl Salicylate Is Required for Signaling Systemic Acquired Resistance Is Dependent on Exposure to Light after Infection. *Plant Physiol.* *157*, 2216–2226. <https://doi.org/10.1104/pp.111.187773>.
- van Loon, L.C., Rep, M., and Pieterse, C.M.J. (2006). Significance of Inducible Defense-related Proteins in Infected Plants. *Annu. Rev. Phytopathol.* *44*, 135–162. <https://doi.org/10.1146/annurev-phyto.44.070505.143425>.

- Lu, Y., and Yao, J. (2018). Chloroplasts at the Crossroad of Photosynthesis, Pathogen Infection and Plant Defense. *Int. J. Mol. Sci.* *19*, 3900. <https://doi.org/10.3390/ijms19123900>.
- Lumba, S., Toh, S., Handfield, L.-F., Swan, M., Liu, R., Youn, J.-Y., Cutler, S.R., Subramaniam, R., Provar, N., Moses, A., et al. (2014). A Mesoscale Abscisic Acid Hormone Interactome Reveals a Dynamic Signaling Landscape in Arabidopsis. *Dev. Cell* *29*, 360–372. <https://doi.org/10.1016/j.devcel.2014.04.004>.
- Ma, L., Li, J., Qu, L., Hager, J., Chen, Z., Zhao, H., and Deng, X.W. (2001). Light Control of Arabidopsis Development Entails Coordinated Regulation of Genome Expression and Cellular Pathways. *Plant Cell* *13*, 2589–2608. <https://doi.org/10.1105/tpc.010229>.
- Mansfield, J., Genin, S., Magori, S., Citovsky, V., Sriariyanum, M., Ronald, P., Dow, M., Verdier, V., Beer, S.V., Machado, M.A., et al. (2012). Top 10 plant pathogenic bacteria in molecular plant pathology. *Mol. Plant Pathol.* *13*, 614–629. <https://doi.org/10.1111/j.1364-3703.2012.00804.x>.
- McCann, H.C., Li, L., Liu, Y., Li, D., Pan, H., Zhong, C., Rikkerink, E.H.A., Templeton, M.D., Straub, C., Colombi, E., et al. (2017). Origin and Evolution of the Kiwifruit Canker Pandemic. *Genome Biol Evol* *13*. .
- Medzhitov, R. (2013). Pattern Recognition Theory and the Launch of Modern Innate Immunity. *J. Immunol.* *191*, 4473–4474. <https://doi.org/10.4049/jimmunol.1302427>.
- Mi, H., Ebert, D., Muruganujan, A., Mills, C., Albu, L.-P., Mushayamaha, T., and Thomas, P.D. (2021). PANTHER version 16: a revised family classification, tree-based classification tool, enhancer regions and extensive API. *Nucleic Acids Res.* *49*, D394–D403. <https://doi.org/10.1093/nar/gkaa1106>.
- Mroginski, M.A., Kaminski, S., von Stetten, D., Ringsdorf, S., Gärtner, W., Essen, L.-O., and Hildebrandt, P. (2011). Structure of the Chromophore Binding Pocket in the Pr State of Plant Phytochrome phyA. *J. Phys. Chem. B* *115*, 1220–1231. <https://doi.org/10.1021/jp108265h>.
- Naveed, Z.A., Wei, X., Chen, J., Mubeen, H., and Ali, G.S. (2020). The PTI to ETI Continuum in Phytophthora-Plant Interactions. *Front. Plant Sci.* *11*, 2030. <https://doi.org/10.3389/fpls.2020.593905>.
- Paik, I., and Huq, E. (2019). Plant photoreceptors: Multi-functional sensory proteins and their signaling networks. *Semin. Cell Dev. Biol.* *92*, 114–121. <https://doi.org/10.1016/j.semdb.2019.03.007>.
- Panchal, S., Roy, D., Chitrakar, R., Price, L., Breitbach, Z.S., Armstrong, D.W., and Melotto, M. (2016). Coronatine Facilitates Pseudomonas syringae Infection of Arabidopsis Leaves at Night. *Front. Plant Sci.* *7*. <https://doi.org/10.3389/fpls.2016.00880>.
- Park, E., Nedo, A., Caplan, J.L., and Dinesh-Kumar, S.P. (2018). Plant-microbe interactions: organelles and the cytoskeleton in action. *New Phytol.* *217*, 1012–1028. <https://doi.org/10.1111/nph.14959>.
- Pedmale, U.V., and Liscum, E. (2007). Regulation of Phototropic Signaling in Arabidopsis via Phosphorylation State Changes in the Phototropin 1-interacting Protein NPH3. *J. Biol. Chem.* *282*, 19992–20001. <https://doi.org/10.1074/jbc.M702551200>.
- Perrella, G., Vellutini, E., Zioutopoulou, A., Patitaki, E., Headland, L.R., and Kaiserli, E. (2020). Let it bloom: cross-talk between light and flowering signaling in Arabidopsis. *Physiol. Plant.* *169*, 301–311. <https://doi.org/10.1111/ppl.13073>.
- Popescu, S.C., Popescu, G.V., Bachan, S., Zhang, Z., Seay, M., Gerstein, M., Snyder, M., and Dinesh-Kumar, S.P. (2007). Differential binding of calmodulin-related proteins to their targets revealed through high-density Arabidopsis protein microarrays. *Proc. Natl. Acad. Sci. U. S. A.* *104*, 4730–4735. <https://doi.org/10.1073/pnas.0611615104>.
- Popescu, S.C., Popescu, G.V., Bachan, S., Zhang, Z., Gerstein, M., Snyder, M., and Dinesh-Kumar, S.P. (2009). MAPK target networks in Arabidopsis thaliana revealed using functional protein microarrays. *Genes Dev.* *23*, 80–92. <https://doi.org/10.1101/gad.1740009>.
- Prasad, K.V.S.K., Abdel-Hameed, A.A.E., Xing, D., and Reddy, A.S.N. (2016). Global gene expression analysis using RNA-seq uncovered a new role for SR1/CAMTA3 transcription factor in salt stress. *Sci. Rep.* *6*, 27021. <https://doi.org/10.1038/srep27021>.
- Redditt, T.J., Chung, E.-H., Karimi, H.Z., Rodibaugh, N., Zhang, Y., Trinidad, J.C., Kim, J.H., Zhou, Q., Shen, M., Dangl, J.L., et al. (2019). AvrRpm1 Functions as an ADP-Ribosyl Transferase to Modify NOI Domain-Containing Proteins, Including Arabidopsis and Soybean RPM1-Interacting Protein4. *Plant Cell* *31*, 2664–2681. <https://doi.org/10.1105/tpc.19.00020>.
- Reuter, L., Schmidt, T., Manishankar, P., Throm, C., Keicher, J., Bock, A., and Oecking, C. (2021). Light-triggered and phosphorylation-dependent 14-3-3 association with NONPHOTOTROPIC HYPOCOTYL 3 is required for hypocotyl phototropism. *BioRxiv* 2021.04.09.439179. <https://doi.org/10.1101/2021.04.09.439179>.

- Río-Álvarez, I., Rodríguez-Herva, J.J., Martínez, P.M., González-Melendi, P., García-Casado, G., Rodríguez-Palenzuela, P., and López-Solanilla, E. (2014). Light regulates motility, attachment and virulence in the plant pathogen *Pseudomonas syringae* pv tomato DC3000. *Environ. Microbiol.* *16*, 2072–2085. <https://doi.org/10.1111/1462-2920.12240>.
- Rivadosi, A., Garlaschi, F.M., Casazza, A.P., Zucchelli, G., and Jennings, R.C. (2008). On phytochrome absorption and the phytochrome photoequilibrium in a green leaf: environmental sensitivity and photoequilibrium time. *Photochem. Photobiol. Sci.* *7*, 986–990. <https://doi.org/10.1039/B806142D>.
- Rooney, W.M., Grinter, R.W., Correia, A., Parkhill, J., Walker, D.C., and Milner, J.J. (2020). Engineering bacteriocin-mediated resistance against the plant pathogen *Pseudomonas syringae*. *Plant Biotechnol. J.* *18*, 1296–1306. <https://doi.org/10.1111/pbi.13294>.
- Rossignol, P., Collier, S., Bush, M., Shaw, P., and Doonan, J.H. (2007). Arabidopsis POT1A interacts with TERT-V(18), an N-terminal splicing variant of telomerase. *J. Cell Sci.* *120*, 3678–3687. <https://doi.org/10.1242/jcs.004119>.
- Sakuraba, Y., Jeong, J., Kang, M.-Y., Kim, J., Paek, N.-C., and Choi, G. (2014). Phytochrome-interacting transcription factors PIF4 and PIF5 induce leaf senescence in Arabidopsis. *Nat. Commun.* *5*, 4636. <https://doi.org/10.1038/ncomms5636>.
- Santamaría-Hernando, S., Rodríguez-Herva, J.J., Martínez-García, P.M., Río-Álvarez, I., González-Melendi, P., Zamorano, J., Tapia, C., Rodríguez-Palenzuela, P., and López-Solanilla, E. (2018). *Pseudomonas syringae* pv. tomato exploits light signals to optimize virulence and colonization of leaves. *Environ. Microbiol.* *20*, 4261–4280. <https://doi.org/10.1111/1462-2920.14331>.
- Savage, Z., Duggan, C., Toufexi, A., Pandey, P., Liang, Y., Eugenia Segretin, M., Him Yuen, L., Gaboriau, D.C.A., Leary, A.Y., Tumtas, Y., et al. (2021). Chloroplasts alter their morphology and accumulate at the pathogen interface during infection by *Phytophthora infestans*. *Plant J.* *107*, 1771–1787. <https://doi.org/10.1111/tpj.15416>.
- Schindelin, J., Arganda-Carreras, I., Frise, E., Kaynig, V., Longair, M., Pietzsch, T., Preibisch, S., Rueden, C., Saalfeld, S., Schmid, B., et al. (2012). Fiji: an open-source platform for biological-image analysis. *Nat. Methods* *9*, 676–682. <https://doi.org/10.1038/nmeth.2019>.
- Sels, J., Mathys, J., De Coninck, B.M.A., Cammue, B.P.A., and De Bolle, M.F.C. (2008). Plant pathogenesis-related (PR) proteins: A focus on PR peptides. *Plant Physiol. Biochem.* *46*, 941–950. <https://doi.org/10.1016/j.plaphy.2008.06.011>.
- Senior, A.W., Evans, R., Jumper, J., Kirkpatrick, J., Sifre, L., Green, T., Qin, C., Žídek, A., Nelson, A.W.R., Bridgland, A., et al. (2020). Improved protein structure prediction using potentials from deep learning. *Nature* *577*, 706–710. <https://doi.org/10.1038/s41586-019-1923-7>.
- Sievers, F., Wilm, A., Dineen, D., Gibson, T.J., Karplus, K., Li, W., Lopez, R., McWilliam, H., Remmert, M., Söding, J., et al. (2011). Fast, scalable generation of high-quality protein multiple sequence alignments using Clustal Omega. *Mol. Syst. Biol.* *7*, 539. <https://doi.org/10.1038/msb.2011.75>.
- Sohn, K.H., Saucet, S.B., Clarke, C.R., Vinatzer, B.A., O'Brien, H.E., Guttman, D.S., and Jones, J.D.G. (2012). HopAS1 recognition significantly contributes to Arabidopsis nonhost resistance to *Pseudomonas syringae* pathogens. *New Phytol.* *193*, 58–66. <https://doi.org/10.1111/j.1469-8137.2011.03950.x>.
- Sowden, R.G., Watson, S.J., and Jarvis, P. (2018). The role of chloroplasts in plant pathology. *Essays Biochem.* *62*, 21–39. <https://doi.org/10.1042/EBC20170020>.
- Spoel, S.H., and Dong, X. (2012). How do plants achieve immunity? Defence without specialized immune cells. *Nat. Rev. Immunol.* *12*, 89–100. <https://doi.org/10.1038/nri3141>.
- Suetsugu, N., and Wada, M. (2007). Chloroplast photorelocation movement mediated by phototropin family proteins in green plants. *Biol. Chem.* *388*, 927–935. <https://doi.org/10.1515/BC.2007.118>.
- Suetsugu, N., and Wada, M. (2017). Two Coiled-Coil Proteins, WEB1 and PM12, Suppress the Signaling Pathway of Chloroplast Accumulation Response that Is Mediated by Two Phototropin-Interacting Proteins, RPT2 and NCH1, in Seed Plants. *Int. J. Mol. Sci.* *18*, 1469. <https://doi.org/10.3390/ijms18071469>.
- Suetsugu, N., Takemiya, A., Kong, S.-G., Higa, T., Komatsu, A., Shimazaki, K., Kohchi, T., and Wada, M. (2016a). RPT2/NCH1 subfamily of NPH3-like proteins is essential for the chloroplast accumulation response in land plants. *Proc. Natl. Acad. Sci.* *113*, 10424–10429. <https://doi.org/10.1073/pnas.1602151113>.
- Suetsugu, N., Higa, T., Gotoh, E., and Wada, M. (2016b). Light-Induced Movements of Chloroplasts and Nuclei Are Regulated in Both Cp-Actin-Filament-Dependent and -Independent Manners in Arabidopsis thaliana. *PLOS ONE* *11*, e0157429. <https://doi.org/10.1371/journal.pone.0157429>.

- Sullivan, A., Purohit, P.K., Freese, N.H., Pasha, A., Esteban, E., Waese, J., Wu, A., Chen, M., Chin, C.Y., Song, R., et al. (2019). An 'eFP-Seq Browser' for visualizing and exploring RNA sequencing data. *Plant J.* *100*, 641–654. <https://doi.org/10.1111/tj.14468>.
- Sullivan, S., Waksman, T., Henderson, L., Paliogianni, D., Lütkemeyer, M., Suetsugu, N., and Christie, J.M. (2021). Regulation of Plant Phototropic Growth by NPH3/RPT2-like Substrate Phosphorylation and 14-3-3 Binding. *BioRxiv* 2021.04.09.439135. <https://doi.org/10.1101/2021.04.09.439135>.
- Tang, D., Wang, G., and Zhou, J.-M. (2017). Receptor Kinases in Plant-Pathogen Interactions: More Than Pattern Recognition. *Plant Cell* *29*, 618–637. <https://doi.org/10.1105/tpc.16.00891>.
- de Torres Zabala, M., Littlejohn, G., Jayaraman, S., Studholme, D., Bailey, T., Lawson, T., Tillich, M., Licht, D., Bölder, B., Delfino, L., et al. (2015). Chloroplasts play a central role in plant defence and are targeted by pathogen effectors. *Nat. Plants* *1*, 15074. <https://doi.org/10.1038/nplants.2015.74>.
- Toum, L., Torres, P.S., Gallego, S.M., Benavides, M.P., Vojnov, A.A., and Gudesblat, G.E. (2016). Coronatine Inhibits Stomatal Closure through Guard Cell-Specific Inhibition of NADPH Oxidase-Dependent ROS Production. *Front. Plant Sci.* *7*, 1851. <https://doi.org/10.3389/fpls.2016.01851>.
- Ueda, H., Ito, T., Inoue, R., Masuda, Y., Nagashima, Y., Kozuka, T., and Kusaba, M. (2020). Genetic Interaction Among Phytochrome, Ethylene and Abscisic Acid Signaling During Dark-Induced Senescence in *Arabidopsis thaliana*. *Front. Plant Sci.* *0*. <https://doi.org/10.3389/fpls.2020.00564>.
- Upton, J.L., Zess, E.K., Białas, A., Wu, C., and Kamoun, S. (2018). The coming of age of EvoMPMI: evolutionary molecular plant–microbe interactions across multiple timescales. *Curr. Opin. Plant Biol.* *44*, 108–116. <https://doi.org/10.1016/j.pbi.2018.03.003>.
- Van Der Biezen, E.A., and Jones, J.D.G. (1998). Plant disease-resistance proteins and the gene-for-gene concept. *Trends Biochem. Sci.* *23*, 454–456. [https://doi.org/10.1016/S0968-0004\(98\)01311-5](https://doi.org/10.1016/S0968-0004(98)01311-5).
- Vieira-Pires, R.S., and Morais-Cabral, J.H. (2010). 310 helices in channels and other membrane proteins. *J. Gen. Physiol.* *136*, 585–592. <https://doi.org/10.1085/jgp.201010508>.
- Waese-Perlman, B., Pasha, A., Ho, C., Azhieh, A., Liu, Y., Sullivan, A., Lau, V., Esteban, E., Waese, J., Ly, G., et al. (2021). ePlant in 2021: New Species, Viewers, Data Sets, and Widgets. 2021.04.28.441805. <https://doi.org/10.1101/2021.04.28.441805>.
- Walter, M., Chaban, C., Schütze, K., Batistic, O., Weckermann, K., Näke, C., Blazevic, D., Grefen, C., Schumacher, K., Oecking, C., et al. (2004). Visualization of protein interactions in living plant cells using bimolecular fluorescence complementation. *Plant J.* *40*, 428–438. <https://doi.org/10.1111/j.1365-313X.2004.02219.x>.
- Wan, Y.-L., Eisinger, W., Ehrhardt, D., Kubitscheck, U., Baluska, F., and Briggs, W. (2008). The Subcellular Localization and Blue-Light-Induced Movement of Phototropin 1-GFP in Etiolated Seedlings of *Arabidopsis thaliana*. *Mol. Plant* *1*, 103–117. <https://doi.org/10.1093/mp/ssm011>.
- Wang, W., Feng, B., Zhou, J.-M., and Tang, D. (2020). Plant immune signaling: Advancing on two frontiers. *J. Integr. Plant Biol.* *62*, 2–24. <https://doi.org/10.1111/jipb.12898>.
- Whalen, M.C., Innes, R.W., Bent, A.F., and Staskawicz, B.J. (1991). Identification of *Pseudomonas syringae* pathogens of *Arabidopsis* and a bacterial locus determining avirulence on both *Arabidopsis* and soybean. *Plant Cell* *3*, 49–59. <https://doi.org/10.1105/tpc.3.1.49>.
- Wildermuth, M.C., Dewdney, J., Wu, G., and Ausubel, F.M. (2001). Isochorismate synthase is required to synthesize salicylic acid for plant defence. *Nature* *414*, 562–565. <https://doi.org/10.1038/35107108>.
- Willems, A.R., Schwab, M., and Tyers, M. (2004). A hitchhiker's guide to the cullin ubiquitin ligases: SCF and its kin. *Biochim. Biophys. Acta BBA - Mol. Cell Res.* *1695*, 133–170. <https://doi.org/10.1016/j.bbamcr.2004.09.027>.
- Win, J., Chaparro-Garcia, A., Belhaj, K., Saunders, D.G.O., Yoshida, K., Dong, S., Schornack, S., Zipfel, C., Robatzek, S., Hogenhout, S.A., et al. (2012). Effector Biology of Plant-Associated Organisms: Concepts and Perspectives. *Cold Spring Harb. Symp. Quant. Biol.* *77*, 235–247. <https://doi.org/10.1101/sqb.2012.77.015933>.
- Winter, D., Vinegar, B., Nahal, H., Ammar, R., Wilson, G.V., and Provart, N.J. (2007). An "Electronic Fluorescent Pictograph" Browser for Exploring and Analyzing Large-Scale Biological Data Sets. *PLoS ONE* *2*, e718. <https://doi.org/10.1371/journal.pone.0000718>.
- Wu, S.-H. (2014). Gene Expression Regulation in Photomorphogenesis from the Perspective of the Central Dogma. *Annu. Rev. Plant Biol.* *65*, 311–333. <https://doi.org/10.1146/annurev-arplant-050213-040337>.

- Xin, X.-F., and He, S.Y. (2013). *Pseudomonas syringae* pv. tomato DC3000: A Model Pathogen for Probing Disease Susceptibility and Hormone Signaling in Plants. *Annu. Rev. Phytopathol.* 51, 473–498. <https://doi.org/10.1146/annurev-phyto-082712-102321>.
- Xin, X.-F., Kvitko, B., and He, S.Y. (2018). *Pseudomonas syringae*: What it takes to be a pathogen. *Nat. Rev. Microbiol.* 16, 316–328. <https://doi.org/10.1038/nrmicro.2018.17>.
- Xu, D. (2020). COP1 and BBXs-HY5-mediated light signal transduction in plants. *New Phytol.* 228, 1748–1753. <https://doi.org/10.1111/nph.16296>.
- Yamaguchi, Y., Huffaker, A., Bryan, A.C., Tax, F.E., and Ryan, C.A. (2010). PEPR2 Is a Second Receptor for the Pep1 and Pep2 Peptides and Contributes to Defense Responses in Arabidopsis[W]. *Plant Cell* 22, 508–522. <https://doi.org/10.1105/tpc.109.068874>.
- Yang, L., McLellan, H., Naqvi, S., He, Q., Boevink, P.C., Armstrong, M., Giuliani, L.M., Zhang, W., Tian, Z., Zhan, J., et al. (2016). Potato NPH3/RPT2-Like Protein StNRL1, Targeted by a *Phytophthora infestans* RXLR Effector, Is a Susceptibility Factor. *Plant Physiol.* 171, 645–657. <https://doi.org/10.1104/pp.16.00178>.
- Zhang, L., Du, L., Shen, C., Yang, Y., and Poovaiah, B.W. (2014a). Regulation of plant immunity through ubiquitin-mediated modulation of Ca²⁺–calmodulin–AtSR1/CAMTA3 signaling. *Plant J.* 78, 269–281. <https://doi.org/10.1111/tpj.12473>.
- Zhang, L., Du, L., Shen, C., Yang, Y., and Poovaiah, B.W. (2014b). Regulation of plant immunity through ubiquitin-mediated modulation of Ca²⁺–calmodulin–AtSR1/CAMTA3 signaling. *Plant J.* 78, 269–281. <https://doi.org/10.1111/tpj.12473>.
- Zimorski, V., Ku, C., Martin, W.F., and Gould, S.B. (2014). Endosymbiotic theory for organelle origins. *Curr. Opin. Microbiol.* 22, 38–48. <https://doi.org/10.1016/j.mib.2014.09.008>.

APPENDIX 1: PCR Thermocycler programmes

A) Mutagenesis PCR

1.	98°C	1min	}	x20
2.	98°C	25s		
3.	60°C	30s		
4.	72°C	5min		
5.	72°C	10min		
6.	10°C	∞		

- *DpnI*-treatment for the product after PCR.

B) Mutagenesis PCR for Gel Extraction

1.	98°C	1min	}	x30
2.	98°C	25s		
3.	60°C	30s		
4.	72°C	2min		
5.	72°C	10min		
6.	10°C	∞		

- *DpnI*-treatment for the product after PCR.

